Sea Grant Program on Marine Corrosion
FINAL REPORT

Volume Three — Supporting Data
Localized Corrosion, Aluminum Alloys

Edited by
S. C. Dexter
and
W. H. Hartt

Submitted to

THE OFFICE OF SEA GRANT PROGRAMS
NATIONAL OCEANIC AND ATMOSPHERIC ADMINISTRATION
UNITED STATES DEPARTMENT OF COMMERCE

APRIL 1985

UNIVERSITY OF DELAWARE
Sea Grant College Program
LEWES, DELAWARE 19958

SEA GRANT PROGRAM ON MARINE CORROSION
FINAL REPORT

VOLUME THREE - SUPPORTING DATA
LOCALIZED CORROSION, ALUMINUM ALLOYS

Submitted to
The Office of Sea Grant Programs
National Oceanic and Atmospheric Administration
United States Department of Commerce

Marine Corrosion Program Leaders:

Stephen C. Dexter, University of Delaware
Overall Program Leader and
Localized Corrosion Project Leader

William H. Hartt, Florida Atlantic University
Calcareous Deposits Project Leader

Aluminum Alloys Project Principal Investigators:

Ronald M. Latanision, Massachusetts Institute of Technology

Stephen C. Dexter, University of Delaware

April 1985
University of Delaware
Sea Grant College Program
Lewes, Delaware 19958
DEL-SG-03-85

PREFACE

The Sea Grant Program on Marine Corrosion began in the fall of 1980 as a cooperative research project involving eight principal investigators from both academia and industry. An important component of the Program was the establishment of an Industrial Advisory Panel, whose primary functions were to keep the investigators aware of developing industrial problems in the area of marine corrosion, and to assist the investigators in technology transfer.

The Program was to last for three years, and was viewed by both the National Sea Grant Office and by the investigators themselves as an experiment in forging closer ties between a substantial academic research effort and its ultimate beneficiaries in industry.

This report, in four volumes, will serve, not only to document the technical results from three years of work by the eight principal investigators with their associates and students, but also to evaluate the success of that experiment, and to recommend whether the structure of the Program should be continued, and perhaps used as a model in other fields of research.

Volume One of the report is a stand-alone document, summarizing and evaluating the results of the entire program, while Volumes Two through Four present the technical details for each of the major segments of the program. Volume One is intended to be readable for the general educated public, whereas Volumes Two, Three and Four are intended to be reference volumes for those interested in specific areas of marine corrosion research and engineering.

Stephen C. Dexter
Overall Program Leader

PREFACE TO VOLUME THREE

The work on Localized Corrosion of Aluminum Alloys was done at the Massachusetts Institute of Technology by Dr. R. M. Latanision and his students, Samuel Smith and Nancy Kackley and at the University of Delaware by Dr. S. C. Dexter and his students, Keith Lucas, James Mihm, Wayne Rigby and Laila Moettus.

Figures and Tables in Volume Three will be found interspersed throughout the text, while references will be indicated in the text by consecutive numerals enclosed in square brackets and listed at the end of each major section.

Stephen C. Dexter
Localized Corrosion
Project Leader

Sea Grant Program on
Marine Corrosion

FINAL REPORT

Table of Contents

I. THE ROLE OF WATER CHEMISTRY

A. Introduction

It is now well established that the corrosion processes which occur on aluminum in seawater are significantly different from those which occur in saltwater (sodium chloride solution). These differences have been documented by both electrochemical and surface analytical techniques [1, 2].

Previous work [3, 4, 5] in quiescent seawater has clarified the roles of variables such as temperature, pH and the concentrations of dissolved gasses, oxygen and CO_2 in determining the corrosion potential and rate of cathodic reduction of oxygen on aluminum surfaces. It has also been demonstrated [1] that the presence of magnesium in the aluminum-water system has an influence on the cathodic reaction during corrosion of aluminum in aerated seawater. It was shown that the behavior of both pure aluminum and aluminum-magnesium alloys in natural seawater could not be reproduced in sodium chloride solutions in the laboratory until bicarbonate and magnesium were introduced into the system. Bicarbonate dissociates into carbonate ions and dissolved molecular carbon dioxide. Its presence allows laboratory simulation of the carbonic acid system which controls the pH of natural seawater.

It was proposed [1] that the role of magnesium is to act as a catalyst for the reduction of percarbonic acid, an intermediate species [6] in the seawater carbonic acid system according to:

$$H_2CO_4 + 2H^+ + 2e^- \xrightarrow{Mg^{++}} CO_2 + 2H_2O.$$

The above reaction would provide another reduction current for depolarization of the cathode in natural seawater but not in sodium chloride solutions. This was viewed as one possible reason why seawater is often observed to be more corrosive than 3 to 3.5% sodium chloride.

Large concentrations of magnesium are present on unalloyed aluminum surfaces corroded in seawater. Because of this it is important to understand how and why magnesium appears on aluminum surfaces corroded in seawater. It is clear that it cannot be due to an exchange reaction since the thermodynamic driving force is in the opposite direction. It

may be due to either precipitation of magnesium hydroxide or an adsorption reaction. If the excess magnesium concentrations can be pinpointed at the corrosion pit site, the participation of magnesium in the cathodic reactions is supported.

In order to examine the surface presence of magnesium, pure aluminum and aluminum alloy 5052 coupons were allowed to corrode in natural seawater. The Scanning Auger Microprobe (SAM) was used to determine the composition of the aluminum surface at various points. In order to examine the relationship between magnesium on the aluminum surface and active corrosion sites, a modified version of the Scanning Vibrating Electrode Technique designed by Isaacs [7] was used. This apparatus is able to map out the relative solution potential just above the freely corroding specimen with resolution on the order of tens of microns. The locations of initiating pits were identified by the local potential gradient in the electrolyte. After removal from the electrolyte, the same pits were identified with the scanning electron microscope and the surface composition around the pit site was analyzed with the SAM.

In order to determine whether precipitation or adsorption processes are the more likely cause of the magnesium surface coverage, the various chemical hypotheses were investigated by computer modeling using the MINEQL [8] program with the Stanford Adsorption Package [9].

Another probable difference between laboratory saline solutions and seawater is the possible effects of copper ions. It is known that even very low concentrations of copper ions in the electrolyte can have a major effect on the corrosion of aluminum due to an exchange reaction which results in depolarization of the cathodic half reaction. However, low levels of copper are difficult to study in laboratory solutions since reagent grade chemicals can contain as much as 5 ppm copper. Seawater generally contains less than 1 ppb, but concentrations may be much higher due to anthropogenic inputs, especially if circulation is restricted. It has been shown that very little of the copper in seawater is present as CU^{++} (< 1%) and that the majority is present as dissolved $Cu(OH)_2$ and $CuCO_3$ [10]. It is important to determine if these species will react with the aluminum surface and if there is a minimum concentration of copper in seawater necessary for the exchange reaction.

Although the effects of copper and magnesium appear quite different, they were amenable to examination by common theoretical and experimental procedures.

The experimental approach was straightforward. Aluminum samples were allowed to corrode in natural seawater and then their surfaces were examined using a Scanning Auger Microprobe (SAM) which allowed the composition of the aluminum surface to be determined at points of interest. SAM has a very thin sample depth (2 to 3 atomic layers) and a lateral resolution of less than 1 micron [11].

Other work was done using wet electrochemical polarization techniques to see if other divalent cations dissolved in natural seawater were capable of producing the same type of effect on the cathode kinetics that has been observed for magnesium. Finally, a set of experiments was done to determine whether magnesium in the alloy would produce the same effect as it does in the electrolyte.

B. Experimental Techniques

B.1. At the University of Delaware

Most of the experimental techniques used in this work have been previously published [1, 3-5], so only essential and/or new information will be presented here. Corrosion potentials and cathodic polarization curves were generated either on long 2 to 4 cm cylindrical electrodes machined from 1.3 cm diameter 99.99% and alloy 5052-0 aluminum rod, or on 13 to 15 cm long tubular electrodes made from commercial 5052-0 drawn tubing of 3.2 cm outside diamter and 0.165 cm wall thickness. Refer to Table I.1 for analyses of these metals. The cylindrical electrodes were mounted with a conventional Teflon compression gasket to avoid crevice effects [12].

Electrodes were prepared identically in order to achieve uniformity of the aluminum surface prior to testing. Specimens were abraded through 600 grit emery paper, degreased with acetone, pickled to 20% nitric acid at 50 to 60°C for 15 to 20 minutes, dipped in 1N sodium hydroxide (50 to 60°C) for 5 to 30 seconds, and rinsed in distilled water. Electrodes were then aged for 1 hour in room temperature (23 $\pm$ 2°C) distilled water, prior to immersion in the test cell. After both pickling and

Table I.1

Composition of Alloys Used

Component	99.99% Aluminum[1] (ppm)	Alloy 5052 Rod[2] (Wt %)	Alloy 5052 Tube[3] (Wt %)
Silicon	3.50	0.08	0.07
Iron	1.20	0.19	0.10
Copper	0.05	0.01	0.03
Manganese	NT	0.02	0.01
Magnesium	1.00	2.44	2.43
Chromium	0.25	0.20	0.19
Nickel	<0.30	0.02	0.00
Zinc	<0.18	0.01	0.04
Lead	<0.25	<0.01	NT
Tin	<0.64	<0.01	NT
Titanium	0.40	<0.01	0.01
Zirconium	0.95	NT	NT
Sodium	<0.50	NT	NT
Oxygen	10.00	NT	NT
Nitrogen	<5.00	NT	NT
Hydrogen	<1.00	NT	NT
Aluminum	Balance	Balance	Balance

[1]Material and analysis supplied by Materials Research Corporation.

[2]Material and analysis supplied by Reynolds Metals Company.

[3]Material supplied by Tube Sales, Inc., analysis done by Alcoa Laboratories.

NT-Indicates component not tested for.

aging, the specimens were examined at 25x in a stereomicroscope. Those with pits, significant surface irregularities, and/or crevices at the Teflon interfrace were reabraded, repickled and reexamined.

The sea water used in these experiments was full strength clean Atlantic Ocean surface water (salinity from 32 to 34 parts per thousand) collected in 55 liter polyethylene jugs at two to three week intervals from 40 to 100 miles off the mouth of Delaware Bay. The water was continuously aerated while stored in the laboratory. Before use, it was passed through glass fiber and 0.2 micrometer membrane filters to remove detritus and marine microorganisms.

Sodium chloride solutions were prepared by dissolving Fisher reagent grade salts in distilled water having a resistivity greater than 0.8 megohm. Other ions such as HCO_3^-, Mg^{++}, Ca^{++} and Sr^{++} were introduced by adding the proper amount of concentrated stock solution to the test electrolyte. HCO_3^- was added as the sodium salt, while Mg^{++}, Ca^{++} and Sr^{++} were added as the chloride.

The temperature of the test cell was controlled by pumping precooled alcohol through a glass cooling coil inserted into the electrolyte. Precooling was done with an FTS Systems Model MC260SV Cooling Unit. Temperature control was achieved to $\pm$ 0.5°C over the temperature range 4 to 25°C. The pH of test solutions was controlled to better than $\pm$ 0.05 pH units by adding 0.01N HCl or NaOH to sodium chloride solutions, or by varying the CO_2 partial pressure in natural seawater. Electrolyte pH was monitored with a Fisher Accument digital pH meter using either Markson or Sargent-Welch combination electrodes. Dissolved oxygen was controlled by varying the oxygen partial pressure and was measured in solution using a YSI Model 57 oxygen meter calibrated by the Winkler titration method. Cathodic polarization experiments were conducted using standard potentiostatic techniques [12]. A freshly pickled and aged electrode was allowed to reach steady state (usually within 45 to 60 minutes) in a 1000 ml six-neck polarization flask containing the test electrolyte. Polarization, controlled by either a Wenking Model 70 TS1 or a Princeton Applied Research Model 173 potentiostat was at a rate of 25 mV every 5 minutes in the active direction. Corrosion potentials were measured either by the potentiostat or by a high impedence Keithley Model 602 electrometer or by a Beckman Model RMS 3060 digital multi-meter using a saturated calomel reference electrode.

The total analytical amount of magnesium in solution in the test electrolytes was verified experimentally to within ± 30 ppm using a standard disodium EDTA titration technique [13]. The endpoint was read on a Bausch and Lomb Spectronic 700 Spectrophotometer.

B.2. At M.I.T.

Exposure

Sample preparation for the simple exposure tests was straightforward. Aluminum metal coupons (one cm^2) with thickness sufficient to prevent perforation during the text were polished to 600 grit with distilled water. After air drying, the sides and back were masked using a commercial lacquer (Stop-Off), and held in a dessicator for 24 hours prior to testing. No specimens prepared by the above procedure were observed to remain at the active corrosion potential, all moved immediately to above the pitting potential. The specimens were exposed to sea water in 100 ml beakers. The seawater was collected at the Woods Hole Oceanographic Institution dock (Woods Hole, MA), for the experiments on pure aluminum (Marz-grade) and was collected at Magnolia, MA, for the exposure tests alloy 5052. The pH of the seawater was adjusted from 7.0 to 8.1, (± 0.1) reflecting the natural range of seawater pH variations with depth, by varying the partial pressure of carbon dioxide. The pH was checked and adjusted at four to eight hour intervals unless the specimens were in seawater in which no pH adjustment was made (8.0 to 8.1), then the value was checked at the beginning and end of the experiment. The temperature was maintained at 20°C ± 3°C. The small temperature fluctuations were not found to contribute significantly to the variability of the data.

After exposure, Auger spectra were taken at two to six sites on the sample surface. The surface compositons recorded by the Auger spectra were adjusted to account for sea salts deposited on the surface by evaporation after removal of the sample from the solution. The concentration of Mg, Ca, and K attributed to sea salt was calculated by assuming all the Na is expected to adsorb. Since these cations have constant concentration ratios in seawater, the amount of Mg, Ca and K due to evaporation of seawater from the surface was calculated and subtracted from the total Auger signal for these ions. The resulting concentration was then defined as the surface excess or amount absorbed.

The distribution of cations was then calculated for each site on the sample. The average surface composition was determined by averaging values for all sites on the sample.

As shown later little sodium is expected to react with the surface, so this ion was used to determine the amount of sea salt on the surface. Since all of the ions of interest are conservative in seawater (all have constant concentration ratios [14]), knowing the concentration of one fixes the concentration of the rest. If the Auger beam is not rastered in order to maximize the signal to noise ratio, the spacial resolution of the Auger is fine enough that the precipitated salts do not appear as an homogenous contamination, but in discrete patches. Therefore, the concentration of any one salt varies over the surface.

To find the average sea salt concentration, the average sodium to aluminum ratio for all sites on the sample was determined. The reason a ratio must be used to compare elemental concentrations between sites is that absolute concentration values are not comparable between spectra. The aluminum concentration was chosen as the second member for the ratio because it is the most abundant of the cations on the surface and is not present in seawater at significant concentrations.

Once the average sodium to aluminum ratio is determined for the specimen, the expected sodium concentration value can be defined as the product of the aluminum concentration and the average sodium to aluminum ratio. Since the ratio of sodium to each of the other cations is constant, the concentration of each of these elements attributable to sea salt is the product of the sodium concentration and the specific element to sodium ratio. These ratios are listed below [14]:

$$[Mg]/[Na] = 0.1270$$
$$[Ca]/[Na] = 0.0667$$
$$[K]/[Na] = 0.0630$$

The concentration of the element attributable to sea salt was subtracted from the total concentration of the element. This concentration was then defined as the surface excess or amount adsorbed. The percentage-wise distribution of cations on the surface could then be calculated for each site on the sample. The average surface composition was determined by averaging values for all sites on the sample.

Modeling

The surface composition of aluminum oxide in seawater was modeled using the computer program MINEQL [8] with the Stanford adsorption package [9]. This program is described in detail elsewhere [15]. Most of the values for the reaction constants necessary to run MINEQL + Stanford are available in the literature. The program MINEQL includes a large source file of thermydynamic data for ligands in solution. This source file is constantly updated as new or more accurate values appear in the literature. The adsorption constants are not included in this data file, since they are specific to each surface composition. In this study it is assumed that the surface oxide layer on aluminum is γ-Alumina. Both Davis et al. [16] and Benjamin (in Davis and Leckie [17] studied adsorption of ions on γ-Alumina. Constants are available in their publications for the adsorption of copper, lead, cadmium, sodium, chloride, and zinc.

The data compiled above, along with that determined in the results section, were entered into the program and the effect of important parameters on the speciation was determined.

SPM

The scanning potential microprobe was designed to achieve high resolution of the localized potential gradients developed over the metal surface as pitting corrosion develops. To achieve higher resolution, the microelectrode must be held very close to the flat, level surface of the sample. A flat sample surface was achieved by careful metallographic preparation. The sample mounting stage was designed and machined to create a mounting surface parallel to the probe's axes of motion.

The probe and auxillary electrodes are platinum wires 100 μm in diameter. A micrometer was used to raise and lower the probe arm and electrodes to position the probe electrode close to the sample surface. The distance of the probe from the surface was measured with a 25X fixed focus microscope lens with a measuring reticle. The probe and auxillary microelectrodes are vibrated vertically by a piezoelectric bimorph ceramic reed driven by a 6-volt sine-wave of fixed frequency. This allows the measurement of an A.C. signal by the probe with the magnitude modulated by the potential gradient in the electrolyte. The

frequency is set by the piezoelectric crystal's vibration frequency (267 Hz). The signals from both electrodes are measured by a lock-in amplifier set at the reference frequency of the sine-wave supply. The output of the amplifier, a D.C. signal reflecting the difference in magnitude between the probe and the auxillary electrode is run through a 12-bit analog to digital converter interfaced to an Apple II+ computer.

The digital signal is accessed by a program running on the computer. This program also moves the probe across the sample surface by advancing the stepping motors by a specified number of steps. Each time the probe is advanced one step, a data point is stored in an array by the program. Simultaneously, the pen of the X-Y plotter is advanced in the x-direction and its y-positions is modulated by the voltage value corresponding to this position on the sample. The result is a quasi-three-dimensional plot where a peak indicates a region of anodic pitting activity and a valley indicates a cathodic area. Square coupons, 1 cm on a side, of aluminum were prepared by polishing to 600 grit on wet silicon carbide paper, and then with 1 cm alumina slurry on a cloth wheel, using only distilled water as a lubricant. The electrolyte for the SPM exposures contained 2.45 mg NaCl, 0.52 mg $MgCl_2$-$6H_2O$ and 0.41 mg Na_2SO_4 in 1 liter of distilled water. This solution contains a subset of the components of ASTM substitute ocean water in diluted concentrations. This diluted solution was chosen so that the interaction of magnesium with the corroding surface could be investigated while keeping the solution con ductivity low.

The probe was positioned at a marked reference point at the beginning of the scan so that the data collected could be correlated to positions on the sample. The scanning electron microscope was used to locate pit sites on the sample which showed activity during the SPM scan. Then, the pits were located again with the scanning Auger microscope (SAM) and analysis of the composition surface was performed.

C. Results and Discussion

C.1. Magnesium and other Divalent Cations

In the earlier work in which the effect of divalent magnesium cations in the water was documented [1], the magnesium was always present in its normal seawater concentration of about 1272 ppm. This is

a large amount of magnesium, and the results presented in Figure I.1 show that much less than that is needed to give the previously observed noble shift in corrosion potential. Mg^{++} was added as the chloride to a 3% NaCl + 140 ppm HCO_3^- solution at 23 $\pm$ 2°C and pH 7.2, the electrolyte in which previous research had shown that the noble shift in corrosion potential of 99.99% aluminum is maximized. Figure I.1 shows that there is no effect of adding Mg^{++} at concentrations less than 50 ppm. At Mg^{++} concentrations greater than 50 ppm there is gradual increase in the magnitude of noble shift in the corrosion potential until at 150 ppm the full effect is achieved. Increasing the Mg^{++} concentration above 150 ppm gives no further increase in the size of the shift. The variability of the corrosion potential data are indicated by the vertical error bars in Figure I.1. In this figure, as in the rest of the data presented in this paper, the vertical error bars represent the envelope of all measurements taken (at least five) at a given set of conditions rather than the standard deviation, which would be smaller.

A series of cathodic polarization curves was run under the same conditions described above for Figure I.1 and the results are shown in Figure I.2. At 50 ppm of added Mg^{++}, the curve remains unchanged. The curve at 150 ppm, however, is indistinguishable (within experimental error) from the one at 1200 ppm. Moreover, the shape of the curve up to the 10 $\mu A\ cm^{-2}$ level is not altered by the addition of Mg^{++}. It is only the corrosion potential that changes.

Since publication of the original observation of the magnesium effect, it has been discovered that in laboratory experiments, the effect tends to decrease or even disappear with time as shown in Figure I.3. Corrosion potentials for 99.99% aluminum in 3% NaCl + 140 ppm HCO_3^- at pH 7.2 typically jump roughly 100 mV noble within 5 minutes (usually within 30 seconds) of the addition of greater than 150 ppm Mg^{++}. Recently, however, we have monitored the corrosion potential for longer times after Mg^{++} addition and have observed that it tends to recover most, or sometimes all, of the noble shift within 24 to 48 hours. This is not strictly an effect of depletion of Mg^{++} in the solution, because addition of more Mg^{++}, even in dosages exceeding 1200 ppm, does not restore the effect.

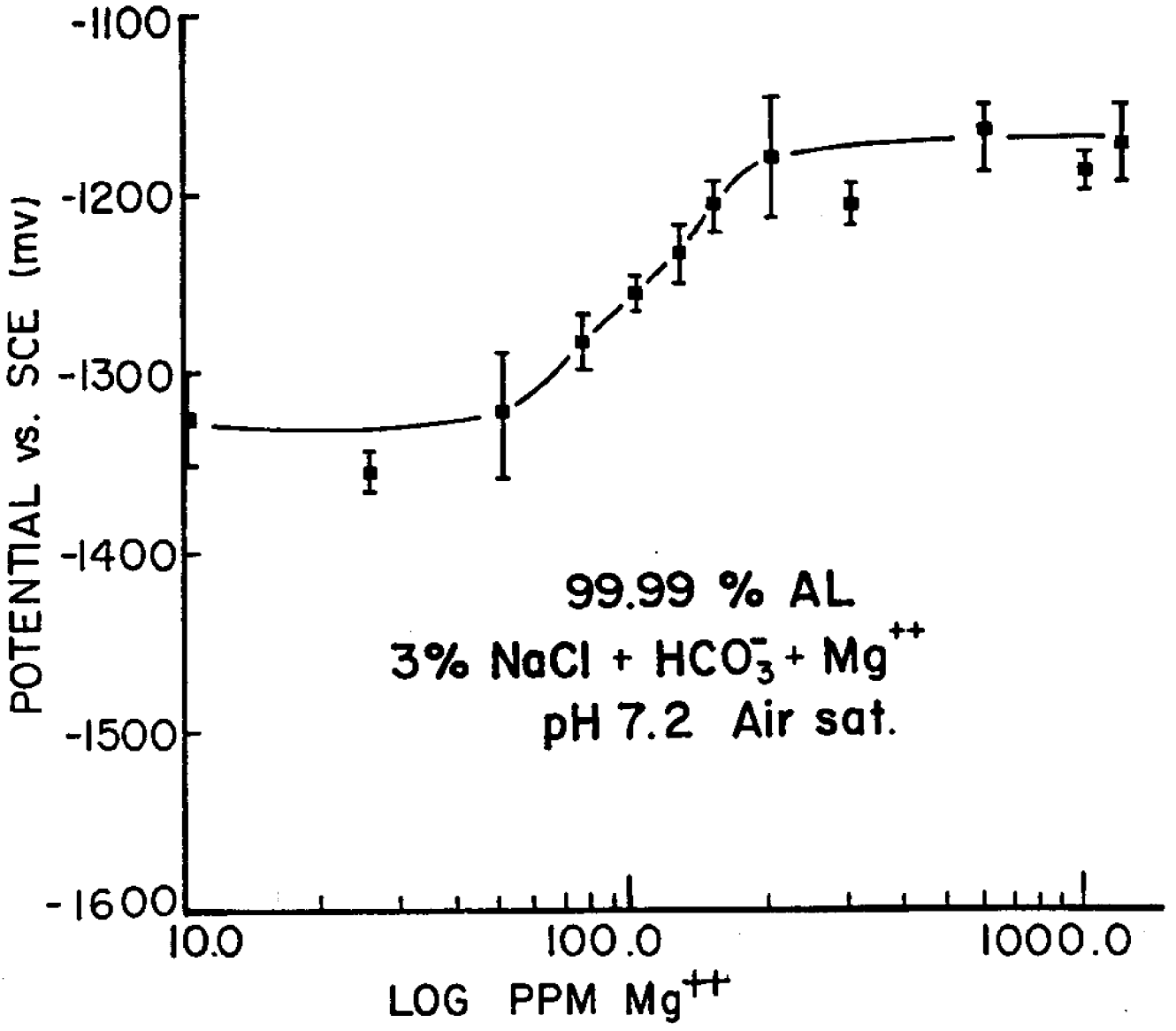

Fig. I.1 Corrosion potential of 99.99% aluminum in 3% NaCl + HCO_3^- solution as a function of magnesium additions at pH 7.2.

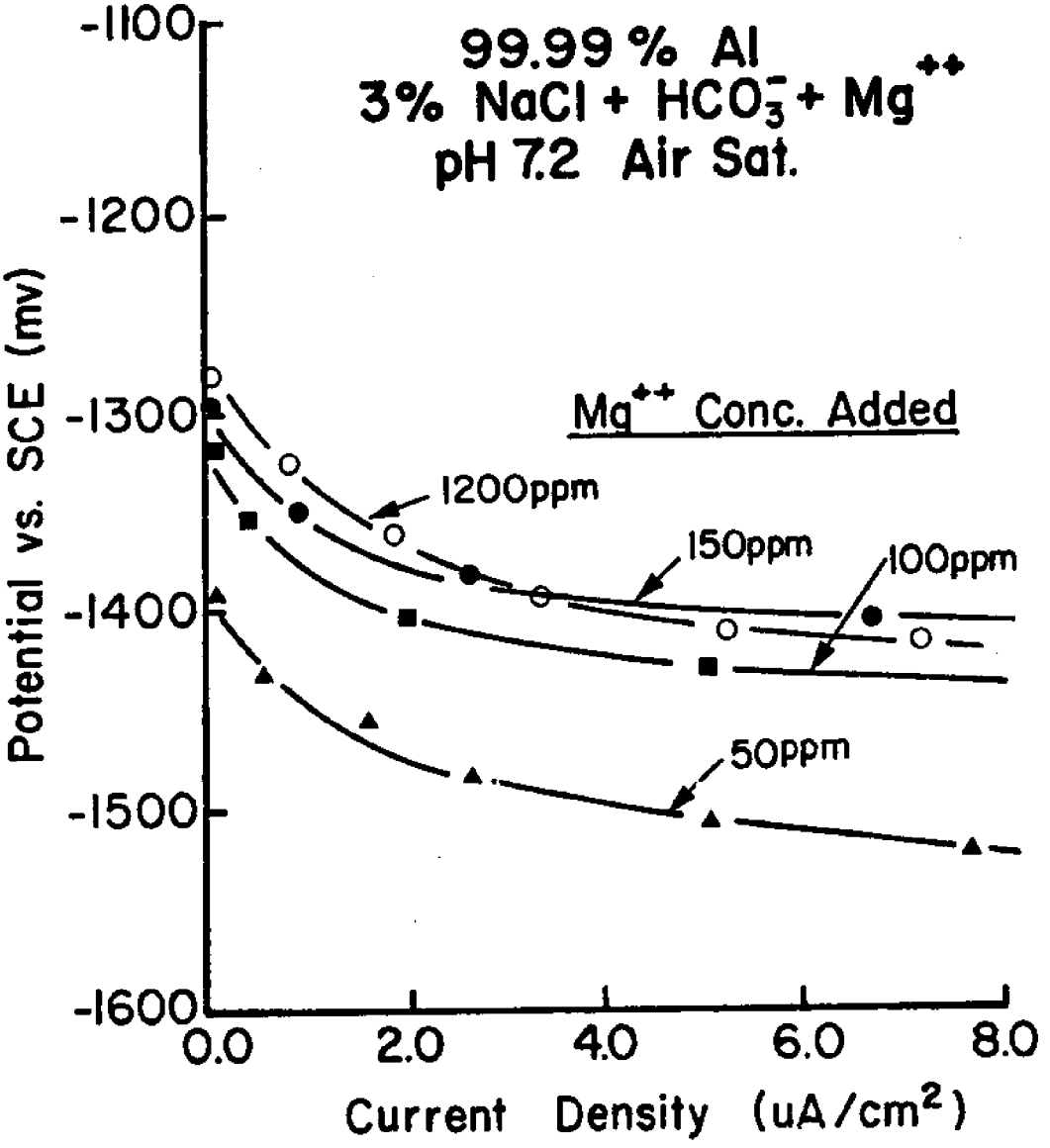

Fig. I.2 Cathodic polarization of 99.99% aluminum in 3% NaCl + HCO_3^- solution as a function of magnesium additions at pH 7.2.

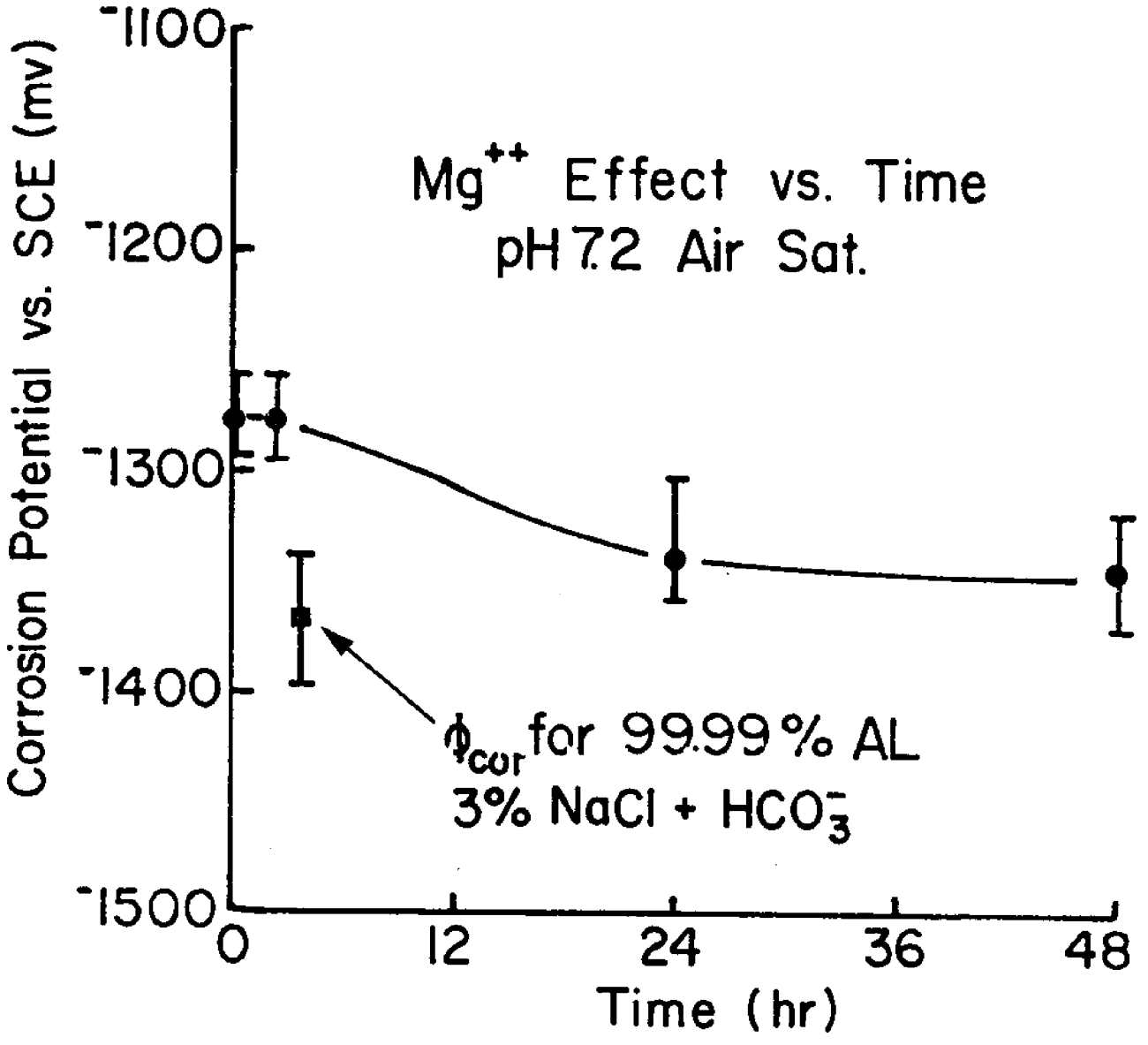

Fig. 3.3 Decay of the magnesium effect with time. The data point indicated by the arrow represents the corrosion potential prior to addition of magnesium.

In order to check further on this, we used an EDTA titration technique to measure the amount of magnesium in solution at various times during the experiment. The results are shown in Table I.2. The first two experiments were controls. In experiment No. 1 with no Mg^{++} added, the corrosion potential of the 99.99% aluminum electrode in 3% NaCl + 140 ppm HCO_3^- was stable over the 24 hour period. In experiment No. 2, 1200 ppm Mg^{++} was added to one liter of the same electrolyte with no electrode in the solution. The EDTA measurements on a sample of the water drawn from the cell after 24 hours showed that there was still 1180 $\pm$ 30 ppm magnesium in the solution. This indicates that significant amounts of Mg^{++} were not being lost to the atmosphere or to the walls of the container. In the last three experiments, the corrosion potential shifted in the noble direction upon addition of Mg^{++} and then recovered to nearly its initial value within 24 hours. The EDTA measurements showed a decrease in the amount of Mg^{++} present in solution in these last three experiments. Presumably this Mg^{++} was deposited on the aluminum electrode surface. In each case, however, there was enough remaining in solution after 24 hours to give the full effect shown in Figure I.1.

Another experiment was done in which we added enough EDTA to the solution containing the electrode to complex all magnesium present. This is depicted in Figure I.4. 1200 ppm Mg^{++} was added at time, -15 min, and gave the usual noble shift in corrosion potential. At time zero, the EDTA was added in such a way as not to change the pH of the electrolyte. Within one hour, the corrosion potential had recovered to its original value, whereas that normally would have taken about 24 hours. Within seconds after the EDTA was added, all free Mg^{++} ions were removed from solution. The magnesium was still there but it was all complexed with EDTA. This indicates that it is the free Mg^{++} ions present in the electrolyte that affect the corrosion potential rather than magnesium containing complexes. This finding is in accord with the proposed mechanism of percarbonic acid reduction as catalyzed by free Mg^{++}.

We have found recently that the details of the electrode surface preparation technique have an influence on whether or not the magnesium effect is observed. All electrodes are pickled after the abrasive

Table I.2

Measurements of Mg^{++} and ϕ_{cor}

Experiment No.	ϕ_{cor} (mV SCE) and [Mg^{++} conc. ($\pm$ 30 ppm) in Sq. Brackets]		
	ϕ_{cor} before Mg^{++} and nominal [Mg^{++}] added	ϕ_{cor} and [Mg^{++}] concentration after 15 min.	ϕ_{cor} and [Mg^{++}] concentration after 24 hrs.
1*	-1375 [none]	-1376 [none]	-1380 [none]
2**	- [1200]	- [1231]	- [1180]
3	-1340 [1200]	-1260 [1235]	-1330 [860]
4	-1414 [600]	-1350 [590]	-1410 [524]
5	-1368 [200]	-1323 [200]	-1350 [174]

*No Mg^{++} Added

** No Electrode

preparation steps in order to remove the work hardened layer formed during abrasion. It was found accidentally that decreasing the time in the final 1N NaOH bath from 30 sec to 5 sec usually caused the magnesium effect to disappear. Scanning electron microscopy of the electrode surfaces revealed that at 5 sec the directionality from the final abrasion step could still be seen in the surface morphology, indicating that the work hardened layer had not yet been fully removed. At 30 sec the directionality was gone and the magnesium effect reappeared.

In order to distinguish between the possible effects of surface morphology and work hardening, we tried removing the work hardened layer by annealing. An electrode which had received only a 5 sec final pickling treatment in 1N NaOH was annealed for one half-hour at 350°C. This annealing treatment alone did not restore the magnesium effect.

The fact that the proposed precarbonic acid mechanism is specific to magnesium also predicts that other divalent cations which may be present in seawater will not have a similar effect when Mg^{++} is absent. To check on this prediction we added Ca^{++} and Sr^{++}, the two most abundant divalent cations in seawater other than Mg^{++}, to 3% NaCl + HCO_3^- solution and measured their effects on the corrosion potential and cathodic polarization behavior of 99.99% aluminum at pH values of 8.2 and 7.2. At pH 8.2 the normal behavior of 99.99% aluminum in 3% NaCL + HCO_3^- is shown in Figure I.5 and that in the same electrolyte with Ca^{++} and Sr^{++} additions at their seawater concentrations in Figures I.6 and I.7 respectively. Sr^{++} has no effects at all. Ca^{++} gives a slight noble shift in the corrosion potential but it is only about half that produced by Mg^{++}. It is hard to draw any conclusions at pH 8.2 because even the shift produced by Mg^{++} is small at that pH [1].

At pH 7.2, the Mg^{++} effect is maximized. According to the proposed mechanism this is because the concentration of dissolved molecular CO_2 from which the percarbonic acid forms is maximized [1]. The normal curve for 99.99% Al in 3% NaCl + HCO_3^- at pH 7.2 is shown in Figure I.8. The corresponding curves with Ca^{++} and Sr^{++} additions again in their seawater concentrations appear as Figures I.9 and I.10. At pH 7.2 the curves in Figures I.8 to I.10 all fall within the same experimental scatterband and it is clear that neither Ca^{++} nor Sr^{++} in their full seawater concentrations produce an effect similar to that of magnesium.

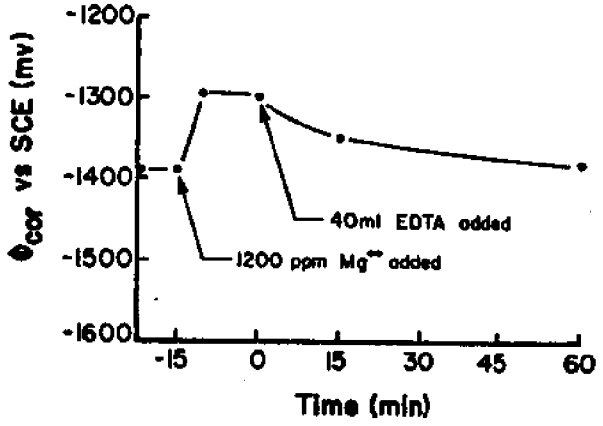

Fig. I.4 -Corrosion potential of pure aluminum as a function of time upon adding magnesium to the solution and subsequently complexing the magnesium with disodium EDTA.

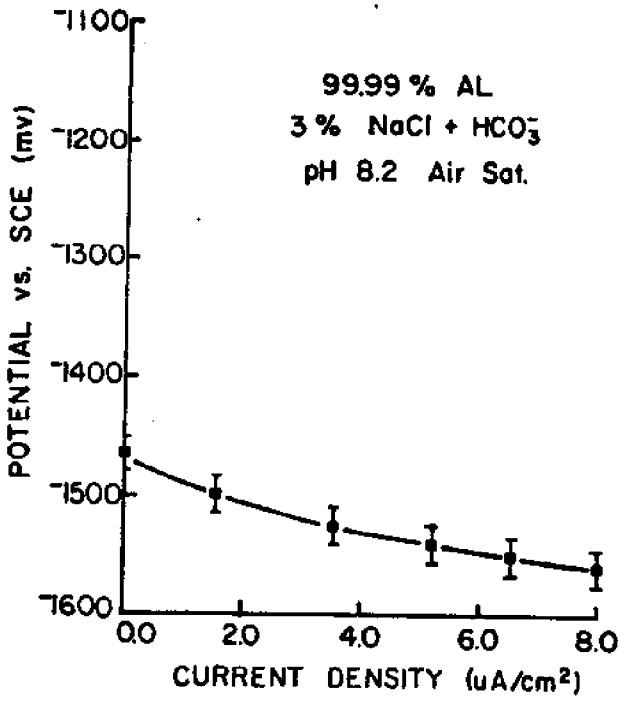

Fig. I.5-Cathodic polarization of pure aluminum in 3% NaCl + HCO_3^- at pH 8.2 for comparison to Figures I.6 and I.7.

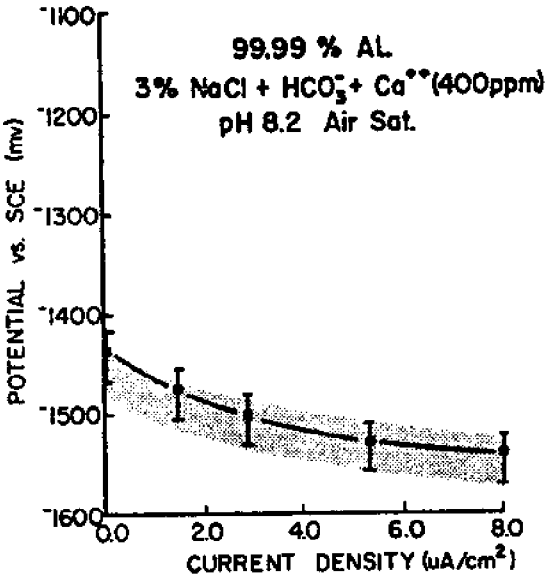

Fig. I.6 Cathodic polarization of pure aluminum as in Figure I.5 after adding 400 ppm Ca^{++} at pH 8.2.

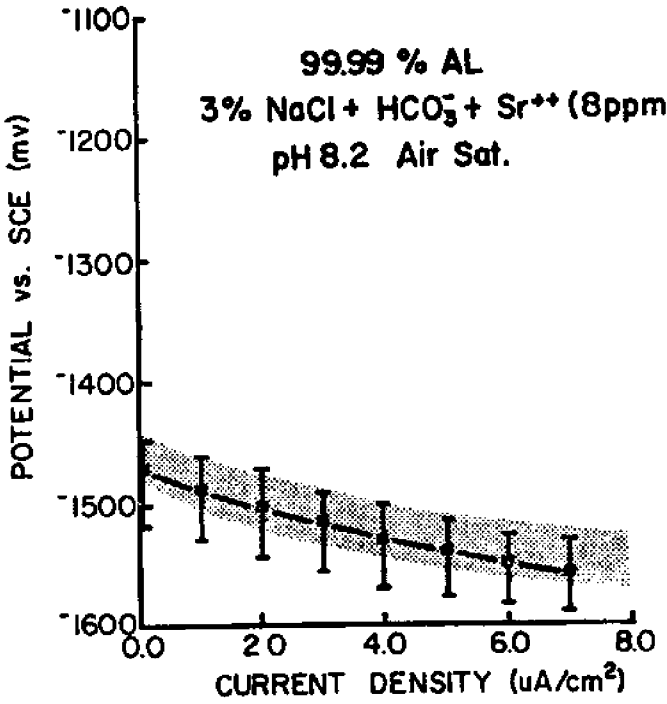

Fig. I.7 Cathodic polarization of pure aluminum as in Figure I.5 after adding 8 ppm Sr^{++} at pH 8.2.

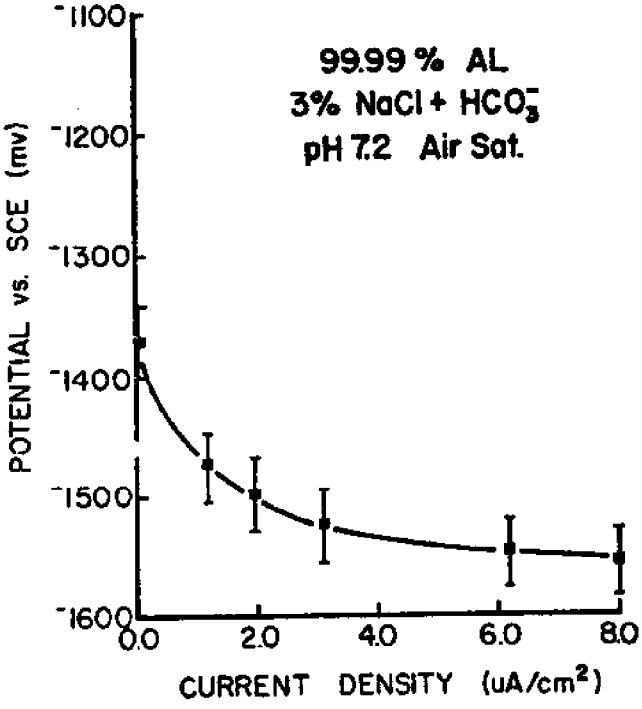

Fig. I.8 Cathodic polarization of pure aluminum in 3% NaCl + HCO_3^- at pH 7.2 for comparison to Figures I.9 and I.10.

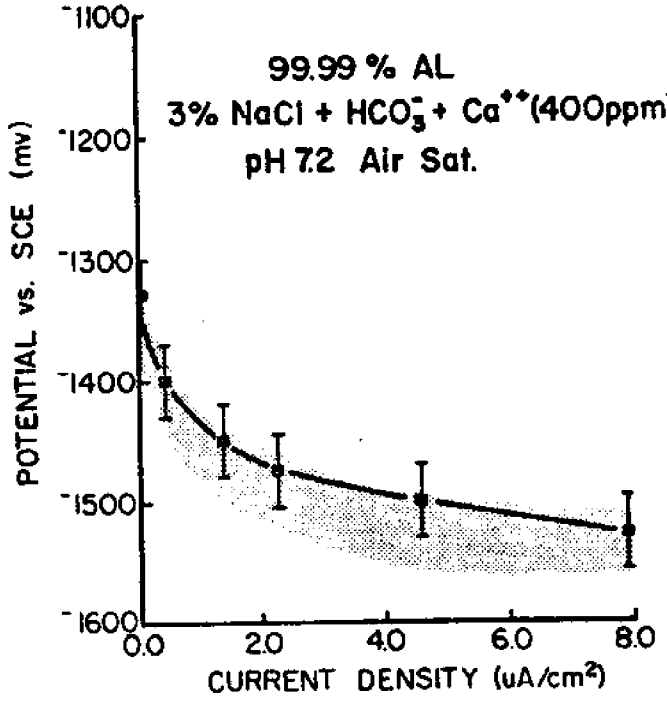

Fig. I.9 Cathodic polarization of pure aluminum as in Figure I.8 after adding 400 ppm Ca^{++} at pH 7.2.

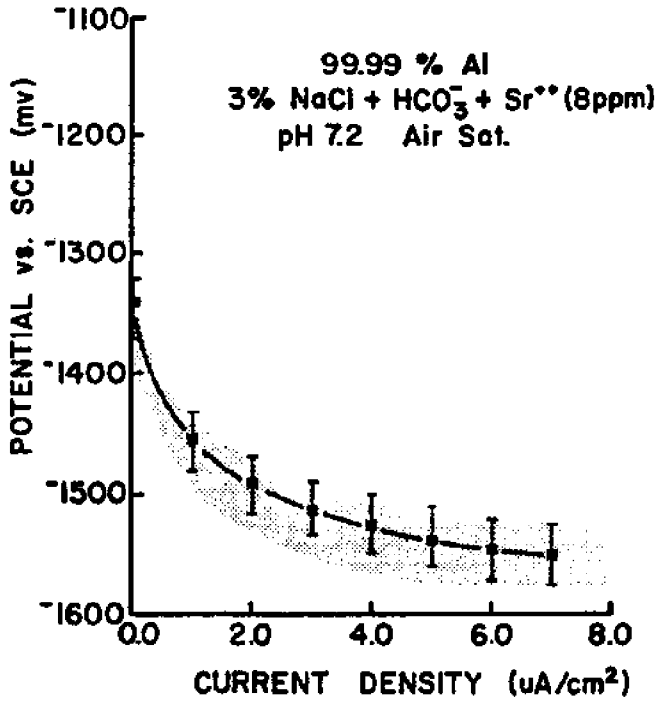

Fig. I.10 Cathodic polarization of pure aluminum as in Figure I.8 after adding 8 ppm Sr^{++} at pH 7.2.

The results which we have presented are consistent with the proposed percarbonic acid mechanism for the observed effect of magnesium on the corrosion potential of aluminum. We have shown that the observed noble jump in corrosion potential is specific to the presence of magnesium in the solution. Such a noble shift is not caused by the other two divalent ions, Ca^{++} and Sr^{++}, which are present at appreciable concentrations in seawater. Moreover, the effect can be made to disappear in the laboratory by complexing all the magnesium present in the solution with EDTA, making it unavailable to act as a catalyst in the percarbonic acid reduction reaction. Thus, it is only the free Mg^{++} ion concentration in the solution that is important. The question then arises as to how much of the total 1272 ppm magnesium present in full strength (35 parts per thousand salinity) natural seawater is present as free Mg^{++}. According to the literature in the field of marine chemistry [18], nearly 90% of the total 54 moles of magnesium per kg of seawter is present as "free" Mg^{++}. The strongest complex is $MgSO_4$, which accounts for nearly 10% of the total magnesium in solution. The missing one percent or so of magnesium is ion paired with OH^-, HCO_3^-, CO_3^{2-} and Cl^-. Thus, there should be plenty of free Mg^{++} in solution to produce the observed effect.

It is not yet understood why the magnesium effect tends to disappear with time. We have shown that this is not due to a gross removal of magnesium from solution. It is also unreasonable to expect it to be due to a complexation type of phenomenon because these take place over fractions of a second, whereas the magnesium effect takes tens of hours to disappear. Magnesium from the water does become incorporated into the passive film on pure aluminum [2], and it is suspected that changes in the passive film over a period of hours are probably involved in the disappearance of the magnesium effect. The details of the changes involved, however, are not clear.

It is also not yet clear how minor changes in the pickling procedure influence the role of magnesium. But again, the structure or thickness of the passive film is implicated. Increasing the length of time in the sodium hydroxide pickle enhances the magnesium effect. It also must lead to a greater removal of the oxide scale, or of the work

hardened surface layer, or to a change in the concentration of surface contaminants, or perhaps all three. It is interesting to note that the magnesium effect is the most pronounced when the passive film is least well established. The magnesium effect tends to be greatly reduced, or even absent, when the passive film is either not well removed during surface preparation, or has had enough time to reform.

In order to determine the chemical mechanism for magnesium incorporation into the barrier film a series of experiments were run in which the variation of surface composition with pH was determined by Auger analysis. Sixteen samples of commercial purity aluminum were exposed in seawater with pH values ranging from 7.0 to 8.1. There was considerable scatter in the data. This was not unexpected since the experiments were run in fresh, natural seawater and aluminum is well-known for extreme variability in corrosion experiments, even under the most carefully controlled conditions [4]. Figure I.13 presents the magnesium surface excess versus pH in graphical form. The error bars in Figure I.13 represent the value of one standard deviation in the data from a single sample. Due to the data scatter, only a linear analysis was justified. In the pH range of 7.0 to 8.1 there is an increase of approximately 7.4% in magnesium coverage per pH unit.

A series of samples of alloy 5052 were exposed to 3.5% NaCl solution and to natural seawater. Since alloy 5052 contains about 2.5% magnesium it might be expected that the oxide film would contain magnesium even after exposure to solutions containing no magnesium. This is suggested by the findings of Rowland and Dexter [1] that the presence of magnesium either in the alloy or in the electrolyte, has a significant effect on the cathodic kinetics of the corrosion reaction. As illustrated in Figure I.14, this hypothesis was not borne out. After exposure to 3.5% NaCl solution, the barrier film is found to consist only of aluminum oxide if known contaminants are excluded. However, when exposed to natural seawater the alloy 5052 specimens showed magnesium concentrations in the barrier film (Figure I.15) comparable to those found previously [19] on pure aluminum surfaces exposed to seawater.

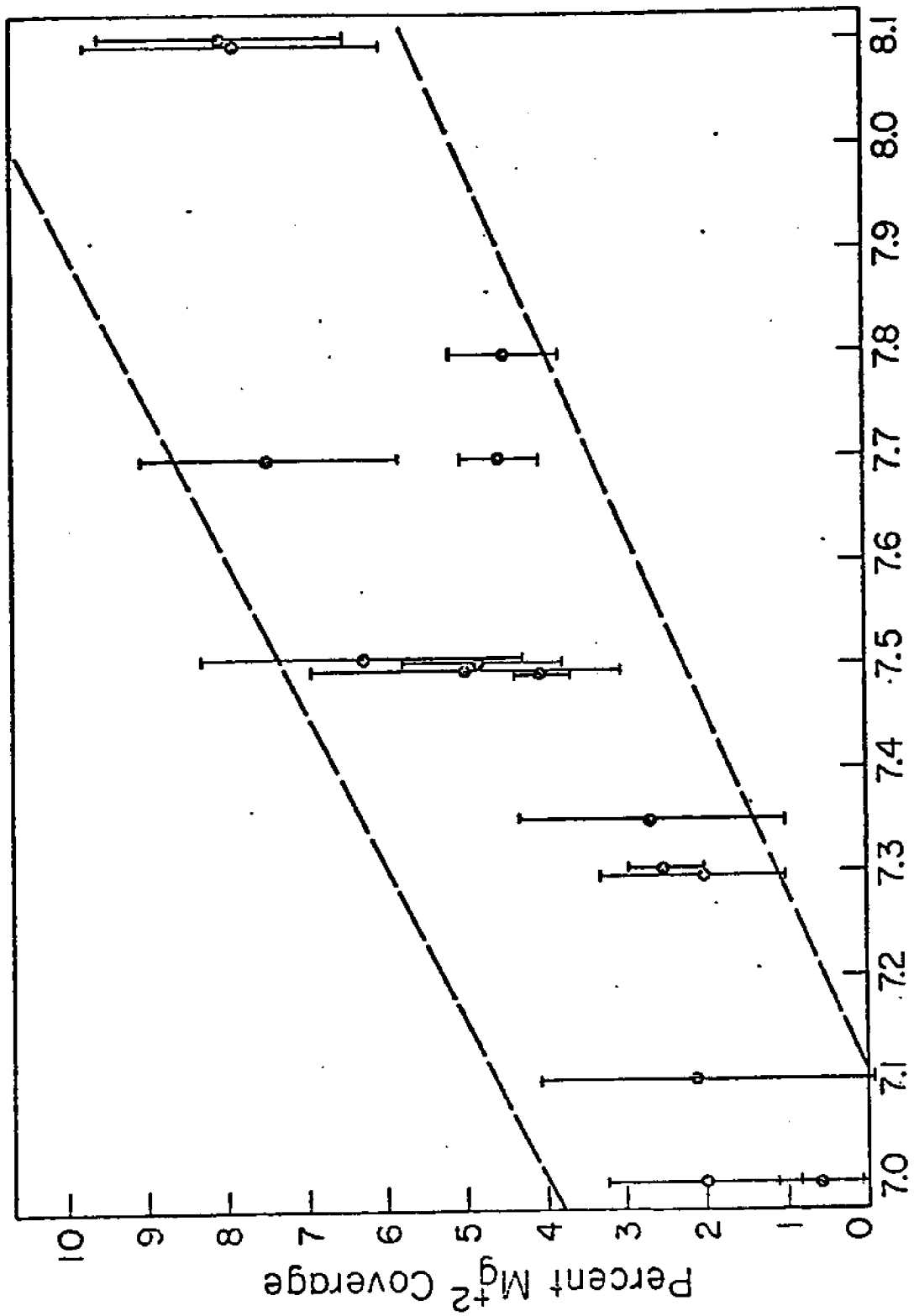

Figure I-13 Experimental Data for Magnesium Coverage Versus pH, Organics Present

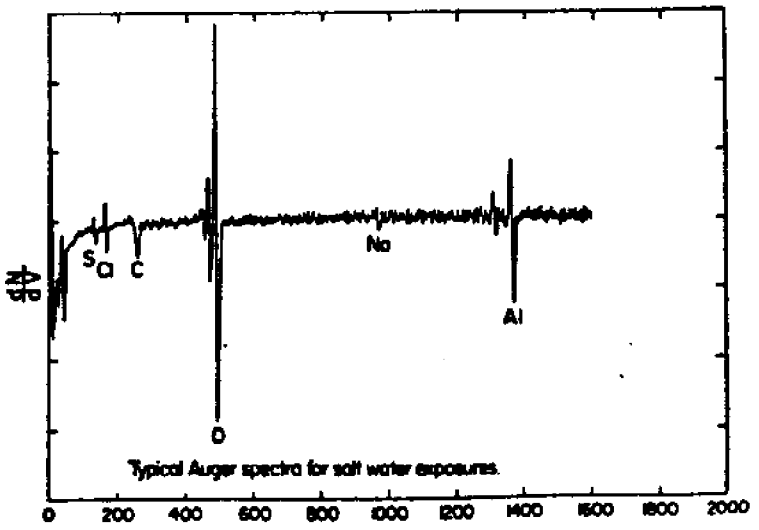

Fig.[I.14] Auger Spectra of Alloy 5052 Surface Corroded in Salt Water.

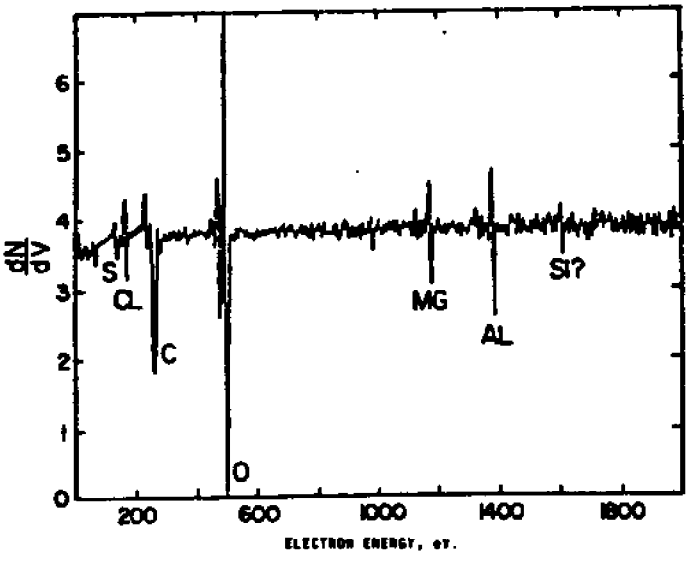

Fig. [I.15] Auger Spectra of Alloy 5052 Surface Corroded in Sea-water.

The surface composition for aluminum in seawater was predicted by the MINEQL [8] computer modeling program using a data file of adsorption chemistry constants [9]. Normal seawater values of temperature (20°C), pH 7.1-8.1 and salinity (35 ppt) with an organic film present on the aluminum surface were used. The pH versus adsorbed magnesium relationship generated by the computer model is shown in Figure I.16. The results of the model lie well within the experimental results.

At a pH of 8.1, the model predicted the following surface composition:

$$SOH = 76.0\%$$
$$Cl_{ads} = 11.9\%$$
$$Mg_{ads} = 8.5\%$$

Where SOH is a surface site (aluminum). The actual surface excess of magnesium measured experimentally was 7.8% with a standard deviation of 2.7%. The major inconsistency in the surface composition is the chloride concentration. The model predicts a much higher concentration of adsorbed chloride than is measured, especially if allowances are made for chloride deposited by evaporating seawater and other contamination during storage and transportation. The lower experimental values for surface chloride concentration are expected since the model is predicting the surface composition in solution where chloride is electrostatically adsorbed in the double layer. The chloride will be released after removal from solution. The chloride removal reaction could be written as follows:

$$SOH_2Cl = SOH + HCl$$

If this reaction occurs chloride would be removed by volatilization of HCl. If the majority of chloride were to desorb, then the sites predicted to be occupied by chloride would appear as aluminum in an Auger spectra.

The possibility that magnesium is present on the aluminum surface as a result of the precipitation of magnesium hydroxide due to an increase in the pH resulting from cathodic activity was considered. The

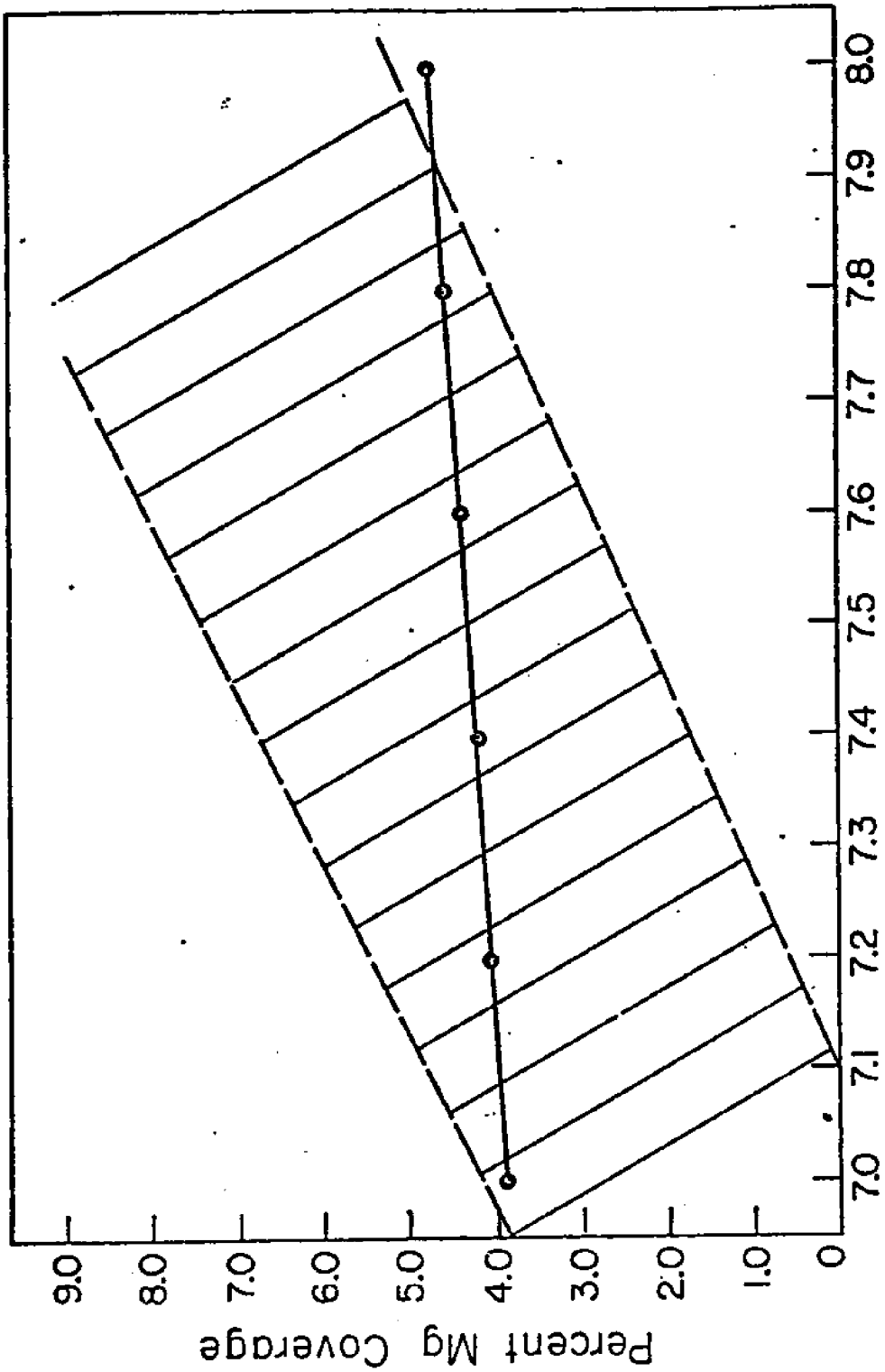

Figure I.16 Predicted Magnesium Coverage for Aluminum in Seawater Versus pH, Organics Present

computer model shows that magnesium hydroxide is not predicted to precipitate until a pH of about 9.0. In addition, pure aluminia colloids show magnesium on their surfaces with no cathodic reactions occurring [20]. For these reasons it is unlikely that precipitation of magnesium hydroxide is the major source of magnesium on aluminum surfaces during seawater exposure.

The scanning potential microprobe (SPM) was used to locate active pitting sites so that the surface composition near pits on alloy 5052 could be analyzed. Previous work [19] has shown increased magnesium concentrations near pits sites on pure aluminum. Using the SPM we are able to analyze pits known to be actively corroding at the time of removal from solution. The spatial position of a pit identified by an SPM scan can be determined from knowledge of the scan step size and the x- and y-position of the feature with respect to the scan starting point. The SPM scan of an alloy 5052 sample exposed to a dilute salt electrolyte is shown in Figure I.17. Several regions of pitting activity are indicated. Most of the pitting activity shows only 1 or 2 mV differences from the background level. An SEM photomicrograph (Figure I.18) was used to visually locate the pits identified in the SPM scan. The location of the pits marked a-f on the SPM scan are noted on the SEM photomicrograph.

The feature marked "d" was selected for further study. It appears as a small peak in the SPM scan of this sample in line 64. This pit was located with SAM using the SEM photomicrograph as a guide. The size of this pit is about 1-2 μm wide and 15 μm long (Figure I.19). The surface region surrounding the pit was analyzed by Auger electron spectroscopy (AES). A line scan was taken across the pit. The region was sputtered for 20 seconds prior to the AES scan to remove surface contaminants.

The AES scan across the pit (Figure I.20) showed an increase in carbon coincident with a decrease in aluminum, oxygen, and magnesium in the pit. Magnesium is present in higher concentrations 4 to 6 μm to the left of the pit. As discussed earlier, this surface excess of magnesium is due to an adsorption reaction. The decrease in Al, O, and Mg at the pit is probably not due merely to a change in surface topography since the carbon signal increases over the pit. A change in topography should affect the strength of all signals equally. However,

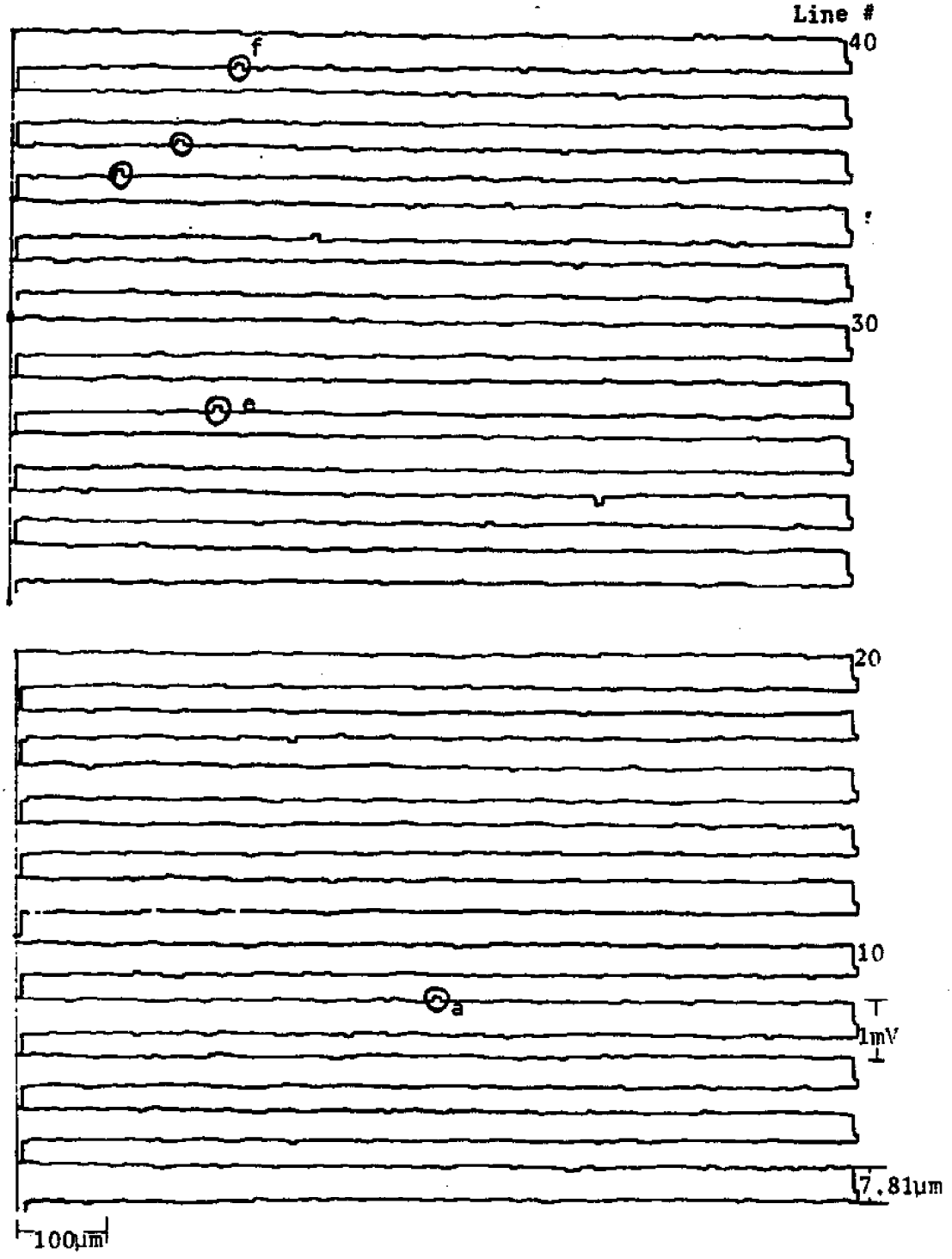

Fig. I.17 SPM scan of Al-5052 in Solution 3.

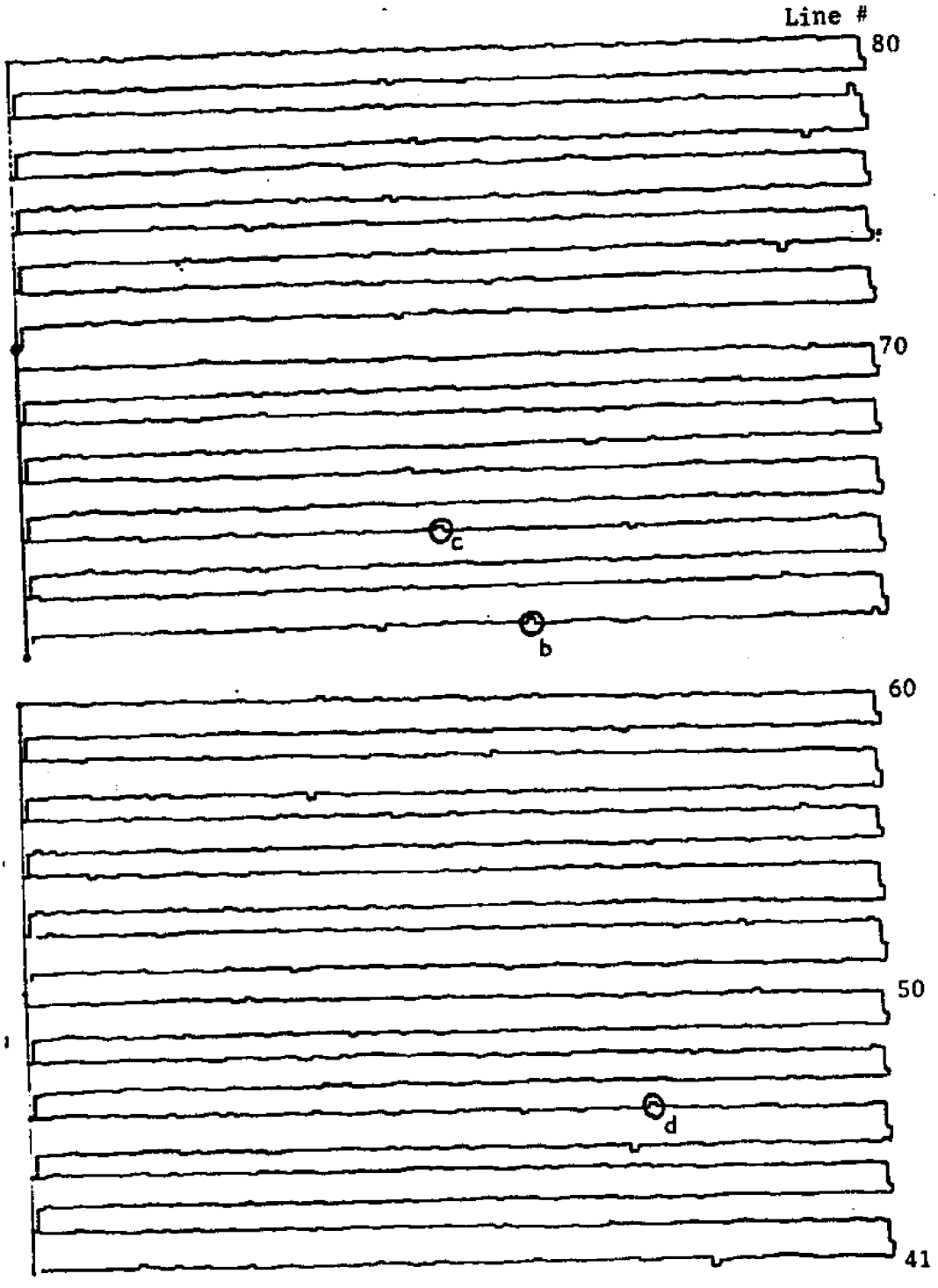

Fig. I.17 continued.

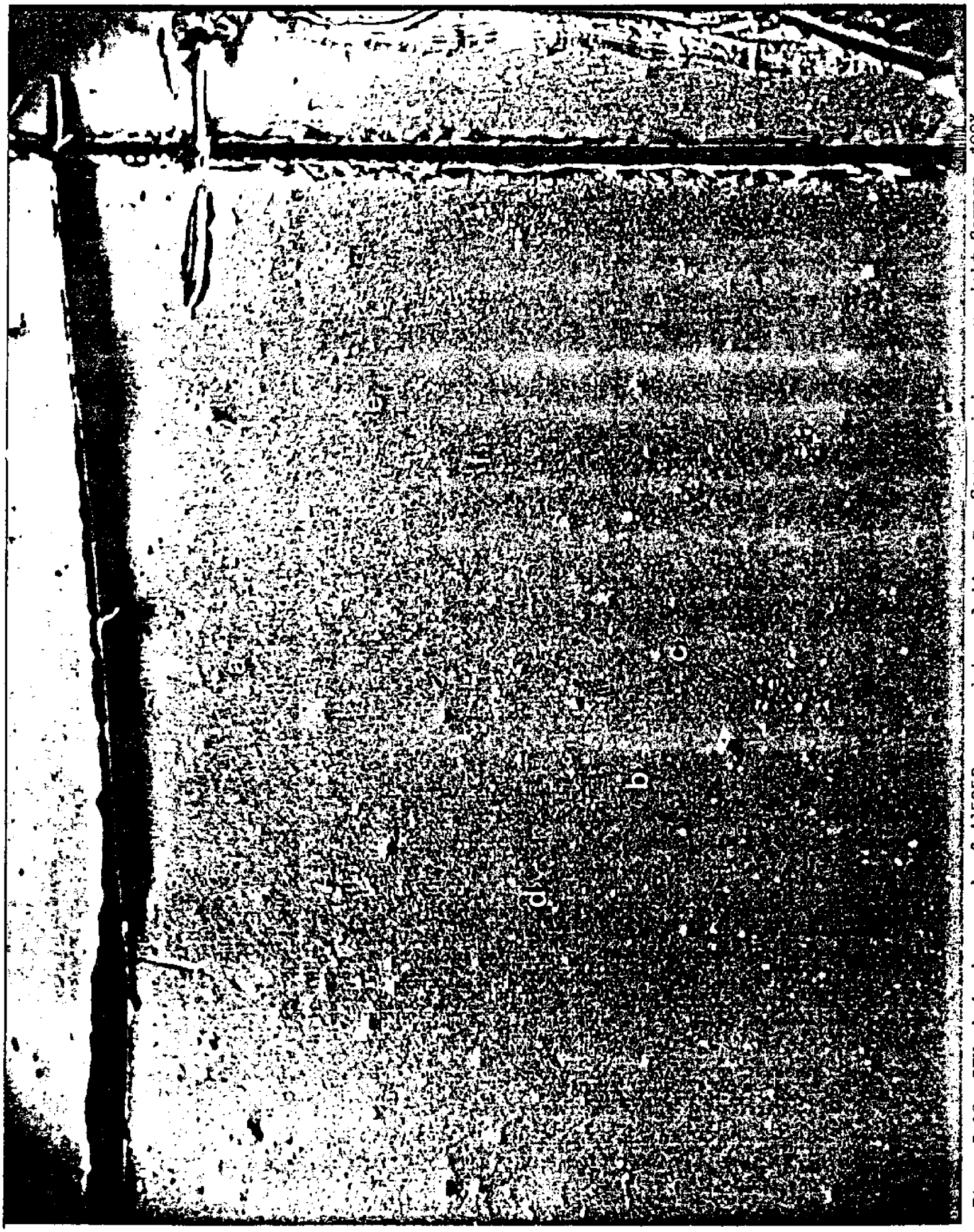

Fig. I.18 SEM photomicrograph of A15052 exposed to solution 3. Scan origin-upper right Corner. 100X

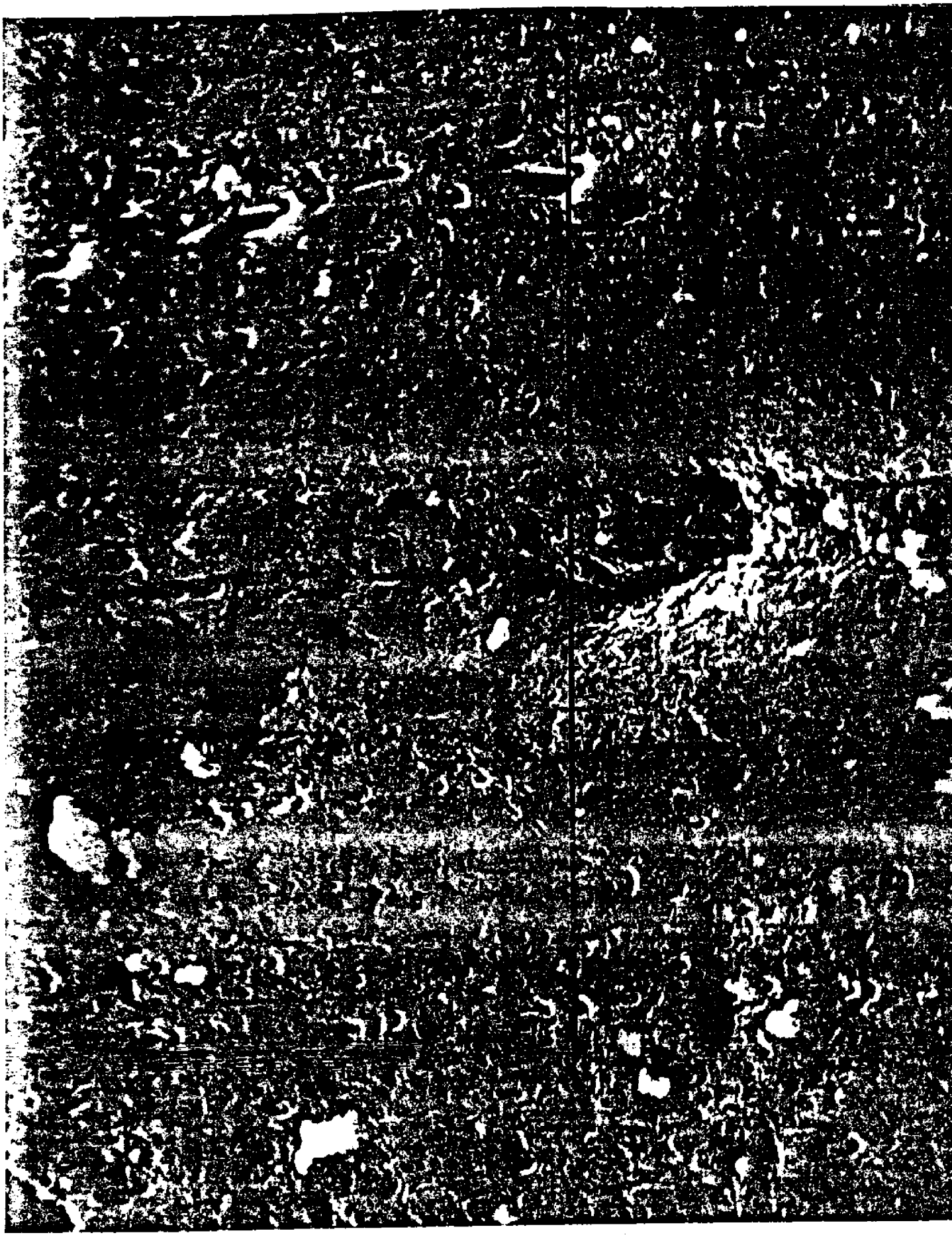

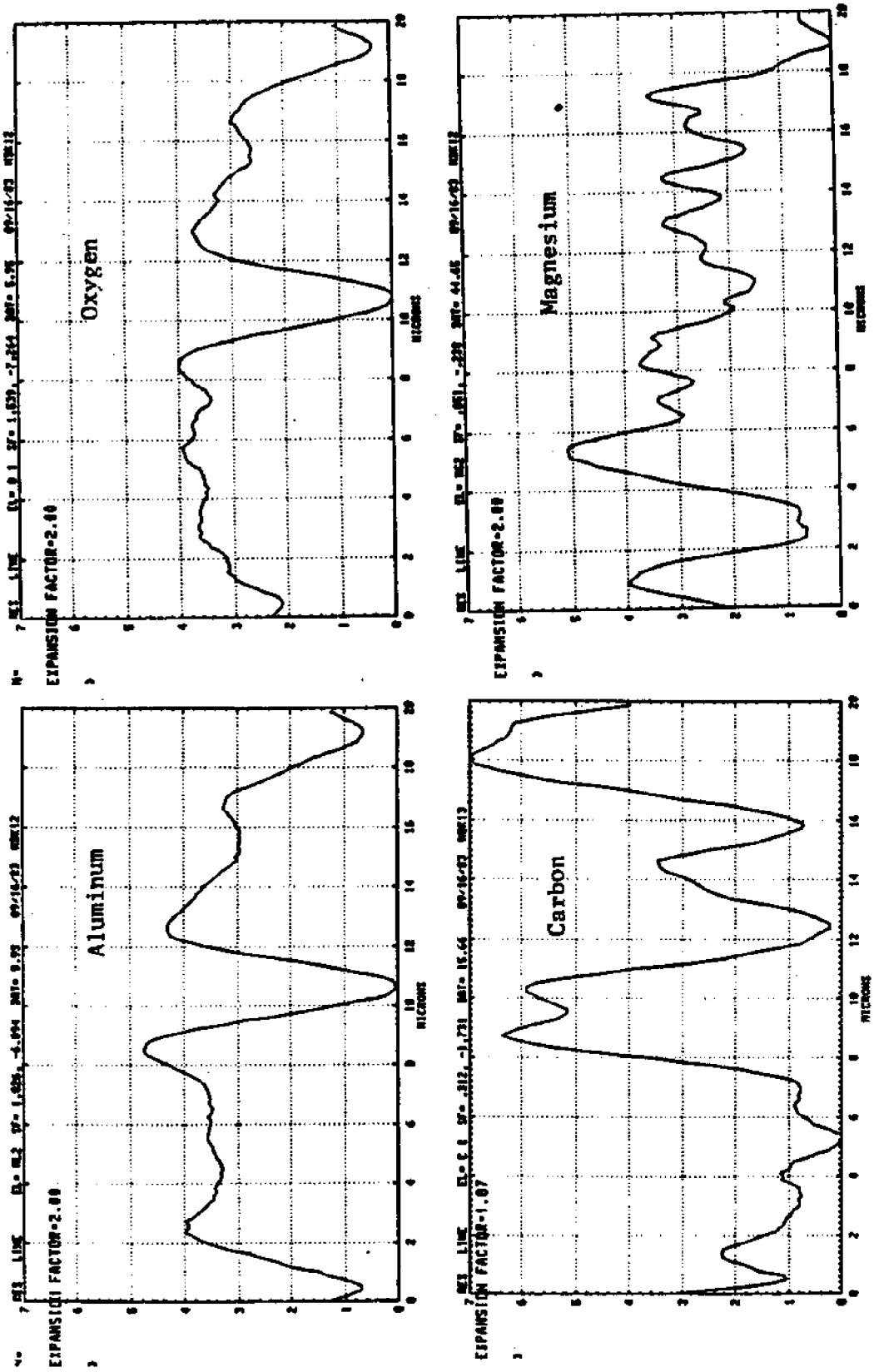

Fig. I-20 Elemental line scans by Auger Electron Spectroscopy (AES) across pit in Fig.I-18.

this effect could be due to the sputtering done before the scan. If the pit interior were not sputtered as cleanly as the rest of the surface, then an increase in the carbon signal at the pit would result. A carbon layer in the pit would also obscure the Al, O and Mg signals.

To answer this question and to confirm the presence of magnesium around the pits, another pit on this sample was located and analyzed. This line scan (Figure I.21) also showed decreases in Al, O and Mg at the pit and relatively constant carbon levels across the pit. (Note the large expansion factor necessary to highlight the small variations in carbon signal across the surface). This scan indicates that the relative excess of carbon in the pit is not a result of incomplete sputtering since no sputtering was done prior to these scans. Also, the decrease in the Al, O and Mg signals are not merely due to a topographical effect, but reflect actual decreases in these elements in the pit. Since no carbon compounds were intentionally added to the electrolyte, the carbon signal is probably due to contamination from exposure of the sample to air or from the vacuum system of the SAM.

These scans also show higher concentrations of magnesium at a distance of 4 to 6 μm from the pit center. After sputtering, (Figure I.23) even more magnesium is present 4 to 6 μm to the right of the pit. (Note lower expansion factors). The carbon level has been decreased and shows an even more definite peak at the pit site, where Al, O and Mg signals decrease.

The results presented show that the surface films of aluminum corroded in seawater are different from those found in sodium chloride solutions. The major difference in the films was the presence of magnesium on the surface. Adsorption chemistry predicts the observed relation between surface magnesium concentration of cations. An adsorption process would not require the large changes in surface pH required if the magnesium were due to precipitated magnesium hydroxide. This compound is soluble in seawater at pH less than 9.0. At the low current densities on freely corroding surfaces the pH is probably lower.

The model predicts much higher concentrations of chloride at the surface of the corrosion specimen than was actually measured. This is possibly due to the volatilization of hydrogen chloride from the surface when the specimen was removed from the electrolyte.

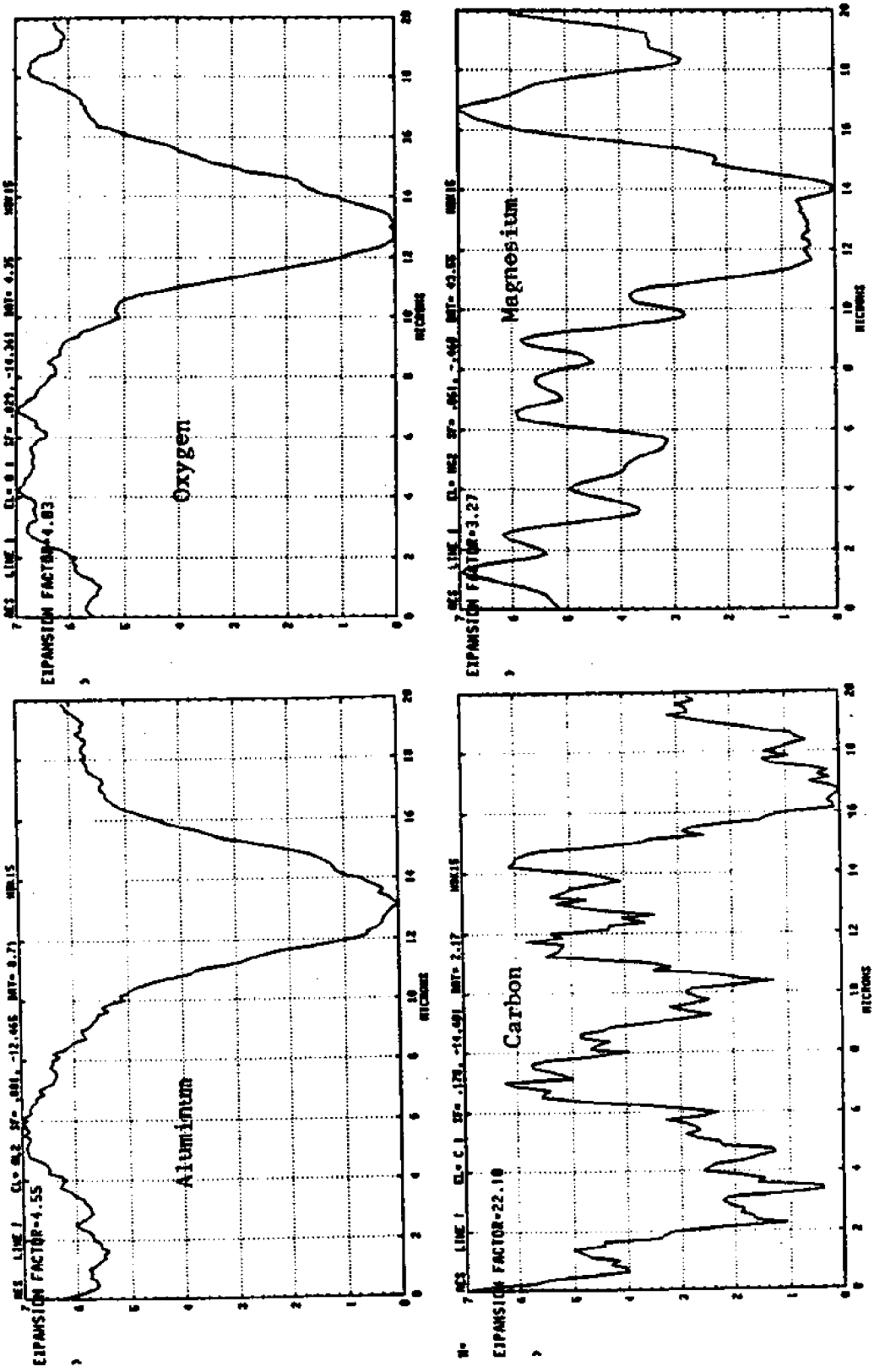

Fig. I.21 Elemental line scans by AES across pit in Al-5052 exposed to Solution 3.

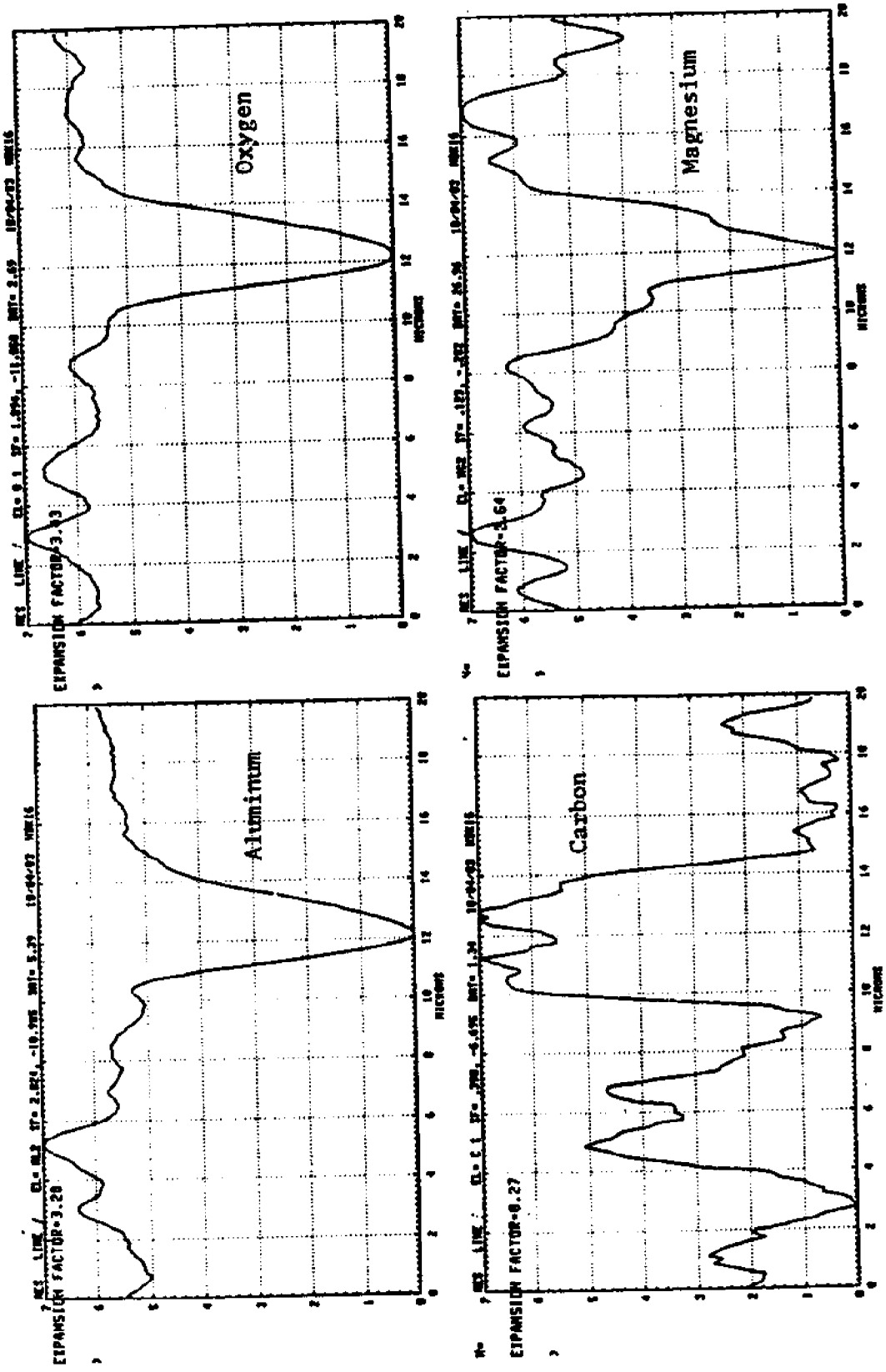

Fig. I.23 Elemental line scans by AES across pit in Al-5052 after 20 sec. sputter.

Using the SPM, pits were located while the aluminum alloy 5052 was actively corroding in a dilute electrolyte containing magnesium chloride. The SPM scan made it much easier to locate pits for chemical analysis using the scanning Auger microscope. Also, the pits studied with the SAM were definitely known to be active at the time of removal from the electrolyte. Therefore, pits which had passivated were eliminated from the surface analysis. When the surface around these pits was analyzed, excess surface concentrations of magnesium were found at a distance of 4 to 6 μm from the pit center. This result agrees with earlier work done with pure aluminum exposed to seawater [19].

A series of specimens were corroded in seawater which had been treated with high intensity ultraviolet radiation [21] to oxidize all the organics present. Since the activity of Mg^{+2} is lower in the presence of organics it might be expected that these specimens would show a higher percentage of surface magnesium than those corroded in seawater with organics present. The experimental data for the series of experiments run in seawater with the organics removed is presented in Figure I.24. At the lowest pH (7.0) the concentration is identical to that found on specimens in untreated seawater. At a pH value of 7.4, the concentration of magnesium is somewhat higher than that found in untreated water, although because of scatter in the data the magnesium concentration values may be in the uppermost range of those corroded in untreated seawater. At a pH value of 7.9, the surface was covered in a dark film which, by Auger analysis, was found to be composed largely of carbon (Figure I.25). Due to the many sources of carbon contamination, for example carbonates in seawater and carbon from the Auger vacuum system, it was not possible to determine conclusively if this black carbon deposit was in fact, carbon or whether it was a black carbon compound. There does not appear to be enough calcium on the surface for the carbon to be due to calcium carbonate precipitation, besides the color is wrong, since even thin calcium carbonate films are white. Rowland Dexter [1] believe an alumino-hydroxy-carbonate is present on aluminum surfaces at higher pH values. The shape of the carbon peak in the Auger spectrum more closely resembled peak shape of graphite than a carbide. The redox potential of pitting aluminum is low enough to

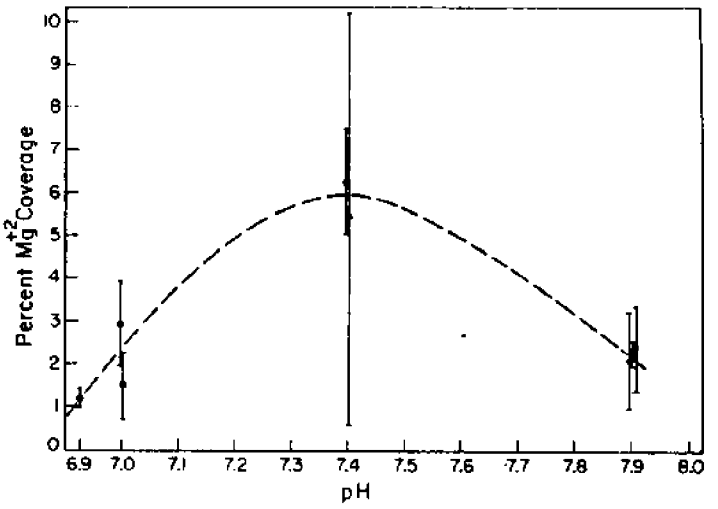

Fig. I.24 Experimental Data for Magnesium Coverage Versus pH, Organics Absent.

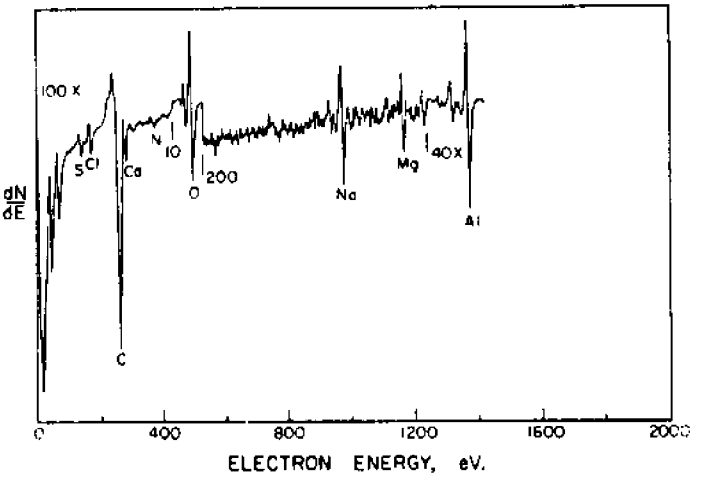

Figure I.25 Auger Spectra of Marz Aluminum Surface Corroded in UV Treated Seawater.

reduce carbonate to either carbon or methane. It could be that carbonate is being reduced to methane at lower pH values and to carbon at higher pH values. Whatever the deposit is, its formation must be strongly inhibited by organics.

On many of the low pH specimens (below a pH of 7.4), there was a significant amount of fluoride on the surface. Fluoride, being a singly charged anion similar to chloride, except at lower concentrations, would most strongly adsorb at the lower pH values. Since hydrogen fluoride is much less volatile than hydrogen chloride, more of the fluoride would be expected to remain on the surface. Fluoride may cause significant changes in the oxidation of aluminum [22].

C.2. Copper

A series of corrosion experiments were run in seawater contaminated with progressively less copper to determine at what point the surface copper contaminations became undetectable. The lowest copper concentration at which copper could be detected on the surface was 100 ppb. Dexter [1, 5] has shown that copper affects the corrosion behavior at an order of magnitude lower concentrations. It is very difficult to detect copper at very low concentrations on the aluminum since the primary copper Auger peak is overlain by a secondary sodium peak. The copper does appear to be at discrete sites at the lower concentrations, whereas the magnesium is more evenly distributed.

When required, copper sulfate was used to add copper ions since, as a salt of a major (highly concentrated) ion in seawater, small additions of sulfate will have an insignificant effect on the total sulfate concentratins in the test solutions.

Although adsorption chemistry appears to predict the proper concentrations and trends with pH for the magnesium on an aluminum surface in seawater, it does not explain the presence of copper on the surface. The concentration of copper on the surface due to adsorption is predicted to be less than 10^{-10} moles per meter square for a seawater solution with 0.3 ppm copper. It has been determined experimentally that there is very significant contamination of the surface even at much lower seawater concentrations of copper.

The mechanism of copper deposition predicted from the literature [2] involves the reduction of copper ions to the metallic state at the surface by aluminum metal oxidation. This mechanism was investigated with the computer model, by examining speciation changes with redox potential. Redox reactions can be treated in the program. The appropriate redox half reactions are entered into the program and the potential specified as a constant. The program calculates the distribution of species at the potential specified. In normal seawater the E_h is assumed to be around +0.75 VSHE. If it is assumed that the aluminum metal controls redox reactions on or 'closely associated with' its surface, then the E_h at a corroding aluminum surface should be set by the potential of the metal. For aluminum in solutions with the concentration of chloride found in seawater the critical pitting potential ($\emptyset_{crit}$) is -0.537 VSHE. This agrees with the potential which was measured for freely pitting aluminum samples in seawater.

At an E_h of +0.75 VSHE, the copper speciation is predicted to be as follows for a seawater copper concentration of 5×10^{-5}M (0.3 ppm):

$CuCO_3$	17.9%
$Cu(OH)_2$	80.4%

Note that the concentration of free copper (Cu^{+2}) is less than one percent. These results agree closely with those in the literature [10].

If the same calculation is made for an E_h of -0.54 VSHE, the model predicts that all the copper will be reduced to the metallic state. Therefore the model predicts the expected result, that the copper on the aluminum surface is due to deposition of metallic copper. This is true even though less than 0.1% of the copper was predicted to be present as free copper ions in the seawater. This clearly illustrates that the distribution of atoms among different species (in this case $CuCO_3$, $Cu(OH)_2$, Cu^{+2} and metallic copper) cannot be assumed constant upon a change in the system, but that the distribution is a competitive process and a new equilibrium will be established with a totally different distribution. For example, the assertion that only free copper ions can react with the aluminum surface is not a valid concept. The speciation of the entire system must be recalculated upon any significant change in that system.

Further calculations for lower concentrations of copper indicate that copper will be present in the reduced state when in contact with pitting aluminum even at much less than 1 ppb. A weakness of this analysis is that it does not take into account the nucleation energy necessary to initiate precipitation. This could be a significant factor at very low concentrations of copper.

The model predicts that all the copper present in the fouling film will be bound to the organics at the normal seawater E_h of 0.75 VSHE. However, at the aluminum surface E_h of -.54 VSHE, reduced copper is again the most stable state. This simply confirms the well-known experimental observation that the mere presence of a fouling film does not render copper inert to aluminum. Further investigation does reveal that the potential at which reduced copper becomes the stable state may be significantly reduced by the presence of the fouling film. In the presence of the fouling film there is an equal partitioning of the copper between reduced copper and dissolved copper at an E_h of 0.06 VSHE, yet when the organics are at a concentration of one ppm, all the copper would be reduced.

The presence of copper on aluminum surfaces exposed to solutions containing dissolved copper does not appear to be due to adsorption, but seems to result from the previously postulated mechanism of reduction to metallic copper [2]. The model results indicated that copper metal was less stable in the presence of an organic fouling film. However the model is based strictly on thermodynamics. A kinetic barrier, such as one due to nucleation energy, is not considered.

References

1. Rowland, H. T., Dexter, S. C., Corrosion, Vol. 36, p. 458 (1980).
2. Smith, S. W., Latanision, R. M., CORROSION/81, preprint No. 204, Toronto, April, 1981.
3. Dexter, S. C., Proc. 7th Intl. Congress on Metallic Corrosion, Rio de Janeiro, October, 1978, p. 1250.
4. Dexter, S. C., Corrosion, Vol. 36, p. 423 (1980).
5. Dexter, S. C., Ocean Science & Engr., Vol. 6, No. 1, p. 109 (1981).
6. Van Rysselbreghe, P., Delahay, P., Gross, A. H., McGeee, J. M., Williams, R. D., Phys. and Colloid Chem., Vol. 54, p. 754 (1950).
7. Isaacs, H. S. and Ishikawa, Y., "Application of the vibrating probe to the study of localized corrosion", Paper presented at the Corrosion Research Symposium, NACE Corrosion/83 (1983).
8. Westfall, J. C., Zachary, J. L. and Morel, F. M. M., "MINEQL: A computer program for the calculation of chemical equilibrium composition of aqueous systems", Technical Note 18, EPA Grant No. R-803738 (No Date).
9. James, R. O. and Parks, G. A., "Application of the computer program MINEQL, to solution of surface chemistry", Unpublished manuscript, (No Date).
10. Zirinio, A., Yamamoto, S., Limnology and Oceanography, Vol. 17, No. 5, p. 661 (1972).
11. MacDonald, N. C., Riach, G. E., Gerlach, R. L., Research Development, Vol. 27, No. 8, p. 42.
12. Leckie, H., Uhlig, H. H., J. Electrochem Soc., Vol. 113, p. 1262 (1966).
13. Grassholf, K., Methods of Seawater Analysis, Verlag Chemi Intl., New York, p. 199 (1976).
14. Stumm, W., Morgan, J. J., Aquatic Chemistry, Wiley-Interscience, NY (1970).
15. Smith, S. W., Brewer, P. G. and Latanision, R. M., To be submitted to Journal of Colloid and Interface Science (1983).
16. Davis, J. A., James, R. O. and Leckie, J. O., Journal of Colloid and Interface Science, 163(3), 480 (1978).
17. Davis, J. A. and Leckie, J. O., Journal of Colloid and Interface Science, 167(1), 90 (1978).

18. Dyrssen, D., Hansson, I., Marine Chemistry, Vol. 1, No. 2, p. 137 (1973).

19. Smith, S. W., "Analysis of the cathodic behavior of aluminum in natural seawater by surface chemistry", Sc.D. Thesis, M.I.T. (1981).

20. Huang, C. and Stumm, W., Journal of Colloid and Interface Science 43, 409 (1973).

21. Armstrong, F. A. J., Williams, P. M., Strickland, J. H. D., Nature, Vol. 211, p. 481 (1966).

22. Sotoudeh, J., Nguyen, T. H., Foley, R. T., Brown, B. F., Corrosion, Vol. 137, No. 6, p. 358 (1981).

II. THE ROLE OF MAGNESIUM AS AN ALLOYING ELEMENT

In order to determine whether magnesium in the alloy has the same effect that it does in seawater, tests have been run on two series of special AlMg alloys made for this project by the Alcoa Technical Center. The first series of alloys, whose compositions are shown in Table II.1, contained varying amount of magnesium from 0.23 to 2.39 wt. % in an alloy 1100 base. The highest of these magnesium contents corresponds to that found in alloy 5052. The second set of alloys was made on a pure aluminum base similar to that shown for 99.99% Al in Table I.1. The first alloy in this series contained a single addition of 0.25% iron. The remaining four alloys in this series contained a single addition each of magnesium in the following amounts: 0.23, 0.4, 1.0, and 2.5 weight percent.

All of the above alloys were tested in 3% NaCl + HCO_3 solution at pH 7.2, and their corrosion potentials and cathodic polarization behaviors were compared to those of 99.99% Al and Al alloy 5052 in the same solution. All of the alloys made on an 1100 alloy base behaved like exactly like the base alloy, regardless of the amount of magnesium present. The corrosion potentials were all at -700 +/- 20 mV SCE, and most samples began to pit immediately upon immersion in the test solution. In these alloys, any influence of magnesium was overwhelmed by the effect of the other alloying elements.

Next, the pure aluminum with 0.25 percent iron was tested. The corrosion potential was between -710 and -730 mV SCE for all specimens tested, and the polarization behavior at pH 7.2 was similar to that of alloy 5052 (see Figure II.1). It was evident that the presence of a quarter percent iron alone is enough to make pure aluminum act like alloy 5052 in our tests.

Finally, the series of alloys with magnesium additions to a pure aluminum base were tested. The samples containing 0.25% Mg had initial corrosion potentials of -1300 to -1325 mV SCE in 3% NaCl + HCO_3 solution at pH 7.2. When magnesium was added as the chloride to the test solution, the corrosion potential jumped 100 to 140 mV noble just as has been shown previously for pure aluminum. This jump is to be distinguished from a 10 to 20 mV temporary jump that always occurs as the

Table II.1

Compositions* of experimental Al-Mg-alloys for University of Delaware/Sea Grant Program

Ident. Number	Si	Fe	Cu	Mn	Mg	Cr	Ni	Zn	Ti
538350	.07	.25	.02	.01	.23	.00	.00	.00	.00
538351	.07	.25	.02	.01	.50	.00	.00	.00	.00
538352	.07	.25	.02	.01	.74	.00	.00	.00	.00
538353	.07	.25	.02	.01	.96	.00	.00	.00	.00
538354	.07	.25	.02	.01	1.44	.00	.00	.00	.00
538355	.07	.24	.02	.01	2.39	.00	.00	.00	.00
538356	.07	.24	.02	.01	2.36	.20	.00	.00	.00
539984 (5052 alloy plate from Williams & Company)	.07	.23	.02	.01	2.38	.19	.02	.01	.02

*Remelt analyses made at Alcoa Technical Center 1981-10-08 and 1981-10-28.

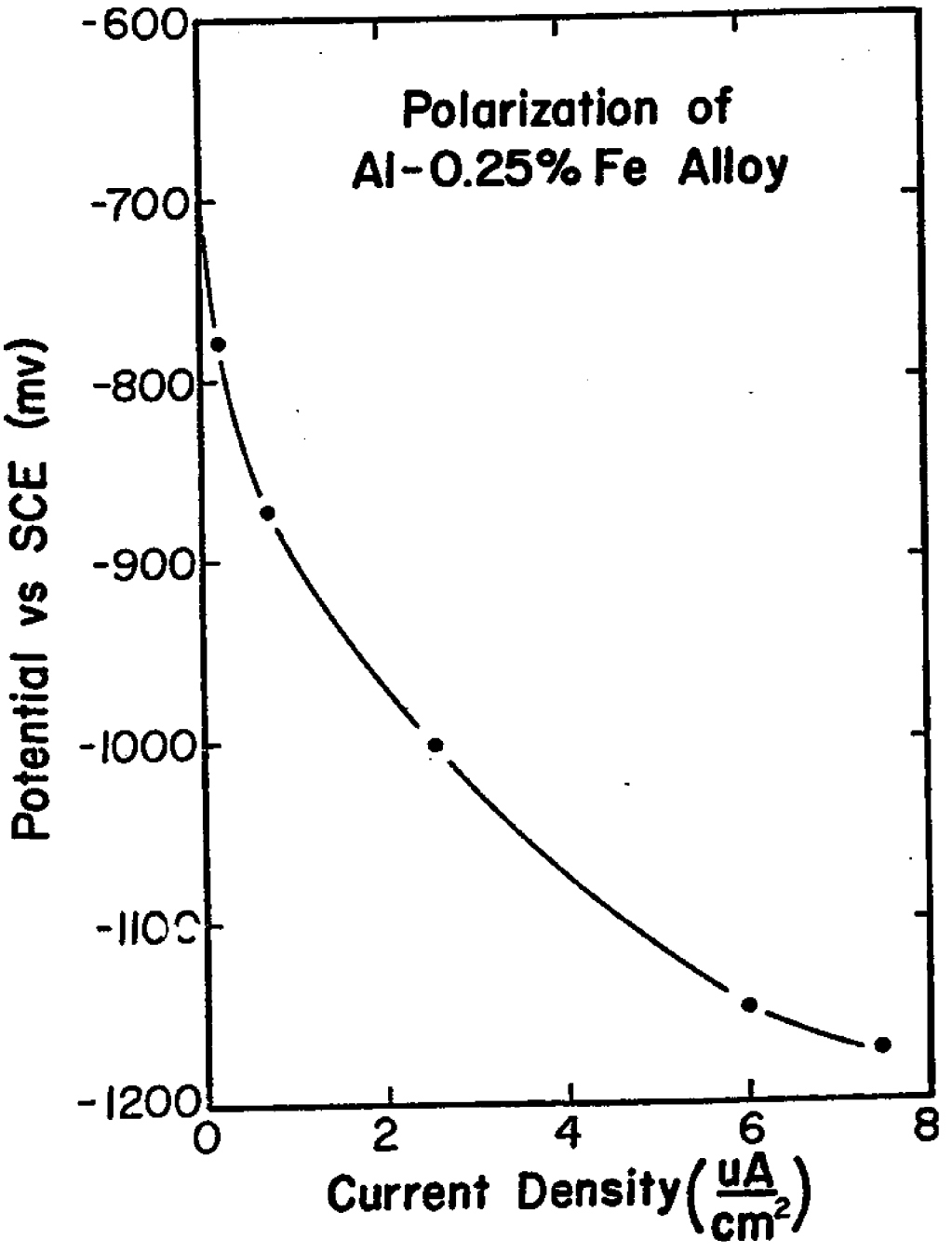

Figure II.1 Cathodic polarization of Al-0.25% Fe alloy (made from 99.99% Al) in 3% NaCl + HCO_3 solution at pH 7.2. Corrosion potential and slope are similar to those for commercial alloy 5052 in the same solution.

$MgCl_2$ is being added. This smaller jump is due to a slight pH change in the electrolyte, and this jump disappears as the pH reequilibrates at the controlled value, usually within two minutes. The magnesium effect is much larger and persists for a period of hours, rather than minutes. It was evident that the 0.25% Mg present in the alloy did not give the magnesium effect, as this effect could be produced subsequently by adding Mg to the water.

The polarization curve of the 0.25% Mg alloy after adding magnesium to the water (Figure II.2) was similar to that previously published for 99.99% Al under these conditions. Usually, the samples would come to a relatively steady corrosion potential in the test solution within one to two hours of immersion, and the cathodic polarization test would begin at that point. Occasionally, the corrosion potential would still be quite noble (-1175 to -1250 mV) after the first two hours. If cathodic polarization were begun under these conditions, the initial slope would be steep and the curves would look like those in Figure II.3. If such a sample was allowed to sit for 24 hours, the corrosion potential would gradually drift back to a value between -1300 and -1350 mV. It is not known why the potential sometimes took so long to equilibrate, but our experience was that the polarization curves looked like those in Figure II.3 whenever polarization was started while the potential was too noble.

The alloys in this final series having 0.5, 1.0 and 2.5 percent Mg also behaved like 99.99% aluminum. Corrosion potentials in air saturated 3% NaCl + HCO_3 were -1400 to -1420 mV at pH 8.2, and -1290 to -1340 mV at pH 7.2. Polarization curves at the two pH levels ran within the scatterband previously published for 99.99% Al.

Tests have not yet been completed to determine whether there is a change in corrosion potential upon adding magnesium chloride to the water, as there usually is with pure aluminum. In the few tests run to date, there has been the small, temporary pH jump mentioned above, but there has not been a magnesium effect. These tests are not conclusive, however, because occasionally pure aluminum does not show the effect either, even with the most careful specimen preparation.

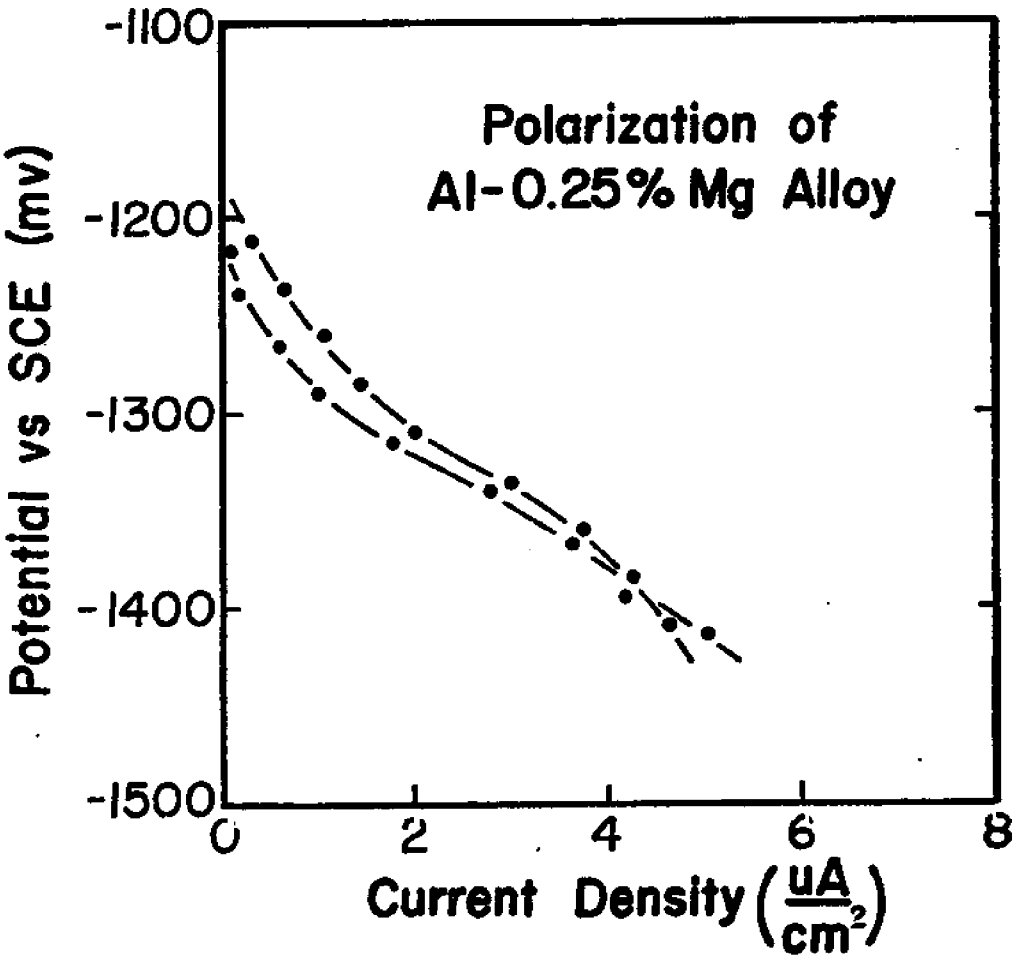

Figure II.2 Cathodic polarization of Al-0.25% Mg (made from 99.99% Al) in 3% NaCl + HCO_3^- + Mg^{++} at pH 7.2. These curves are similar to those for pure aluminum in the same solution.

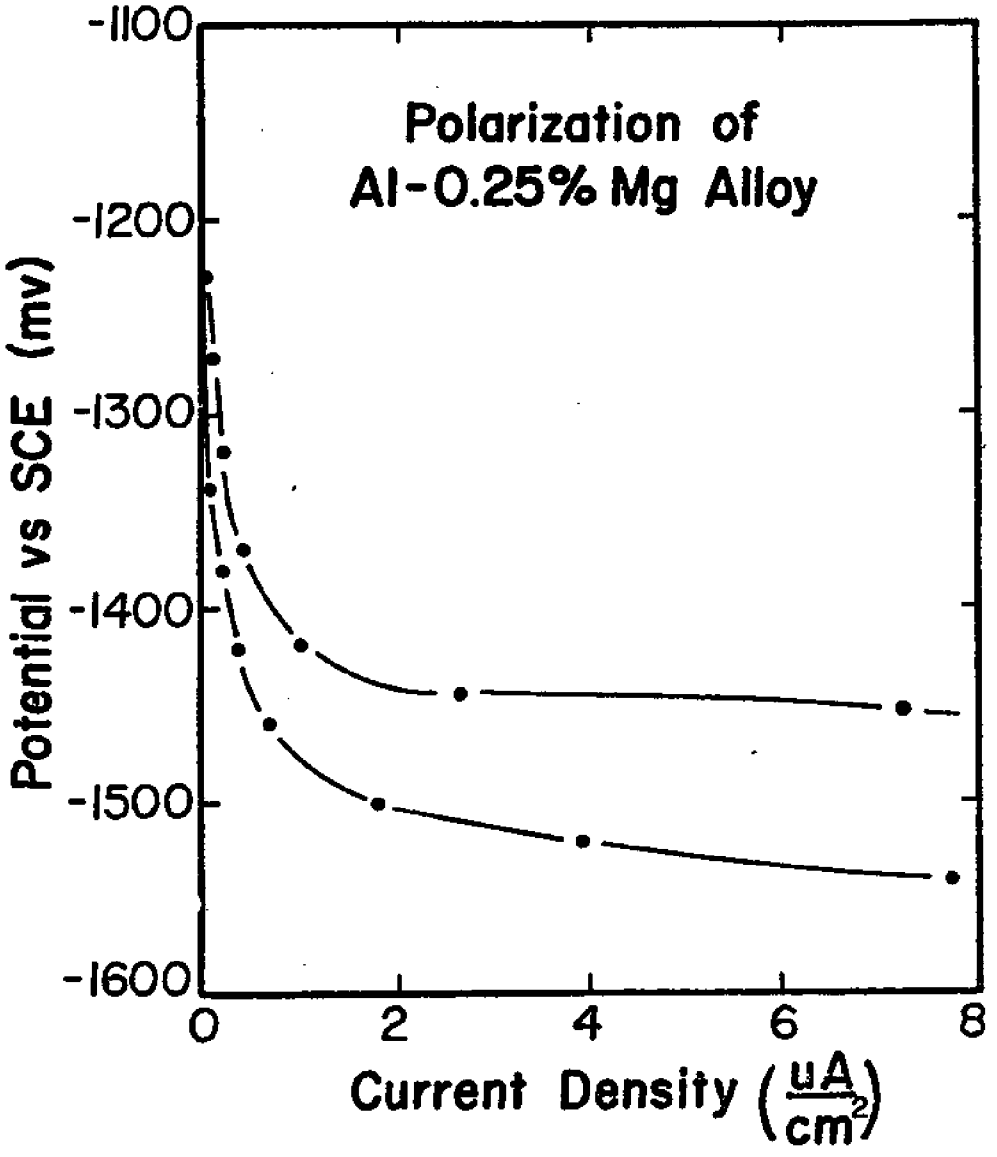

Figure II.3 Typical shape of cathodic polarization curves for 99.99% Al or the Al-0.25% Mg alloy in 3% NaCl + HCO_3 at pH 7.2 when polarization was started before reaching steady state conditions.

It does not appear that magnesium in the alloy plays the same role that it does in the water. The corrosion potential of the binary Al-Mg alloys comes to the same steady value, in about the same way and in about the same length of time as it does for pure aluminum. If magnesium in the alloy were capable of causing the same effect on the corrosion potential that it does when added to the water, then one would expect the corrosion potential of the binary alloys to stay about 100 mV more noble than it does for the first 10 to 12 hours, and then slowly decay to the stable value as was shown in Figure I.3.

It has not yet been proven that magnesium in the alloy has no effect on the cathodic behavior of aluminum in aerated 3% sodium chloride solutions. All data to date, however, are consistent with the idea that magnesium in the alloy has no effect. The mechanism that has been proposed to explain the effect of magnesium in the water requires free Mg^{++} to act as a catalyst for the reduction of percarbonic acid. In order to affect the corrosion potential of an aluminum electrode, this reaction must take place in the boundary layer of water adjacent to the solid/liquid interface. The fact that up to 2.5% magnesium in the alloy seems to have no effect on the corrosion potential, may indicate that passive wastage of the aluminum surface in the first few minutes of immersion does not put more than the 50 ppm of Mg^{++} needed (see Figure I.1) into the boundary layer of water. This is probably reasonable because there is only 2.5% or less of Mg in the alloy. If one assumes that passive wastage of the alloy surface proceeds at a rate of one mil per year, then about $2.2\ 10^{-10}$ gm of magnesium are going into the boundary layer of water per minute of immersion for the 2.5% Mg alloy, and proportionally less for the other alloys. If the boundary layer is one micrometer thick, then for one cm^2 of surface, the above amount of Mg is going into 10^{-4} cm^3 (or gm) of water each minute. That is, Mg is being pumped into the water at a rate of slightly greater than 2 ppm per minute. At this rate it would take about 25 minutes to reach the 50 ppm threshold, and 1.75 Hr to reach the 200 ppm needed for the full effect. This is probably an optimistically short estimate. The passive wastage rate is probably closer to 0.1 mil per year, and much of the magnesium corroded is probably trapped in the corrosion product film. Thus, it

may well take on the order of 10 hours or more for enough magnesium to enter the water from the alloy to give the effect. Moreover, this ten hours is about the same length of time in which the magnesium effect produced by $MgCl_2$ additions to the water begins to decay. Therefore, based on the work done to date, it is suspected that magnesium in the alloy, at least up to the 2.5% level of commercial alloy 5052, will not have any practical effect on the cathodic reaction.

It is clear that magnesium plays a role in the cathodic reactions on aluminum in seawater but it would probably be a mistake to assign too much practical significance to that role. The effect appears to be important only while the passive film is becoming established. Since the effect tends to make the corrosion potential more noble, and since it is maximized at low pH (7.2 to 7.5), it may have some practical impact on initiation of pitting during the first day or so of exposure of an aluminum structure in the deep ocean. It is less likely to have an effect in surface waters where the pH is greater than 8, and it certainly does not play nearly as significant a role as that of the chloride ion.

III. THE ROLE OF WATER FLOW VELOCITY

A. Introduction

Dexter has recently speculated that velocity effects might cause "super" corrosion rates by accelerating relatively sluggish reaction kinetics at the low temperatures found in deep ocean water [1]. This possibility stimulated the work reported in this section on the effect of velocity of seawater flow from 0-1 m/sec on the corrosion of 5000 series Aluminum-Magnesium alloys.

The effects of electrolyte flow on aluminum corrosion have been previously examined at high velocities (3 to 30 m/sec), especially with respect to erosion-corrosion [2-7]. Little work has been done, however, at velocities below 3 m/sec. This is particularly important to OTEC applications where expected heat exchanger tubing velocities are less than 2 m/sec [8, 9]. These lower velocities are also characteristic of tidal or oceanic currents where 1 m/sec (4 km/hr) is near the upper limit of observed flow rates [10]. Therefore, the effects of the velocity range considered in this work could be applied to conditions at

fixed structures in the ocean. This study focuses on the cathodic reactions on non-pitting electrodes and how these reactions are influenced by low velocity seawater flow.

A brief summary of previous methods used to examine velocity effects will be presented. This discussion will be limited to low velocity methods, as high velocity corrosion test methods have been discussed extensively by the National Association of Corrosion Engineers Task Group T-7C-5 [4]. Velocity measurement systems may be categorized as rotating cylinders, rotating discs, ring discs, mechanically driven electrodes and flow-through systems.

Rotating cylindrical electrodes have been used to study the corrosion of iron in chloride solutions by DeCastro and Wilde [11] and in high purity water by Foroulis [12]. Sato et al., found that high speed rotation stablized the rate of individual pit growth in stainless steel exposed to chloride solutions [13]. Silverman used rotating cylindrical electrodes to simulate flow rates equivalent to 5 m/sec through tubing [14]. But, no work was reported using either aluminum or seawater.

Mansfeld and Kenkel used rotating cylindrical electrodes to test galvanic couples and single metals [15, 16]. Both anodic and cathodic polarization measurements were made. For Type 304 stainless steel in 3.5% NaCl, substantial shifts of polarization curves were reported, but no changes in pitting or protection potentials. Both cathodic and anodic currents were decreased as rotation rates increased. 6061 aluminum tested in ASTM substitute ocean water produced polarization curves that indicated higher cathodic and anodic currents as rotation increased, while the pitting potential remained constant. Corrosion rates were found to be proportional to the square root of velocity up to 95 cm/sec.

Prentice and Craig used copper disc electrodes as oxygen and/or corrosion probes in natural seawater [17]. They observed that the corrosion potentials became more active as rotation rates increased. De Sanchez and Schiffrin reported on copper alloy disc electrodes used in sulphide-contaminated seawater [18]. They found that anodic polarization curves were shifted in the active direction by increased rotation, but Tafel slopes and cathodic polarization curves were not affected.

Do Duc and Tissot used combination disc and ring disc electrodes [19] to study tin in phosphate solution and copper in KCl solution. Franze and Novak have used 99.99% aluminum disc electrodes in 0.1N NaCl [20]. Rotational speed varied from 410 to 2000 rpm. They found the pitting potential shifted positive (noble) and that pitting current decreased with increased rotation.

A hydrofoil shaped specimen holder driven in a circle around a one meter diameter tank was used by Perkins et al. to test Cu-Ni alloy and K-monel galvanically coupled to low carbon steel in synthetic seawater [21]. They found galvanic currents increased by a factor of 4-8 over static conditions at velocities of 3.0 m/sec, but found little difference between galvanic currents at 1.5 and 3.0 m/sec. Davis and Gehring tested aluminum alloys 5086-H117 and 5456-H117 with a high speed water wheel in natural seawater [6]. Linear polarizations as well as weight loss data were used. Aluminum corrosion was found to increase with velocity from 0 to 90 knots, but ten knots was the lowest non-zero flow rate tested. Similar increases in corrosion with velocity were found for other non-aluminum alloys.

Flow-through electrodes have been used by several researchers and can be divided into two classifications: open channels and closed systems. Ailor has reported extensive work on corrosion potentials of 38 Al alloys in troughs of flowing natural seawater [22]. The flow rate was predominantly 2.83 m/sec using coastal seawater with pH ranging from 7.8 - 8.1 [23]. Corrosion potentials varied from -800 to -1150 mV (SCE) for 5000 series alloys. 5052-H34 alloy produced E_{corr} values from -1000 to -1100 mV (SCE).

Ailor demonstrated that copper concentrations in the alloy greater than 0.3% caused corrosion potentials of approximately -700 mV (SCE). In the absence of high copper content in the alloys, zinc caused corrosion potentials more active than -1000 mV (SCE). 5052 was found to be very corrosion resistant, showing no apparent pits and a 5 mpy corrosion rate when exposed to 2.38 m/sec seawater flow. The results of increasing the flow from 2.38 to 3.97 m/sec were mixed. They can be summarized as:

Alloy	ΔE_{corr} for increased flow
5083-0	40 mV noble
5086-0	<10 mV active
5054-0	<10 mV active
6061-T6	120 mV active

Ailor also reported that 1000, 4000, 5000, and 6000 series alloys had corrosion potential variations of up to 100 mV/day over the 45 days tested. The corrosion potentials of the 7000 and 2000 series alloys tested were more stable, generally having E_{corr} values of -700 mV (SCE). It is apparent from Ailor's data that the corrosion potentials of many of the alloys varied concurrently. The variations seem to be systematic, with many electrodes following the same active and noble trends. In light of Dexter's work on the effects of variations of pH, temperature, and dissolved oxygen [24-26] it seems likely that variations in seawater chemistry caused these corrosion potential variations.

Lennox et al. exposed sixteen nickel alloys to both quiescent and 23 cm/sec flow conditions using coastal seawater either at a pier or flowing through an open trough system [27]. They found that the effect of increased flow was to shift corrosion potentials noble from those measured during quiescent conditions, although the most noble potentials were measured on the pier mounted specimens.

Beck and Chan mounted high purity iron and Type 304 stainless steel electrodes in the walls of flow channels carrying NaCl solutions [28]. They found a threshold velocity existed below which flow was not important and a critical velocity existed above which current density was limited by ohmic drop in the solution. These velocities varied with pit diameter, but were of the order of 4 cm/sec for threshold velocity and 1.5 m/sec for critical limiting velocity. Efird used seawater in a flow-through system to test the effect of velocity on corrosion of flat copper alloy specimens centered in rectangular channels [29]. A critical velocity ranging from 1.3 m/sec to 12.0 m/sec (depending on the alloy tested) was found for each alloy where removal of corrosion product by shear stress increased the corrosion rate.

K. S. Rajagoplan et al. reported on the effects of flow on two aluminum alloys, 6061-T6 and Indal 3S (1.2% Mn alloy) used for heat exchanger tubings [30]. Samples were tested under static, flow and galvanic coupling conditions with deionized and natural waters. For 6061, the corrosion rate was seen to increase by a factor of 5.5 as flow was increased from 30 to 150 cm/sec with hard water (high chloride and carbonate concentrations). Corrosion measurements were by weight loss, and electrochemical measurements were not made. Severe pitting of 6061-T6 was observed.

Gehring tested 5456-H117 alloy in seawater using a 3 to 30 m/sec closed system [5, 7]. Using both weight loss and polarization resistance measurements, he found an increase in corrosion rate from 0.4 to 6.0 mdd as flow increased. Increases of flow rate from 3 to 30 m/sec caused the E_{corr} to shift from -780 to -820 mV (SCE) in direct proportion to the change in velocity.

Gehring's earlier work included tests of 1100-H14 alloy [7]. He found the corrosion rates of both 5456 and 1100 alloys were velocity dependent, increasing linearly with increased flow. Unlike the 5456 alloy, the 1100 alloy showed almost no shift in corrosion potential from 700 mV (SCE). Cathodic polarizations of both alloys plotted logarithmically showed no systematic velocity effects.

Ryncwicz and Nagrodsky tested Alclad 3003, Alclad 3004, 3004 and 5052 tubing in natural seawater using a non-recirculating system and a flow rate of 1.8 m/sec [8]. They visually inspected the tubing at three month intervals and measured all pits. They found the Alclad samples superior, as the unclad alloys suffered pitting. No electrochemical measurements were conducted, nor were comparisons of flow rates.

As part of the OTEC feasibility studies, Munier and Craig reported on a flow-through system that was barge mounted and used to test aluminum tubing in surface seawater near St. Croix, U.S., Virgin Islands [31]. They exposed one inch I.D. sections of 6061-T6 and 5052-0 tubing to seawater flowing at either 0.9 or 1.8 m/sec for 72 days (6061) or 14 days (5052). They found that corrosion potentials for the alloys reached active peaks of -1145 mV (6061) and -1325 mV (5052) (Data converted to SCE) in 2 days and gradually stabilized in 10 days to -950 mv (6061) and -1050 mV (5052). They were unable to accurately determine

weight loss due to the size of their specimens (2.6 feet long). Using a scanning electron microscope (SEM) and Energy Dispersive Analysis by X-ray (EDAX), they were able to analyze the corrosion products and determine that S, Fe, and Ca showed greater concentrations in the corrosion product than in the alloy. They observed no pitting of 5052 and attributed pitting of 6061 in one experiment to an artifact of the experimental set up. They noted a 2 to 8 mV active shift of corrosion potential as flow rates increased from 1.8 to 2.5 m/sec or 0.9 to 1.2 m/sec as tubes were being changed for inspection. This research is noteworthy as one of the few that thoroughly reported seawater conditions at the test site. These may be summarized as:

Temperature	28.0 $\pm$ 0.5° C
Salinity	35.5 $\pm$ 1.0 $^{o}/_{oo}$
pH	8.15 $\pm$ 0.05
Dissolved Oxygen	4.5 $\pm$ 0.2 ml/l

The literature on the non-aluminum alloys indicates that various flow effects exist. For some alloys, corrosion potential shifted noble; for others, it shifted active. In most cases, flow increased corrosion or corrosion currents. In a few, it had no effect or reduced corrosion or corrosion currents. In some cases, both anodic and cathodic polarizations were shifted. For other alloys, only one polarization seemed affected by flow rate changes. It can be concluded that some interesting and potentially important electrochemical effects seem to be caused by changes in relatively low flow rates of the electrolyte.

For aluminum alloys, the literature appears to agree only that increased flow rate increases the corrosion rate. It was the intent of this research to determine the effects of low velocity flow on the corrosion potentials and cathodic polarization curves of aluminum alloy 5052, and to predict their effects on the corrosion rate of this alloy in seawater.

Flow of electrolyte past the specimen surface was achieved either by varying the rate of stirring in the cylindrical polarization flask by means of a magnetic stirrer, or by varying the flow rate in a specially

constructed flow through system using the tubular electrodes. Quantitative control of flow speed and flow character (i.e., laminar or turbulent) were possible only in the flow through system. The electrodes for the flow through system, however, were time consuming to prepare, so the amount of data that could be taken with the flow through system was limited. For this reason, supplementary data were obtained by varying the stirring rate in the polarization flask from zero (quiescent conditions) to 1200 rpm.

B. Experimental Techniques

The flow through system is shown schematically in Figure III.1 and the test section is shown in detail in Figure III.2. The main features of the system include a 12 liter polypropylene holding tank with PVC bulkhead fittings in which the dissolved oxygen, temperature and pH of the circulating electrolyte are controlled; a March Model AC-3C-MD magnetic drive pump having nonmetallic rotor, chamber and seals; PVC ball and metering valves; and Tygon grade R-3603 tubing. The metering valve was capable of controlling the flow rate to within $\pm$ 5% over the range 0.5 to 35 cm/sec. To obtain the maximum flow rate of 71 cm/sec, the metering valve was removed and replaced with a short section of PVC tubing.

In order to minimize their influence on the hydrodynamics of flow, the pump and metering valve were placed downstream of the electrochemical test section. A 70 cm length of Tygon tubing preceded the test section to allow the flow characteristics to become fully established. The speed of flow was measured volumetrically by disconnecting the Tygon tubing from the inlet reservoir bulkhead fitting and allowing the water to discharge through an identical fitting at the same pressure head as provided by the reservoir. The flow character was determined both by theoretical calculations and flow visualization experiments in the test section. The critical Reynolds number for the laminar to turbulent transition is 2000-4000 for tubing [32]. For the flow through electrode this corresponds to 7-14 cm/sec. Mean flow rates were from 0.5 to 70 cm/sec and should therefore include laminar, transition, and turbulent flow. This was confirmed by pitot tube measurements and observations of suspended threads with a glass tube replacing the aluminum electrode in the test section.

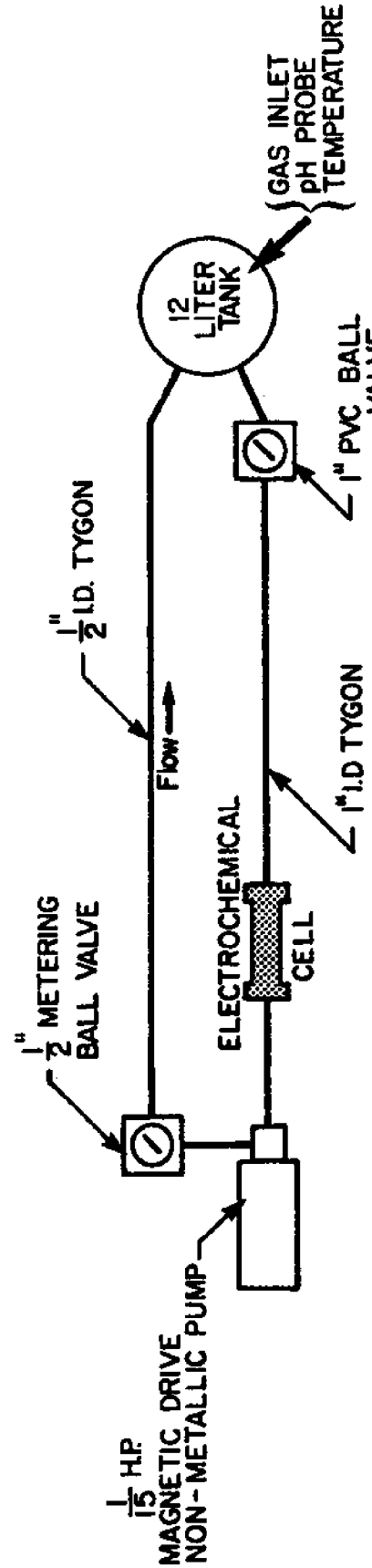

Fig. III.1 Schematic diagram of recirculating flow through system for flow speed measurements.

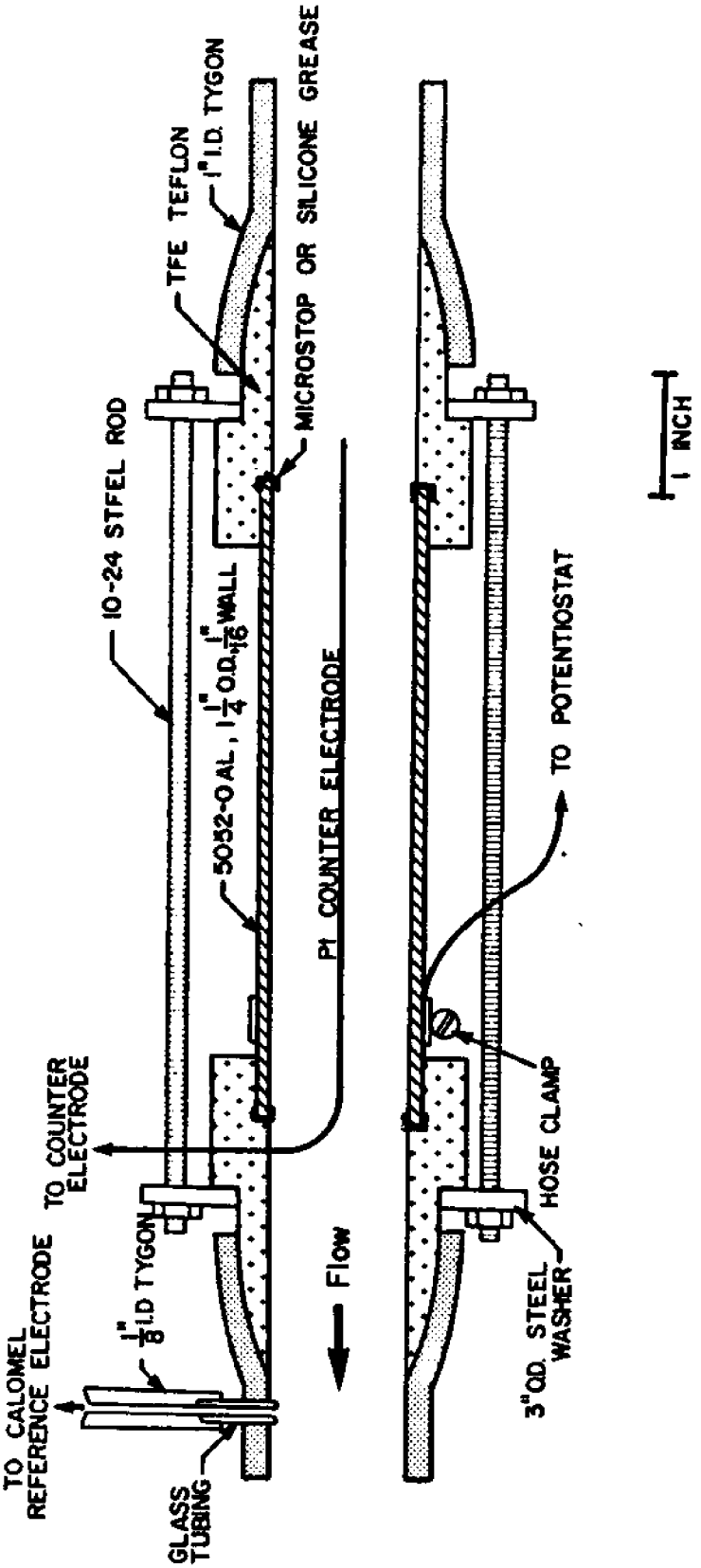

Fig. III.2 The electrochemical test section in the flow through system.

The test section (see Figure III.2) consisted of a tubular electrode held at each end in machined Teflon holders with an external threaded compression fitting as shown. The joints between the Tygon tubing, Teflon holders and aluminum tube specimen were made as smooth as possible to minimize the introduction of flow discontinuities in the test section. To minimize crevice corrosion where the tube joined the Teflon holder, the tube ends were coated after the pickling step with Microstop, an insulating lacquer manufactured by Michigan Chrome and Chemical Company.

The counter electrode in the test section consisted of a length of 18 gage platinum wire inserted through the downstream Teflon holder as shown. Flow visualization experiments done by replacing the aluminum tube section with glass revealed that this wire introduced very little flow disturbance and was stiff enough to resist vibrational strumming at all test flow speeds. The salt bridge connection to the reference electrode chamber was also placed downstream to avoid disturbing the flow. It was found that conductivity of all our electrolytes was high enough that IR drop was insignificant.

Preliminary results on seawater flow effects were obtained using cylindrical electrodes 2 to 4 cm long and nominally 1 cm in diameter. These electrodes were tested in standard six- or seven-necked polarization flasks. Seawater flow was produced by stirring with a magnetic stirrer. Cylindrical electrodes were machined from 5052 aluminum alloy rod supplied by Reynolds Metals Company. A few experiments were conducted with 99.99% aluminum electrodes similar in size to the 5052 electrodes. These 99.99% Al electrodes were machined from 1.3 cm rod supplied by Materials Research Corporation. Analyses of the electrodes are given in Table III.1.

The flow-through electrodes were machined from commercial grade 5052-O Alcoa drawn tubing purchased from Tube Sales, Inc. The outside diameter of the tubing was 1.250 inch (3.20 cm) and the wall thickness 0.065 inch (0.165 cm) as received from the supplier. The inside diameter was $2.850 \pm .010$ cm. These dimensions are typical of those proposed for OTEC tubing [8]. An analysis of a sample of the tubing showed that it was very similar in composition to the cylindrical electrodes, and well within accepted alloy limits for 5052 alloy (Table III.2).

Table III.1

Electrode Analyses

Element	99.99* (ppm)	5052 Cylindrical Electrodes** (%)	5052 Tubular Electrodes*** (%)	5052 Limits Ref. 20 (%)
Si	3.50	0.07	0.08	0.45 < 0.25
Fe	1.20	0.10	0.19	Total < 0.40
Cu	0.05	0.03	0.01	0.10
Mn	N.T.	0.01	0.02	0.10
Mg	1.00	2.43	2.44	2.2-2.8
Cr	0.25	0.19	0.20	0.15-0.35
Ni	<0.30	0.00	0.02	0.05
Zn	<0.18	0.04	0.01	0.10
Ti	0.40	0.01	0.01	0.05
Zr	0.95	N.T.	N.T.	N.T.

*Materials and analysis by Materials Research Corporation

**Analysis by Reynolds Metals Company

***Analysis by ALCOA Technical Center, Alcoa Center, PA

N.T. = Not Tested

A series of marks or irregularities was noted on the inside of all the tubing parallel to the longitudinal axis. A sample was sent to the Alcoa Technical Center in Alcoa Center, Pennsylvania, for inspection and comments. The Alcoa representative described the irregularities as an extrusion flaw only a few mils deep [33]. When the flow-through electrodes were tested in seawater, it was found that pitting often initiated along this flaw. If sufficient sanding was done to eliminate traces of the flaw when inspected at 25x, no pits would initiate at its previous location.

Flow-through electrodes from 13 to 16 cm long were cut from the tubing. Electrodes were prepared by abrading the inner surface with 240, 320, 400, and 600 grit silicon carbide grinding paper. Removal of the extrusion flaws required heavy abrasion using approximately two sheets of 240 grit paper per electrode. Electrodes were then pickled in modified graduate cylinders under conditions identical to those used with the cylindrical electrodes. A special inspection tool was constructed to facilitate internal inspection of the tubular electrodes with a binocular microscope. A small front-silvered mirror was mounted on an aluminum support which could be raised and lowered by a rack and pinion gear. A small electric light bulb was mounted at the top of the mirror to illuminate the specimen surface. Rotating the tube being inspected and raising or lowering the mirror allowed all parts of the electrodes to be thoroughly inspected at 25 to 50x. Use of a reticle in one eyepiece of the microscope allowed detection of pits as small as 0.01 mm diameter through this technique.

Additional information on the polarization techniques and control of various water quality parameters can be found in Section I.B.1. of this Volume, and a thorough discussion of the flow through system set-up, calibration and specimen surface preparation has been given previously by Rigby [34].

C. Results

An increase in the speed of water flowing past the electrode surface always shifted the corrosion potential in the active direction. Figure III.3 shows the change in corrosion potential for aluminum alloy 5052 upon increasing the rotational speed of a stirring bar in the

bottom of a conventional spherical polarization flask from zero to 1200 rpm as a function of pH. The estimated average flow speed past the surface of a 1 cm diameter cylindrical electrode under such conditions was 10 $\pm$ 5 cm/sec. The flow was turbulent and highly erratic due to vortex shedding from the gas bubbler, pH electrode and counter electrodes protruding into the flow. Thus, it is not surprising that there is considerable scatter in the data in Figure III.3. Despite the scatter, the general trend of a decrease in $\Delta\phi_{cor}$ with decreasing pH is clear.

Increasing the flow speed gives an active shift in corrosion potential of alloy 5052 as shown in Figure III.4 for a pH of 7.5. This data shows considerably less scatter because it was done with the flow through system in which the hydrodynamics are controllable. The corrosion potential changed linearly with the logarithm of the flow speed over the range from 1 to 70 cm/sec. The shift was 80 mV in the active direction for each tenfold increase in flow speed within that range at pH 7.5.

Data from the flow through system on both corrosion potential and cathodic polarization are summarized for alloy 5052 at pH 8.2 in Figure III.5 and at pH 7.4 to 7.5 in Figure III.6. Each of the shaded bands in these figures represents the envelope of all the individual curves. The uppermost band in Figure III.5 is the quiescent seawater data for alloy 5052 from previously published work. At pH 8.2 in Figure III.5 each increase in flow speed produces a further active shift in the corrosion potential and decreases the slope of the initial part of the cathodic polarization curve. At current densities up to 5 $\mu A/cm^2$, however, the shift in corrosion potential is the larger of the two effects so that the net result of an increase in velocity is always an increase in polarization of the cathode.

At the lower pH in Figure III.6, the same two trends are in evidence. This time, however, the decrease in slope at the higher flow speeds more than compensates for the active shift in corrosion potential, with the net result being a depolarization of the cathode at current densities greater than 3 $\mu A/cm^2$.

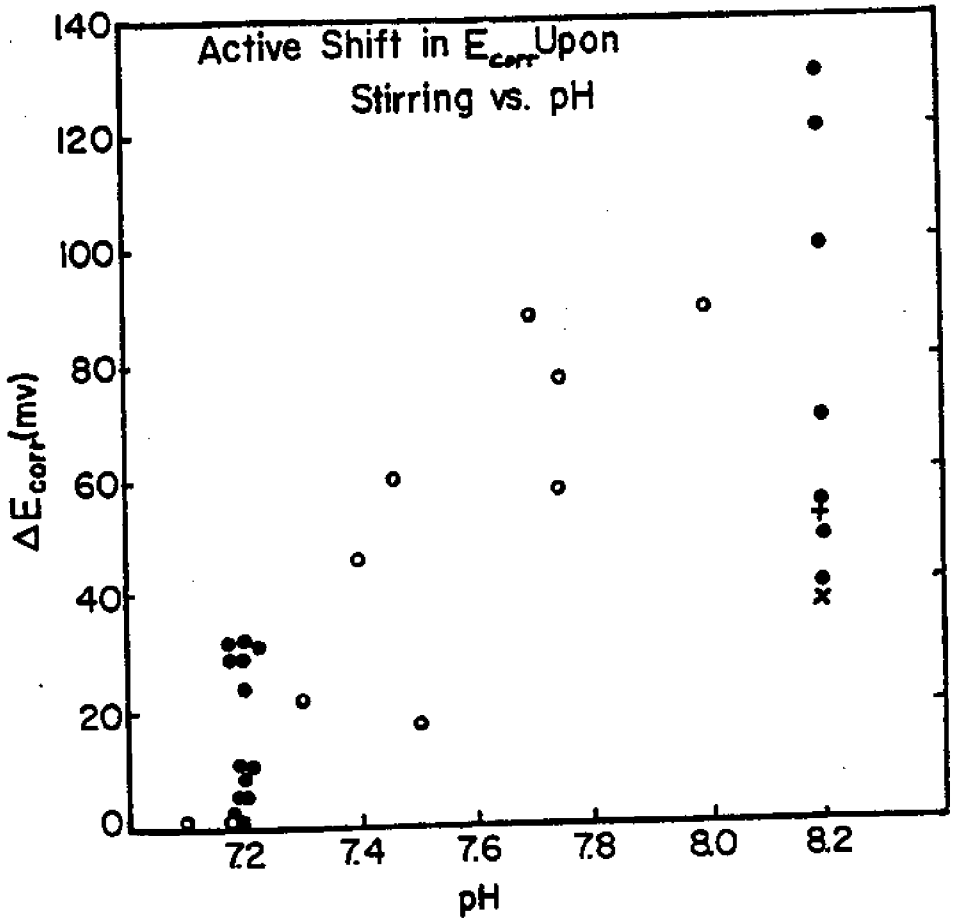

● 5052 in seawater; shift determined before cathodic polarization
○ 5052 in seawater; shift determined during △ pH experiment
× 99.99% Al in seawater
+ 99.99% Al in 3% NaCl + 140 ppm $NaHCO_3$

Figure III.3 Active shift in E_{corr} upon stirring in polarization flask.

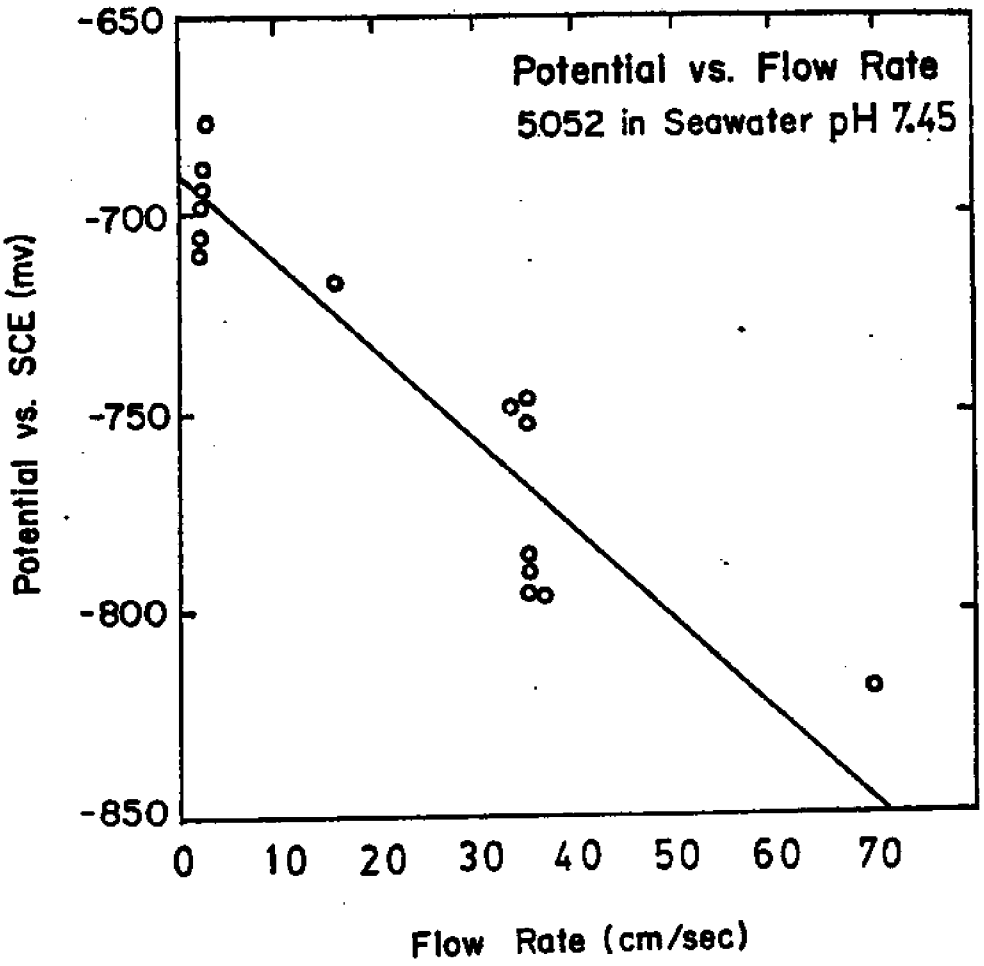

Figure III.4 Effect of flow rate on corrosion potentials for the flow-through electrodes at pH 7.45, air saturation, 23°C.

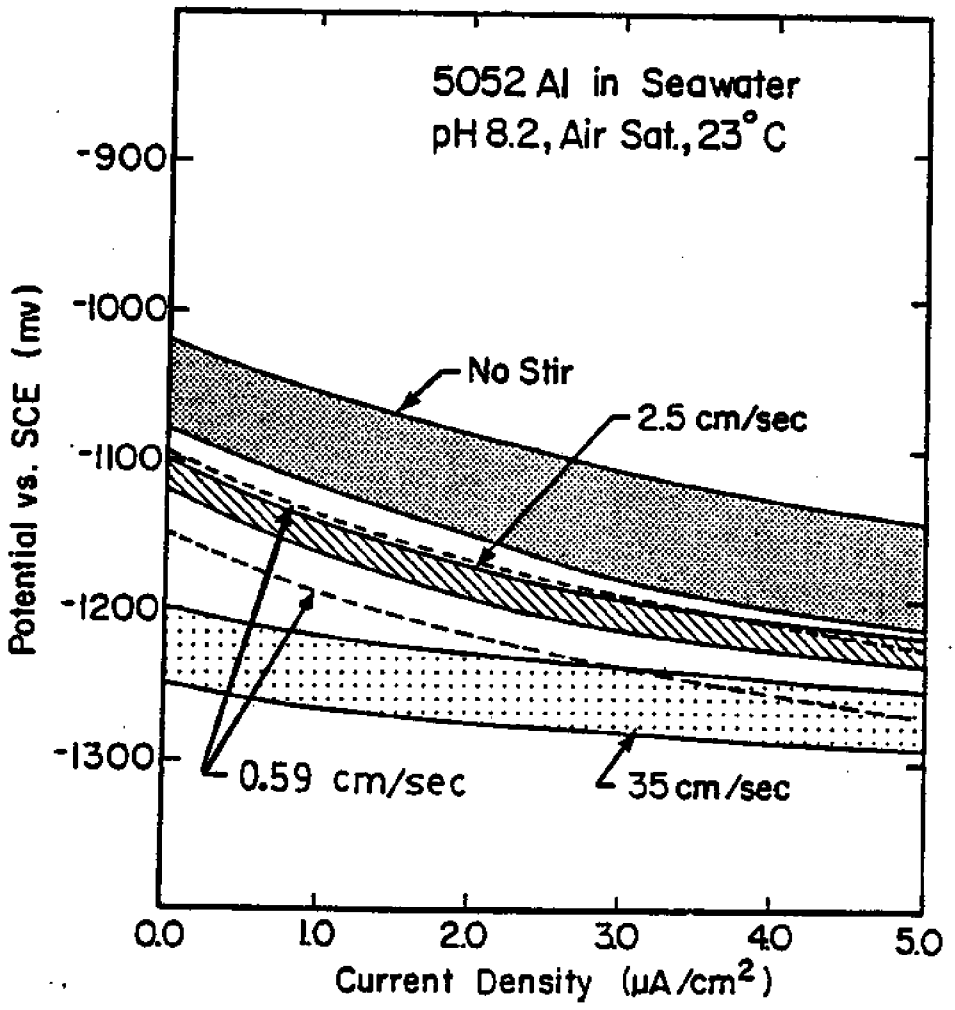

Figure III.5 Cathodic polarizations using the flow-through system at pH 8.2, air saturation, and 23°C. Shaded area, "No Stir", represents five trials using cylindrical electrodes in the polarization flask.

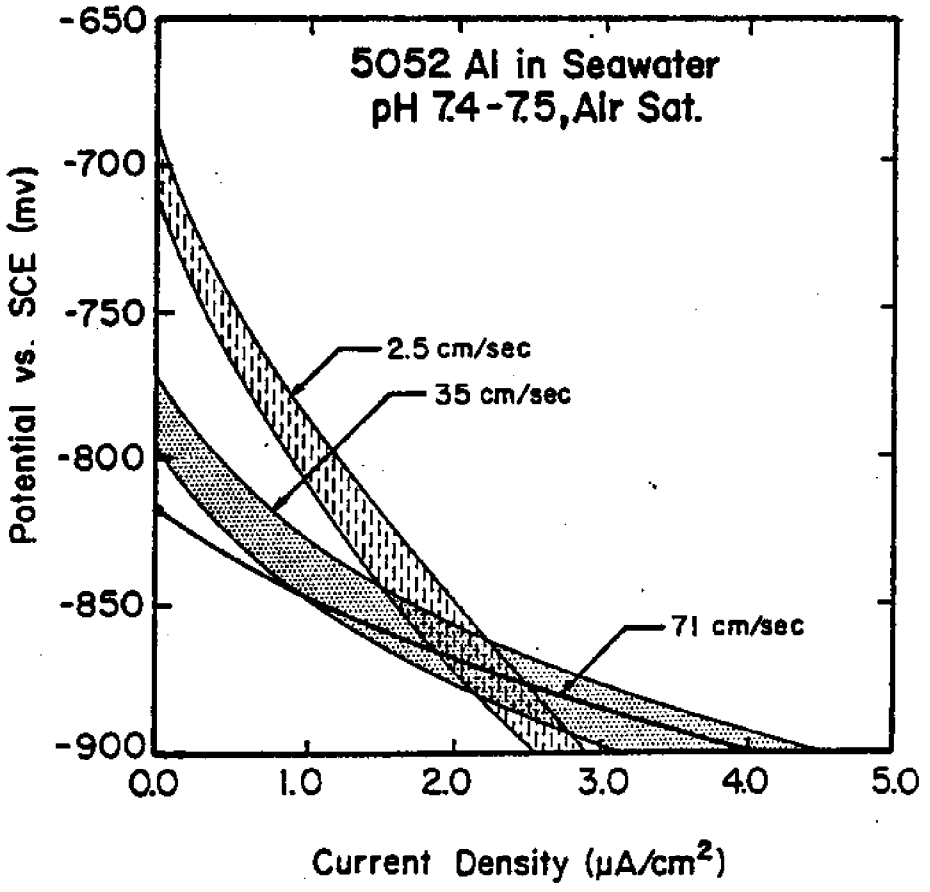

Figure III.6 Cathodic polarizations using the flow-through system at pH 7.45, air saturation and 23°C.

It had been suggested earlier [1, 24] that this decrease in slope of the cathodic curve with increasing velocity might create a super-corrosive condition in the deep ocean. The combination of low temperature and low pH of the deep ocean makes the corrosion potential of alloy 5052 very noble [24], which would encourage pit initiation. The dissolved oxygen, however, is also low, which tends to limit pit growth rates. But an increase in flow rate would increase the mass transport of oxygen to the metal surface, thus leading to rapid growth along with initiation. To investigate this possibility, the stirring rate in the polarization flask was varied while controlling the other variables at simulated deep ocean conditions as follows: pH 7.2, DO 1.3, and temperature 5°C. Under these conditions, the systematic effects of an increase in flow speed disappeared as shown in Figure III.7. It was not possible to be precise about the flow speeds in this figure because the experiments were done in the polarization flask.. Qualitatively the flow speed probably varied from about 0.1 cm/sec with no stirring to about 10 cm/sec at the maximum. Note that the individual curves in Figure 17 do not vary in any systematic way with flow speed but appear to be distributed randomly within a fairly narrow scatterband.

After considerable work had been done to determine the effect of stirring on cathodic polarizations, it became apparent that the shift of corrosion potential with stirring could not be understood without also measuring the effect of velocity of flow on the anodic polarization curve. Anodic polarizations were conducted at pH 8.2 so that the corrosion potential would be sufficiently active to the pitting or transpassive potential to allow the passive region to be examined.

Figure III.8 shows the results of the anodic polarizations. The stirring shifted the passive current density (ip) from 3.5 $\mu A/cm^2$ to 10.1 $\mu A/cm^2$. The current increase indicative of the transpassive region occurred 20 mV more noble when stirring, a change of doubtful significance as the currents became somewhat erratic at polarizations more noble than -750 m/V.

Polarization resistance (R_p) measurements were made immediately before anodic polarizations. The electrodes were polarized from 25 mV active of E_{corr} to 25 mV noble. Figure III.9 shows that stirring

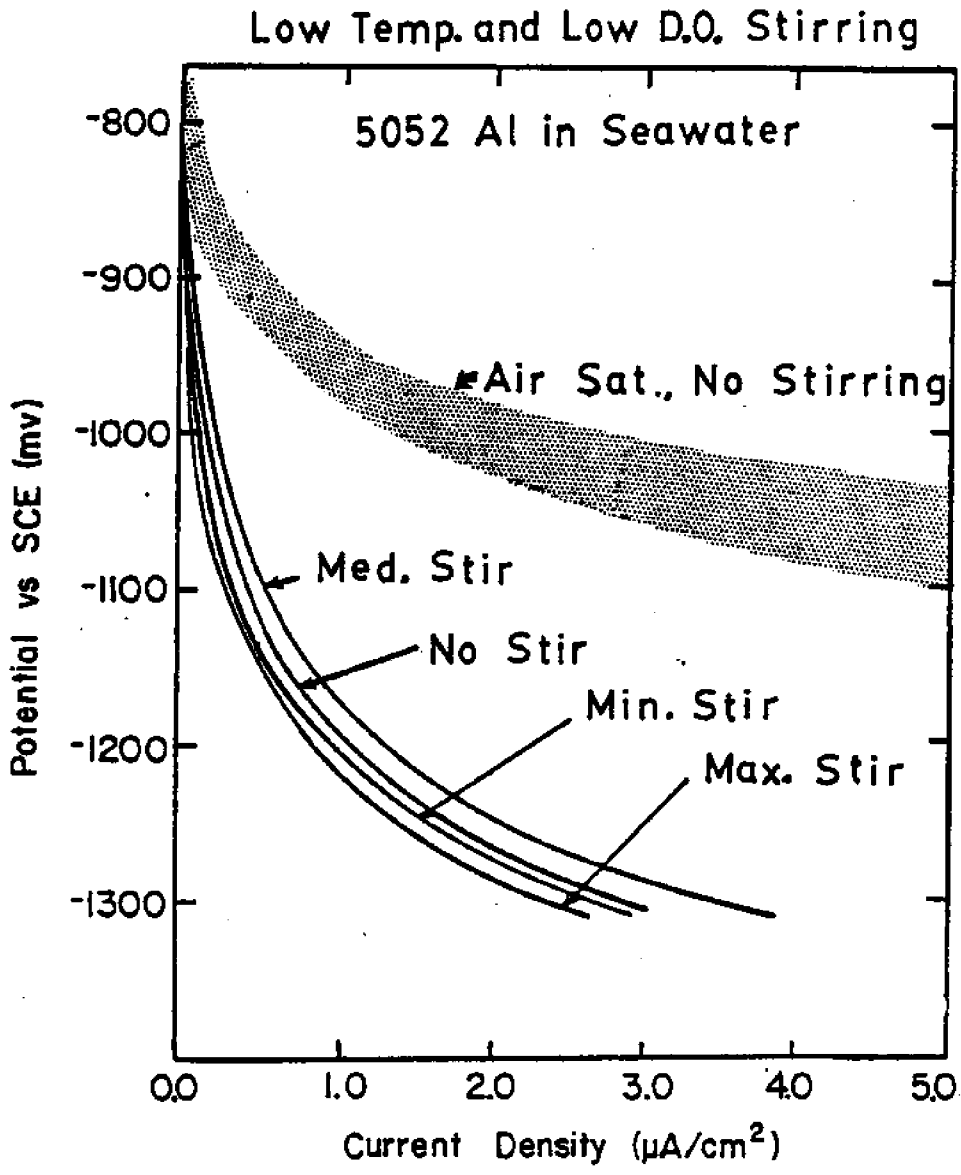

Figure III.7 Effects of stirring on cathodic polarization at pH 7.2, low dissolved oxygen (2.1 ppm), 5°C. Shaded area represents four no stirring trials at pH 7.2, air saturation, 22°C. Estimated (see text) flow rates: No Stir - 0 cm/sec, Min. Stir - 1 cm/sec, Med. Stir - 5 cm/sec, Max. Stir - 10 cm/sec.

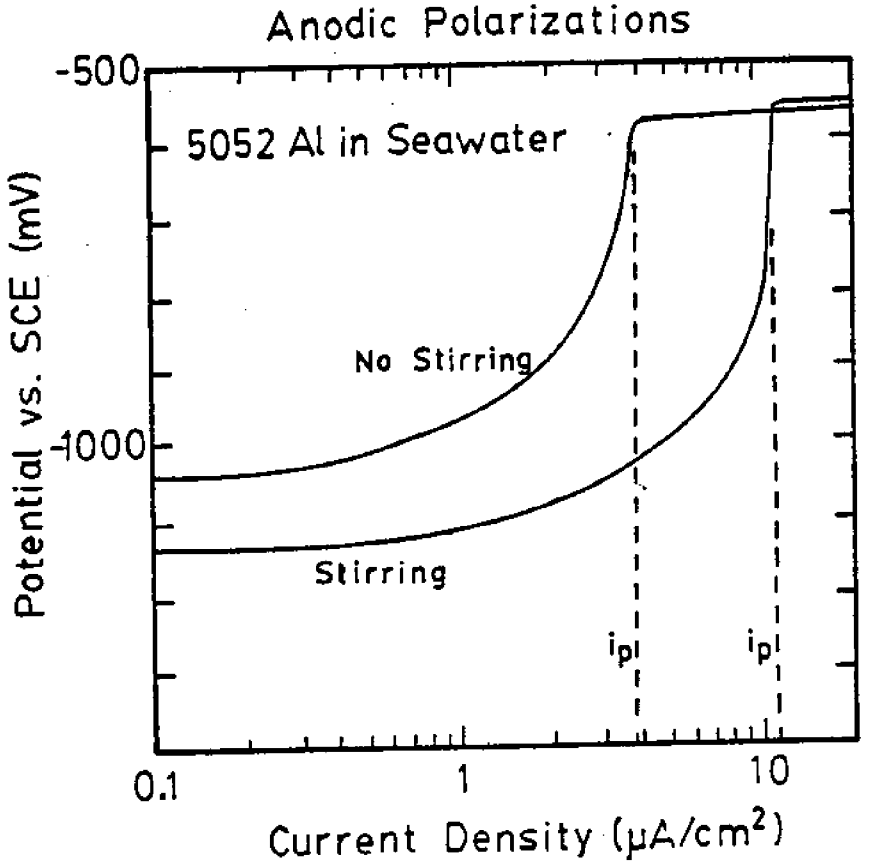

Figure III.8 Effects of stirring on anodic polarizations at pH 8.2 , air saturation, and 20°C. Maximum passive current density shown by i_p.

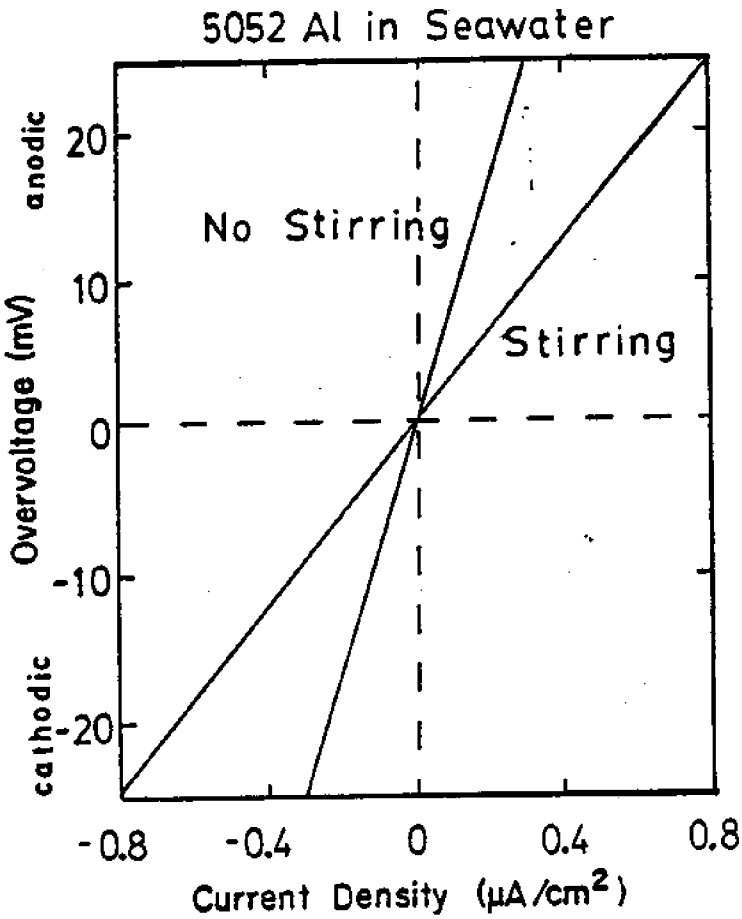

Figure III.9 Effect of stirring on linear polarizations of ±25 mV from E_{corr}. Polarization resistance measurements were calculated from these trials. Seawater pH 8.2, air saturated, 20°C.

decreased the polarization resistance. The slope of the no stirring line is 86 kohm-cm^2. The slope of the stirring line is 31 kohm-cm^2. The deviation from linear E vs. i behavior was estimated as <10%.

During several experiments, the cathodic polarizations were continued to current densities greater than 10 $\mu A/cm^2$. Figure III.10 shows the results of these polarizations plotted logarithmically to show four orders of magnitude of current density. From this plot, the deviation of the aluminum electrodes from linear or Tafel behavior can be observed [35, 36]. From 1.0 to approximately 30 $\mu A/cm^2$, the curves all show smoothly increasing slope. Tafel slopes calculated for this range of current densities produce values of -180 to -250 mV/decade.

After polarization to -1500 mV, the polarization slope is seen to decrease. After these high current density polarizations, the electrodes had large numbers of shallow pits uniformly distributed across the surface and whitish deposits on the surface. The appearance was quite unlike electrodes polarized to less active potentials.

Two groups of the cathodic polarization curves shown in Figure III.10 appear to show a linear or Tafel behavior. These have lower slopes and more active corrosion potentials than the other polarization curves. These "linear" polarizations have been replotted in Figure III.11. With the larger scale of this graph, it can be seen that these curves are not linear but have gradually increasing slopes. The more noble group of curves in Figure III.11 consists of: one 0.59 cm/sec run, four 2.5 cm/sec runs, and two stirring runs. The more active group of curves consists of: seven 35 cm/sec runs, two stirring runs and one 2.5 cm/sec run.

D. Discussion

Two major effects have been observed throughout this research on velocity effects: (1) the corrosion potential of 5052 Aluminum is shifted in the active direction by any increase in the rate of seawater flow across the aluminum surface for the entire range of velocities from 0-0.71 m/sec, and (2) the slopes of the cathodic polarization curves are reduced by any increase in flow rate. Although the magnitudes of these effects vary with pH, the effects were present in all trials (over

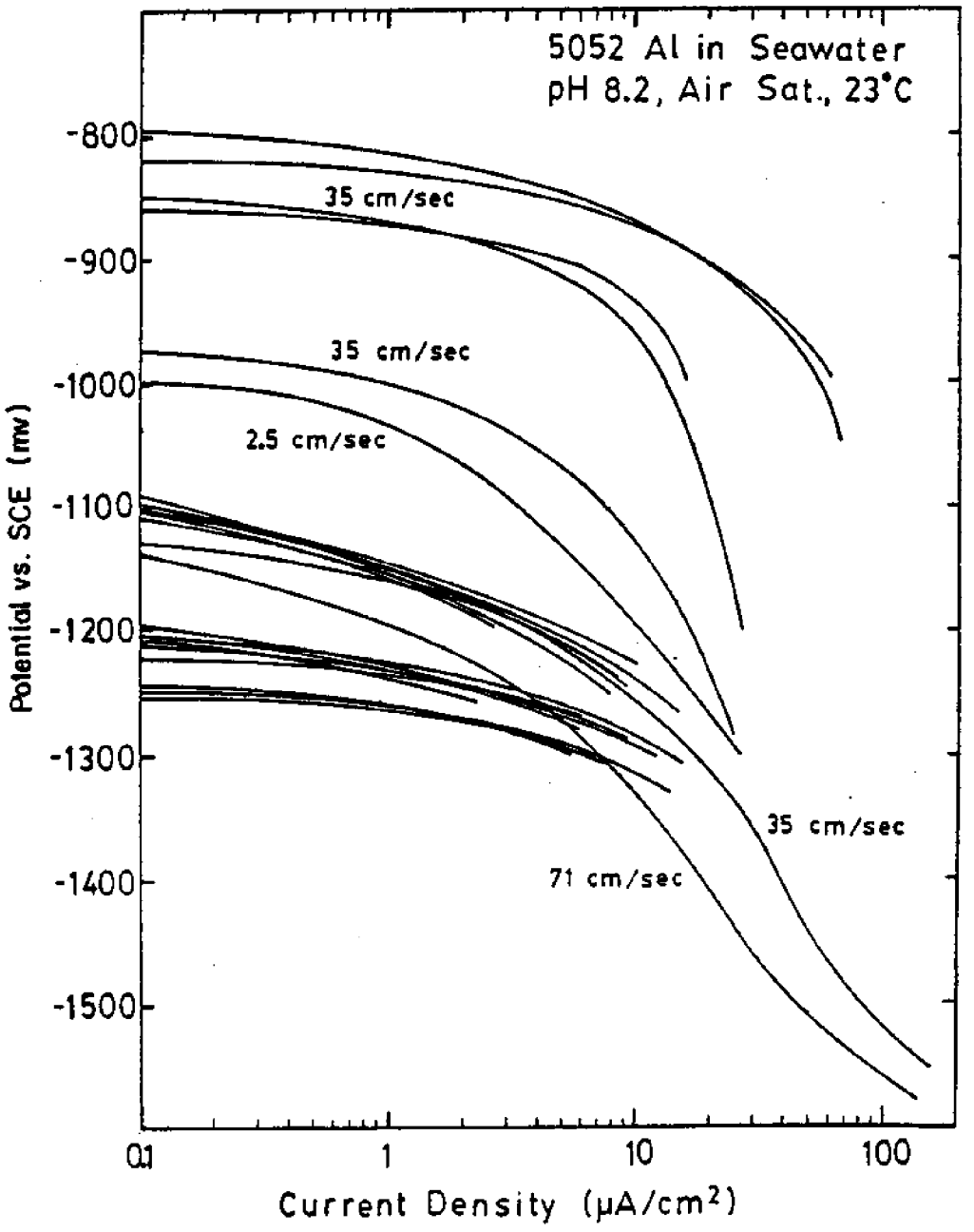

Figure III.10 Cathodic polarizations to high current densities at pH 8.2, air saturation and 23°C. (See also Figure 21)

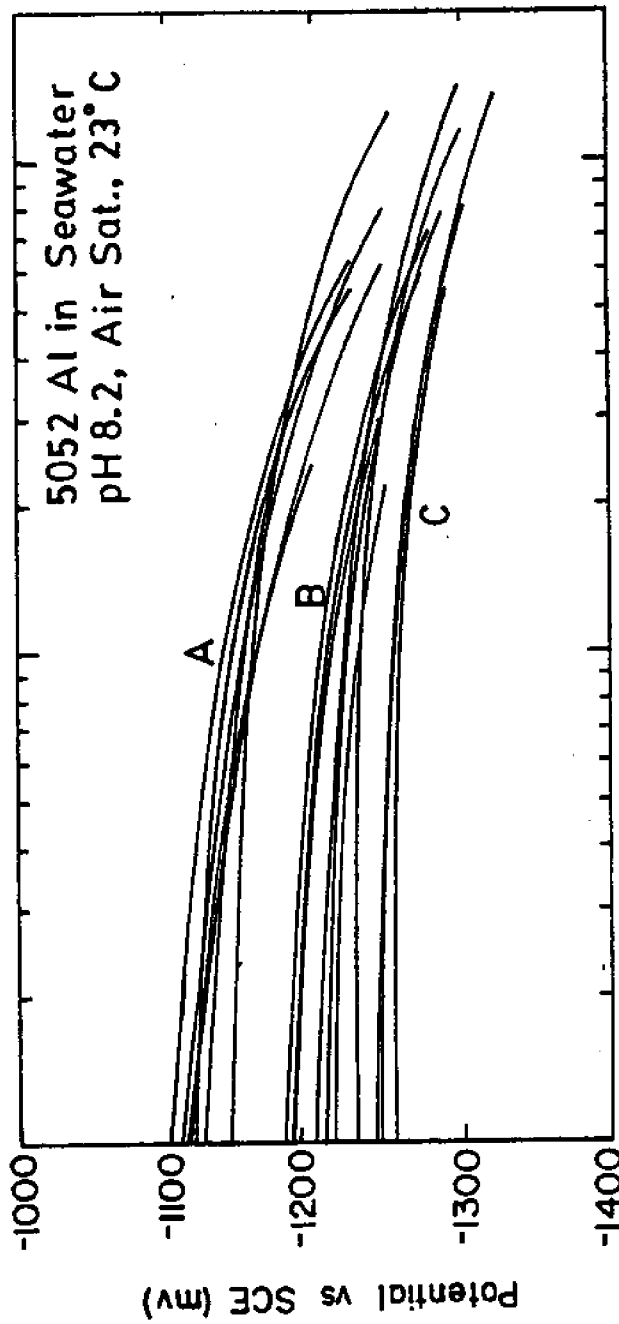

Figure III.11 Cathodic polarizations to high current densities as in Figure 20. Group A represents one 0.59 cm/sec run, two stirring runs and four 2.5 cm/sec runs. Group B represents one 2.5 cm/sec run, two stirring runs, and four 35 cm/sec runs. Group C represents three 35 cm/sec runs.

80) conducted at 20-23°C. The implications of these two effects for the corrosion of aluminum alloys and a discussion of possible causes of the effects will now be presented.

D.1. Implications of the Active Shift of Corrosion Potential

For pure aluminum in 3% NaCl solution, the critical pitting potential is -690 ± 10 mV (SCE) [35]. This potential has been confirmed by Dexter for 5052 alloy in seawater and found to be independent of pH, dissolved oxygen and temperature over the ranges normally present in the ocean [24].

If corrosion potential (E_{corr}) is noble to the critical pitting potential (E_{cpp}), pits will initiate. This phenomena has been previously observed for both aluminum and stainless steel [35, 36] and is confirmed in this work. All electrodes tested that were allowed to remain at a potential noble to -690 mV showed pitting. If E_{corr} is active to E_{cpp}, pits will initiate at a reduced rate [24, 38]. Uhlig claims that no pits will initiate if E_{corr} is active to E_{pit} and that the reduced rate of initiation is due to the fluctuations of E_{corr} which cause it to become equal to or noble of the E_{cpp} [35, 37]. Other authors, notably LaQue and Wood, discount the importance of E_{cpp} and explain the decreased pitting at more active potentials in terms of more stable oxide films [3, 37, 39]. In either case, two points are agreed upon:

(1) Pitting will occur if E_{corr} is noble to E_{cpp}.

(2) When E_{corr} is active to E_{cpp}, pitting becomes less severe as the difference between the two increases.

The active shift of E_{corr} caused by increased flow will therefore increase the pit initiation time.

For pH 7.2 to 7.8, Dexter reports average pit initiation times from 2 to 3 days, increasing at the higher pH conditions [24, 25]. It is expected that an active shift of E_{corr} with increased flow should retard the initiation of pits. Unfortunately, the stirring data (Figure III.3) shows that, at these low pH conditions, the least amount of E_{corr} shift occurs, ranging from 0 to 40 mV at pH 7.2. The flow-through electrode data at pH 7.45 (Figure III.6) shows a somewhat larger shift than would be expected from the stirring departments. The active shift as flow

increased from 2.5 to 35 cm/sec was approximately 80 mV and the additional shift as flow was further increased to 71 cm/sec was approximately 30 mV. Although this is over 100 mV of active shift for seawater flow of less than 1 m/sec, it is doubtful that it is sufficient to protect aluminum in real ocean conditions, since Groover found that all Al alloys he tested with E_{corr} noble to -900 mV suffered some pitting. Dexter reports that 100% of electrodes tested at pH 7.6 (E_{corr} equal to 800 $\pm$ 50 mV) initiated pits within 3 days. This is the same potential as a flow-through electrode at pH 7.4 and 35-71 cm/sec flow. More experimentation is needed to determine the magnitude of protection offered by this E_{corr} shift at pH values typical of deep ocean water.

It may be hypothesized that the maximum beneficial effect of the active shift in E_{corr} with increased flow would occur in locations where the pH is from 7.8 - 8.2. This is the typical range found in large areas of the Pacific and Atlantic Oceans [40-42]. Expected E_{corr} values for 5052 alloy at pH 7.8 - 8.2 would be -900 to -1100 mV [24]. The addition of a 100 to 200 mV active shift of E_{corr} provided by flow rates >35 cm/sec would be predicted by Figures III.3 and III.5. This should provide substantial retardation of pit initiation as long as flow is maintained. Dexter has shown that a pH induced shift of the average E_{corr} from -925 to -1050 mV doubled average pit initiation time from three days to seven days [24]. He found that 70% of 5052 electrodes in pH 8.2 seawater (-1000 to -1100 mV) did not pit during a one month experiment. Low velocity flow should retard pit initiation further by shifting E_{corr} even further from E_{cpp}. It has been generally thought that flow rates higher than 2 m/sec are required to suppress pitting [2, 3]. For aluminum in large areas of the ocean, constant flow rates greater than 35 cm/sec may be sufficient. It has been clearly demonstrated in this research that reduction of flow causes a noble shift in E_{corr}, which would favor pit initiation during periods of zero flow. This confirms previous suggestions that flow be maintained at all times in applications such as OTEC heat exchangers [7].

D.2. Implications of the Changes in Cathodic Polarizations

After pits have initiated, the current from the propagating pit may polarize the electrode towards a more active potential [24, 37]. The rate of pit growth will then be controlled by the reactions represented

by the cathodic polarization curve. Figure III.5 indicates that, at pH 8.2, an increase in corrosion current can be expected from the effects of low velocity seawater flow. A polarization of -25 mV from E_{corr} will produce less than 1 $\mu A/cm^2$ current density at 0.59-2.5 cm/sec flow, but 3 $\mu A/cm^2$ at 35 cm/sec. Similarly, polarization of -50 mV produces 1-2 $\mu A/cm^2$ at 0.59-2.5 cm/sec vs. 6 $\mu A/cm^2$ at 35 cm/sec. This prediction of a factor of three increase in corrosion current as the flow rate is increased from 2.5 to 35 cm/sec will be supported by other analyses in this section.

At pH 7.45, Figure III.6 shows effects similar to those observed at pH 8.2. Polarization of -50 mV from E_{corr} produces currents of 0.3 $\mu A/cm^2$ at 2.5 cm/sec, 1.0 $\mu A/cm^2$ at 35 cm/sec and 2.0 $\mu A/cm^2$ at 71 cm/sec. Corrosion currents are again seen to increase by a factor of 3 as the flow increases from 2.5 to 35 cm/sec and by a factor of 6 from 2.5 to 71 cm/sec. These proportionalities hold true for all other polarizations shown in Figure III.6. As pitting is very likely at pH 7.45, and since the shift in E_{corr} caused by flow is unlikely to be sufficient to significantly slow pit initiation, this increase in available cathodic current caused by low velocity flow may be predicted to be quite harmful to 5052 alloy in low pH seawater, increasing the rate of pit growth or crevice corrosion.

The most corrosive seawater conditions reported for 5000 series aluminum alloys have been in the Pacific Ocean at depths of 500 to 900 m [43]. This water may be characterized by pH 7.5, dissolved oxygen 0.4 ppm, temperature 4-6°C, and salinity 34 $^{o}/oo$. The data indicate that low velocity flow will decrease the slope of the cathodic polarization curves for conditions of low pH and low dissolved oxygen at 22°C. The effect of stirring was to offset the increase in slope caused by the low dissolved oxygen and to increase the corrosion current at any given amount of polarization. This possibility had led to speculation that conditions of low pH, mid-range dissolved oxygen and low temperature combined with flow rates of approximately 1 m/sec would produce very high rates of pitting in 5052 alloy [1].

In contrast to the effect of velocity at 22°C, it was found that low temperatures suppressed the reaction kinetics sufficiently that no effect of stirring could be detected. Figure III.7 shows that the four

trials conducted at conditions of low pH, low dissolved oxygen and low temperature fall within the normal scatter for cathodic polarizations of aluminum. It is concluded that, for dissolved oxygen concentrations of 2.1 ppm, pH 7.2, and 5°C, "super" corrosion will not be produced by low velocity flow. It is possible that flow effects may create very high corrosion rates at higher D.O. concentrations and temperatures, but this possibility remains to be investigated.

D.3. Explanation of the Flow Induced Shift of Corrosion Potential

Variations in corrosion potentials can best be understood by an application of mixed potential theory. An electrode immersed in an electrolyte such as seawater has both anodic and cathodic areas present. The corrosion potential of the metal is the result of the polarization of these areas away from their equilibrium anodic and cathodic half cell potentials to a common mixed potential (E_{corr}).

Any mechanism that shifts the position or slope of either the cathodic or anodic polarization curve will shift the intersection of the two curves and may alter E_{corr} and I_{corr}. For aluminum undergoing uniform passive wastage, the anodic polarization curve may be assumed to be similar to those reported in Figure III.8. Reduction of oxygen is believed to be the cathodic reaction [35, 44, 45]. No data concerning the behavior of an oxygen electrode on aluminum exists in the literature; however, the reduction of oxygen on platinum is well documented by Hoare [36]. It has been reported that cathodic polarization curves for aluminum in neutral solutions over a range of 10 to 10^4 $\mu A/cm^2$ are similar in shape to those on platinum, although shifted in the active direction approximately 400 mV [45].

Mixed potential theory will now be applied to examine possible causes of the observed active shift of E_{corr} as flow rate increases. Figure III.12 has been constructed by assuming the cathodic polarization E vs. log i) relationship is linear and the Tafel slope constant. The anodic curves show the increase in passive current density, i_p, previously reported in Figure III.8. Since both curves have been constructed as a function of current density rather than total current, it is necessary to assume that the cathodic and anodic areas remain constant. Barnartt has shown that changes in the ratio of the two areas

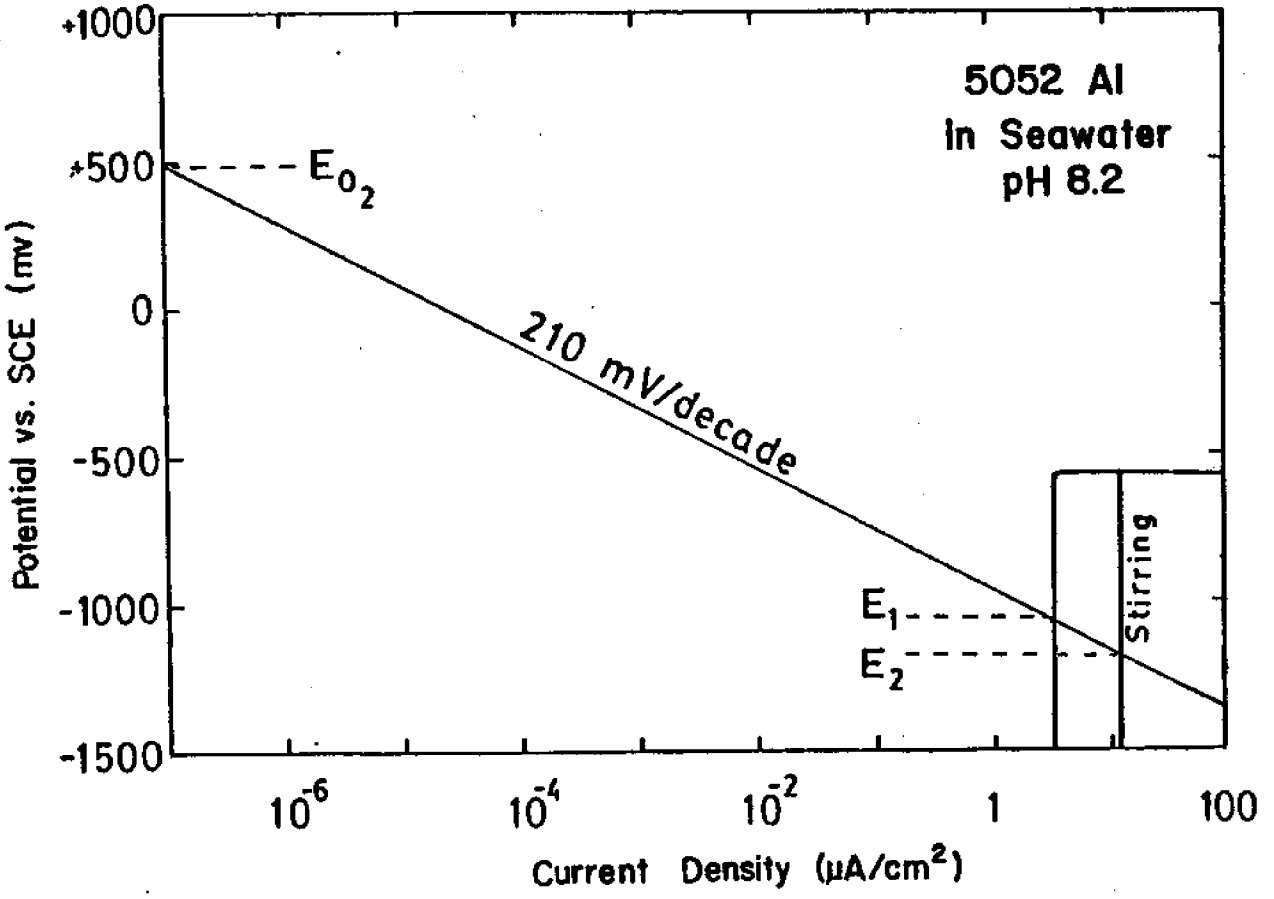

Figure III.12 Prediction of corrosion potentials from mixed potential theory at pH 8.2, air saturation and 20°C.

may effect both E_{corr} and i_{corr} [46]. From theoretical calculations, he maintains that an active shift in E_{corr} of 100 mV would be produced by an increase in the anodic surface area from 50% to 99% of the total electrode surface area. Such a shift for an active/passive metal seem highly unlikely.

Such a redistribution of electrode area would mean the cathodic current densities would be greatly increased at the higher flow rates due to the small cathodic area. It would be expected that limited oxygen diffusion would alter the cathodic polarization curves at the higher flow rates (35 and 71 cm/sec) if cathodic area was greatly reduced. But examination of Figures III.10 and III.11 show only slight changes in the polarization curves as velocity increases. Certainly, if the electrode pits, the anode area shifts in the wrong direction. Although some shift of the proportions of anodic to cathodic surface areas may exist, it does not appear to be a major cause of the velocity induced shift of E_{corr}, noted throughout this research.

Another set of possibilities for the active shift in E_{corr} with velocity would center on changes in the oxygen electrode. Velocity induced changes in the exchange current density, the oxygen half cell potential E_{O_2}, or the shape of the cathodic polarization curve could shift E_{corr}.[2] Each of these three possibilities will now be considered.

A variation in the exchange current density ($i_{\circ O_2}$) would cause a horizontal shift of the cathodic polarization curves.[2] Hoare reports an exchange current density for oxygen on Pt ranging from 10^{-3} to 10^{-4} $\mu A/cm^2$ and a specific value of 1.3×10^{-3} $\mu A/cm^2$ on bright Pt in O_2 saturated 2N H_2SO_4 [36]. However, it seems more realistic to consider the results on an active metal. Hoare does not report on aluminum, but does report on silver and nickel, due to the interest in these electrodes in batteries. For silver, he reports a Tafel Slope of 0.112 V, which was dependent on the partial pressure of O_2. Unfortunately, no $i_{\circ O_2}$ values are reported. Hoare does report results on nickel showing it has lower exchange current densities than Pt. No results appear to exist on the effects of velocity of electrolyte flow on exchange current. From Figure III.12 it may be estimated that a decrease of $i_{\circ O_2}$ by a factor of three would result in the observed 100 mV active shift of

E_{corr} as flow increases from 2.5 to 35 cm/sec. Further investigation of this possibility is needed, but it seems more logical that increased flow would increase, not decrease, exchange current density.

Changes in the half cell potential E_{O_2} could also cause the observed shift of E_{corr}. Equilibrium E_{O_2} values may be calculated by the Nernst Equation [35, 44, 47]:

$$E = E^o + \frac{0.0592}{n} \log \frac{(a_i\ a_j\ a_k\ \ldots)}{(a_r\ a_s\ a_t\ \ldots)}$$

Where:
E is the reduction potential
E^o is the standard reduction potential
n is the number of electrons transferred
a_i, a_j, a_k ... are the activities of reactants
a_r, a_s, a_t ... are the activities of products

The cathodic reaction for n = 1 is:

$$e^- + 1/4\ O_2 + 1/2\ H_2O \longrightarrow OH^-$$

and:

$$E^o = +0.401\ V\ (SHE)$$

$$a_{O_2} = 0.2\ atm$$

$$a_{H_2O} = 1$$

$$K_{H_2O} = (a_{OH^-})\ (a_{H^+})$$

Since the ionization constant (K_{H_2O}) for pure water is 1.008×10^{-14}, the Nernst Equation gives:

$$E_{O_2} = +0.734\ V\ (SHE),\ or = +0.493\ V\ (SCE)$$

This half cell potential has been plotted as E_{O_2} on Figure III. 12. By varying the pH and the partial pressure of oxygen, various possible electrode conditions can be considered.

It seems reasonable to assume that increased seawater flow across the electrode surface should remove some soluble oxygen reduction products (OH^-), while low flow rates should allow more hydroxide to accumulate at the electrode surface. Thus, low flow rates would allow the surface pH to be more basic than at higher flow 5ates. If the surface pH reached values greater than 10, however, one would expect to find greatly increased corrosion [35]. Indeed this was observed in cathodic polarizations beyond 100 $\mu A/cm^2$ where the electrode surface after polarization was markedly different than observed after trials at lower maximum current densities. For a surface pH of 10 and partial pressure of oxygen 0.2 atm, E_{O_2} = +0.388. Increasing the flow would tend to shift the surface pH back towards the bulk value where E_{O_2} = +0.492 V. Thus, a velocity increase would shift E_{O_2} in the noble direction, which should result in a similar change in E_{corr}. Since increased flow shifts E_{corr} active, not noble as predicted by these calculations, any variation of surface pH with flow must be too small to significantly effect E_{corr}.

The second variable affecting the calculated E_{O_2} is the concentration of dissolved oxygen at the electrode surface. If the partial pressure of oxygen in the bulk solution is 0.2 atm, it is reasonable to assume that, under quiescent conditions, it will be less than at the electrode surface due to the cathodic reaction. The effect of increased flow rates would be to increase the oxygen concentration at the electrode. The results of Nernst Equation calculations for three oxygen concentrations, pH 8.2 and 25°C are:

Oxygen Concentration (atm)	E_{O_2} (V SCE)
0.20	+0.493
0.10	+0.488
0.02	+0.478

An order of magnitude increase in oxygen concentration results in just 15 mV of potential change, and the resulting shift in E_{corr} would be in the opposite direction to that which was observed. From the above calculations, it can be concluded that shifts of the potential of the oxygen electrode due to dissolved O_2 or pH are not responsible for the observed shift in E_{corr}.

Consider now how changes in the anodic polarization curves would affect E_{corr} as the flow rate increased. Theoretically, shifts in aluminum exchange current density, $i_{o_{Al}}$, or half cell potential, E_{Al}, or in the passive current density could produce a change in E_{corr}. A shift in E_{Al} would be unlikely to have much effect on E_{corr} because the anodic curve has a very high slope in the passive region.

It is seen from Figure III.8 however that the passive current density i_p is increased by a factor of three by stirring the seawater. In Figure III.12 it is seen that the cathodic polarization curve intersects the no-stirring anodic polarization curve at E_1. Assuming no change in the cathodic polarization curve as stirring begins, the potential will shift to E_2 as the anodic curve moves to the stirring position. This is a shift of 125 mV in the active direction and approximately the shift observed from no-stirring to stirring at pH 8.2. Any reduction of slope of the cathodic polarization curve with stirring would oppose this active shift. But it is seen in Figures III.10 and III.11 that observed changes in cathodic slope virtually disappear when plotted logarithmically as they are in Figure III.12. The increase in i_p with flow rate could be due to either an increase in $i_{o_{Al}}$ or to a reduction in the passive film thickness. The data presented here are not sufficient to distinguish between these two mechanisms.

In conclusion, it has been seen that observed or theoretical changes in the cathodic polarization curve are either too small, in the wrong direction or unsupported by observations and cannot explain the active E_{corr} shift as flow rate increases. The dominant change observed for the anodic polarization curve was the increase of the passive current density, i_p, with stirring. This increase is the mechanism indicated by this research as most likely responsible for the active shift of corrosion potential as seawater flow increases.

D.4. Explanation of Observed Changes in the Cathodic Polarization Curve

Mechanisms which may be responsible for the decreases in cathodic polarization slopes observed as flow increased will now be discussed. Comparison of polarization curves plotted linearly with those plotted logarithmically (Figures III.10 and III.11) demonstrates that the linear plots provide details of changes that are effectively lost in the logarithmic plots. Other researchers have reported no velocity induced differences in cathodic polarizations for aluminum [5, 7] probably because all of their polarization curves were logarithmically plotted.

If the cathodic polarization curve is the result of a single electrochemical reaction, such as the reduction of oxygen, it would be expected that the potential would be proportional to the log of the current density in accord with the Tafel equations [46, 48].

From Figure III.10, it can be seen that most cathodic polarizations measured during this work did not show Tafel behavior. Both Hoare [36] and Stern [48] have reported deviations from linear Tafel behavior for cathodic polarizations with varius electrodes. Stern attributes these variations to four causes: (1) internal electrode currents, (2) concentration polarization, (3) changes in the predominant electrode reaction, and (4) high electrolyte resistance (IR drop). Since the conductivity of seawater is very high, the fourth cause can be eliminated.

It is generally concluded that internal electrode currents are responsible for the deviation of measured polarization curves from Tafel behavior for polarizations less than 100 mV from E_{corr} [46, 49].

Interference of internal currents with measured currents at higher current densities is a more complex problem. The increase in slope at high current density shown in Figure III.10 for the polarizations conducted with E_{corr} noble to -900 mV suggests that active pits may have been supplying current to the electrode. Self-polarization of pitting electrodes has been observed by other investigators [24, 37] and would reduce the measured currents. Although none of the trials reported in Figure III.10 had visible pits, it is possible that the pits had not grown large enough to be observed in the short time the electrode was polarized.

It is seen on Figure III.10 that most electrodes with E_{corr} active to -1100 mV produced polarization curves with lower slopes than electrodes with more noble corrosion potentials. From Figure III.11 the slope for the 1st decade of polarization is 80 $\pm$ 20 mV/decade. The slopes of the more noble polarization curves in Figure III.10 are 250 $\pm$ 50 mV/decade. Unwanted internal electrode currents may explain the different sets of data. The more active E_{corr} values were obtained on either cylindrical electrodes or pre-polarized tubular electrodes. It is hypothesized that these electrodes were past the protective pitting potential [37] and had completely passive surfaces with no active or incipient pits. Therefore, they represent the most accurate measurement made of the cathodic reaction. Hoare reports Tafel constants for oxygen reduction on Pt ranging from 40-120 mV/decade [36] showing general agreement with the lower slopes measured for these active polarizations.

At more active E_{corr} values, it is less likely that pits could initiate on the electrode. Electrodes with E_{corr} active to -1100 mV showed generally linear behavior in Figure III.10. In Figure III.11, however, the larger scale shows that these curves also have increased slope at high current densities. To sustain the cathodic reaction, oxygen must migrate to the electrode surface and be reduced. Concentration polarization occurs when oxygen cannot reach the surface rapidly enough and the solution adjacent to the electrode becomes depleted [48]. This reduces the current below that predicted by the Tafel equation. This type of behavior was seen in all cathodic polarization curves above i_c = 10 $\mu A/cm^2$.

It is expected that concentration polarization effects would be reduced by an increase in flow rate [35, 49]. In Figures III.10 and III.11, it is seen that increased flow had little if any effect on the deviation from Tafel behavior seen at high current densities. This is especially evident in Figure III.11 where flow rates of 2.5 and 35 cm/sec at similar potentials are easily compared. It is possible that the rate controlling reaction is the passage of electrons through the surface oxide film. In this case, flow would not effect the concentration polarization as it would if depletion of oxygen in the electrolyte were rate controlling. The exact surface film present on aluminum has been the subject of much research but is not yet clearly defined [39, 50].

The cathodic curves do show reduced slope as flow rate increases if plotted as a function of i_c rather than a function of log i_c. This reduction of slope is predicted for reduced concentration polarization as flow increases [35, 49]. Apparently, the reduction in concentration polarization at the low flow rates of these experiments is too small to be seen on logarithmic plots such as Figures III.10 and III.11. The effect of increased flow is clearly seen on the linearly plots such as Figures III.5 and III.6.

The final mechanism to explain deviations from Tafel behavior is competing cathodic reactions. Although the literature concludes that oxygen reduction is the controlling reaction for aluminum corrosion, it has been reported that hydrogen ion reduction occurs during cathodic polarizations [51]. From potential-pH equilibrium diagrams, it can be seen that H_2 production is thermodynamically possible at any potential active to -650 mV (SCE) for conditions of 25°C and pH 78 [52].

Polarization to potentials more active than -1400 mV (Figure III.10) produced curves with decreasing slope. This is probably due to the intersection of the oxygen and hydrogen reduction curves and the beginning of a potential region where H_2 evolution is an important cathodic reaction [48]. Although H_2 reduction may not be a significant cathodic reaction for aluminum corrosion at potentials in the range of -700 to -1200 mV expected for 5052, it could contribute significantly to the total cathodic current at more active potentials during polarization.

Thus, it appears that the deviations of measured cathodic polarization curves from the theoretical Tafel behavior can be explained by several interacting mechanisms.

(1) Internal currents reduce the slope at small (<100 mV) polarization from E_{corr}.

(2) Internal currents may increase the slope if active pits initiate and self-polarize the electrode.

(3) Concentration polarization increases the slope at high current densities.

(4) Hydrogen evolution reduces the slope at potentials active to -1400 mV.

Reduction of concentration polarization seems the most likely explanation for the slope reduction of cathodic polarization curves with increased flow. For the low velocities examined during this research, linear rather than logarithmic plots were required to observe the changes in the cathodic polarization curves.

E. Summary

An increase in the speed of flow past the surface always had two effects in our tests. First, it shifted the corrosion potential in the active direction. This agrees with previous work [57] on aluminum alloy 5456 in high velocity seawater flows where they found an active shift in the corrosion potential. Second, it decreased the initial slope of the cathodic polarization curve. Under surface water conditions where the pH is greater than 8, the corrosion potential effect always predominated. This predicts that the increases in flow speed normally associated with tidal and wind driven currents in coastal and estuarine waters should lead to less corrosive conditions than those in stagnant water. Although service experience tells us that a continuous flow of about 2 meters/sec is necessary to suppress pitting altogether, these results indicate that some benefit should be expected even from small flow speeds.

Finally, the lack of any systematic variation of cathodic behavior with flow speed under simulated deep ocean conditions (see Figure III.7) indicates that previous concern over the possibility of triggering a set of highly corrosive conditions in the deep ocean by an increase in flow speed probably will not happen. The concern arose in the Ocean Thermal Energy Conversion Program where deep ocean water might be passing through aluminum condenser tubing at an elevated velocity. We attribute the lack of response to flow demonstrated in Figure III.7 to sluggish reaction kinetics at the low temperature. The data are convincing that there should be no problem under the conditions and short time period of our tests. There may still be cause for concern, however, over longer time periods, or at intermediate temperatures in the 10 to 15°C range.

F. References

1. S. C. Dexter, "Localized Corrosion of Aluminum Alloys for OTEC Heat Exchangers," Ocean Science and Engineering, 6 (1), pp. 109-148 (1981).
2. G. Butler and H. C. K. Ison, Corrosion and its Prevention in Water, R. F. Kreiger Publishing Co., Huntington, New York (1978).
3. F. La Que, Marine Corrosion, Wiley-Interscience, New York (1975).
4. J. A. Davis, "Review of High Velocity Sea Water Corrosion," T-7C-5 Task group report, CORROSION/77, NACE, Houston, Texas (1977).
5. G. A. Gehring, Jr. and M. A. Peterson, "Corrosion of 5456-H117 Aluminum in High Velocity Sea Water," Corrosion, Vol. 37, No. 4 (1981).
6. J. A. Davis and G. A. Gehring, Jr., "The Effect and Velocity on the Sea Water Corrosion Behavior of High Performance Ship Material," Materials Performance, Vol. 14, No. 4, pp. 32-39 (1975).
7. G. A. Gehring, Jr., "Corrosion of Aluminum Alloys in High Velocity Seawater," Final Report for Office of Naval Research Metallurgy Program - Code 471, OCR-ORN-3, Arlington, Virginia (1979).
8. J. F. Rynewicz and N. Nagrodsky, "Corrosion Test Results on Seawater Heat Exchanger Materials," CORROSION/82, Paper No. 52, Houston, Texas (1982).
9. R. O. Lewis and F. L. La Que, "Evaluation of Copper-Nickel Alloys for OTEC Applications," ANL/OTEC-BCM-019 (1981).
10. W. K. Boyd and F. W. Fink, "Corrosion of Metals in Marine Environments, "MCIC-78-37, Metals and Ceramics Information Center, Columbus, Ohio (1978).
11. M. A. C. de Castro and B. E. Wilde, "The Effect of Peripheral Velocity on the Corrosion and Passivation of Iron in Chloride Containing Media," Corrosion, Vol. 35, No. 12, pp. 560-565 (1979).
12. Z. A. Foroulis, "The Influence of Velocity and Dissolved Oxygen on the Initial Corrosion Behavior of Iron in High Purity Water," Corrosion, Vol. 35, No. 8 (1979).
13. N. Sato, T. Nakagawa, K. Kudo and M. Sakashita, "Chloride Pitting Dissolution of Rotating Stainless Steel Electrode in Acid Solution," Electrochemical Techniques for Corrosion, NACE, Houston, Texas (1977).

14. D. C. Silverman, "Rotating Cylinder Electrode for Velocity Sensitivity Testing," Paper No. 258, CORROSION/83, Anaheim, California (1983).

15. F. Mansfeld and J. V. Kenkel, "The Effects of Rotation on Pitting Behavior of Aluminum and Stainless Steel," Corrosion, Vol. 35, No. 1 (1979).

16. F. Mansfeld and J. V. Kenkel, "The Effect of Velocity on Galvanic Corrosion of Al Alloys," Paper No. 100; CORROSION/77, National Association of Corrosion Engineers, San Franciso, California (1977).

17. J. Prentice and H. Craig, Jr., "Rotating Disc Electrode Oxygen Sensor and Corrosion Rate Probe," IEEE Journal of Oceanic Engineering, Vol. OE-4, No. 4 (1979).

18. S. R. de Sanchez and D. J. Schiffrin, "The Flow Corrosion Mechanisms of Copper Base Alloys in Sea Water in the Presence of Sulfide Contamination," Corrosion Science, Vol. 22, No. 6, pp. 585-607, Great Britain (1982).

19. H. Do Duc and P. Tissot, "Rotating Disc and Ring Disc Electrode Studies of Tin in Neutral Phosphate Solutions," Corrosion Science, Vol. 19, pp. 191-197, Pergamon Press (1979).

20. F. Franz and P. Novak, "Effect of Rotation on the Pitting Corrosion of Aluminum Electrodes," Localized Corrosion NACE-3, p. 576 (1971).

21. T. Perkins, K. Graham. G. Storm, G. Leamer and R. Schock, "Flow Effects on Corrosion of Galvanic Couples in Sea Water," Corrosion, Vol. 35, No. 1 (1979).

22. W. H. Ailor, "Flowing Seawater Corrosion Potentials of Aluminum Alloys," NACE Preprint No. 36, National Association of Corrosion Engineers, Houston, Texas (1970).

23. T. S. Lee, Francis LaQue Corrosion Laboratories, The International Nickel Company, Harbor Island, North Carolina, Personal Communication (1982).

24. S. C. Dexter, "Effects of Variations in Seawater upon the Corrosion of Aluminum," Corrosion, Vol. 36, No. 8, pp. 423-432 (1980).

25. S. C. Dexter, "Effect of pH and Dissolved Oxygen on the Corrosion Behavior of Aluminum in Seawater," Proceedings of the 7th International Congress on Metallic Corrosion, Rio de Janeiro (1978).

26. H. Rowland and S. Dexter, "Effects of Sea Water Carbon Dioxide System on the Corrosion of Aluminum," Corrosion, Vol. 36, No. 9, pp. 458-467 (1980).

27. T. J. Lennox, Jr., M. H. Peterson and C. W. Billow, "Corrosion Resistance and Response to Cathodic Protection of Advanced Alloys in Seawater," Paper No. 64, CORROSION/82, Houston, Texas (1982).

28. T. R. Beck and S. G. Chan, "Experimental Observations and Analysis of Hydrodynamic Effects on Growth of Small Pits," Corrosion, Vol. 35, No. 11, pp. 665-671 (1981).

29. K. D. Efird, "Effect of Fluid Dynamics on the Corrosion of Copper-Base Alloys in Sea Water," Corrosion, Vol. 33, No. 1, pp. 3-8 (1977).

30. K. S. Rajogopalan, M. Raghavan, N. S. Rengaswamy, T. M. Balasubramanian and G. Venkatachari, "Corrosion Studies on Aluminum Alloys for Heat Exchanger Applications," Proceedings of the 7th International Congress on Metallic Corrosion, Rio de Janeiro (1978).

31. R. S. C. Munier and H. L. Craig, "Ocean Thermal Energy Conversion (OTEC) Biofouling and Corrosion Experiment," St. Croix, U.S. OTEC Report, PNL-2739 (1978).

32. Vennard, J. K., Elementary Fluid Mechanics, 4th edition, John Wiley, New York, p. 225 (1961).

33. G. Sowinski, Staff Engineer, Alloy Technical Division, Alcoa Laboratories, Alcoa Center, Pennsylvania, Personal Communications (1983).

34. W. E. Rigby, "Aluminum Alloy 5052 Corrosion in Low Velocity Seawater," Master's Thesis, University of Delaware, College of Marine Studies, December, 1983.

35. H. H. Uhlig, Corrosion and Corrosion Control, 2nd Ed., John Wiley and Sons, New York (1971).

36. J. P. Hoare, The Electrochemistry of Oxygen, John Wiley and Sons, New York (1968).

37. F. L. LaQue and H. H. Uhlig, "An Essay on Pitting, Crevice Corrosion and Related Potentials," Materials Performance, Vol. 22, No. 8, pp. 34-36 (1983).

38. R. E. Groover, T. J. Lennox, Jr. and M. H. Peterson, "Cathodic Protection of 19 Aluminum Alloys Exposed to Sea Water-Corrosion Behavior," Materials Protection, pp. 25-30 (1969).

39. G. C. Wood, W. H. Sutton, J. A. Richardson, T. N. K. Riley and A. G. Malherbe, "The Mechanism of Pitting of Aluminum and its Alloys," Localized Corrosion NACE-3, R. W. Staehle, Ed., Houston, Texas, pp. 526-544 (1974).

40. J. P. Riley and G. Skirrow, Chemical Oceanography, 2nd Ed., Vol. 1, Academic Press, Inc., New York (1975).

41. F. M. Reinhart, "Testing in Hydrospace," Handbook on Corrosion Testing and Evaluation, John Wiley and Sons, New York, pp. 531-535 (1971).

42. S. C. Dexter and C. H. Culberson, "Global Variability of Natural Seawater," Paper presented at NACE CORROSION/79, Atlanta, Georgia (1979).

43. F. M. Reinhart, "Corrosion of Metals and Alloys in the Deep Ocean," Technical Report R834, Civil Engineering Laboratory, Port Hueneme, California, February (1976).

44. M. G. Fontana and N. D. Green, Corrosion Engineering, 2nd Ed., McGraw-Hill, New York (1978).

45. B. Bianchi, F. Mazzo, T. Mussini, "Electrochemical Processes of Oxygen and Hydrogen Peroxide in Metal Corrosion and Protection," Electrochim Acta, Vol. 7, pp. 893-904 (1962).

46. S. Barnartt, "Electrochemical Nature of Corrosion," Electrochemical Techniques for Corrosion, R. Baboian, Ed., Houston, Texas (1977).

47. P. W. Adkins, Physical Chemistry, W. H. Freeman and Company, San Francisco, California, pp. 213-215 (1978).

48. M. Stearn and A. L. Geary, "Electrochemical Polarization I. A. Theoretical Analysis of the Shape of Polarization Curves," Journal of the Electrochemical Society, Vol 104, No. 1, pp. 56-63 (1957).

49. J. O'M. Bockris and A. K. N. Reddy, Modern Electrochemistry, Plenum Press, New York (1973).

50. M. J. Pryor, "The Influence of the Defect Structure of Aluminum Oxide Films on the Pitting of Aluminum in Chloride Solutions," Localized Corrosion, NACE-3, R. S. Staehle, Ed., Houston, Texas, pp. 2-11 (1974).

51. R. M. Latanision, N. D. Kackley and S. W. Smith, "Corrosion of Aluminum in Salt and Seawater as Influenced by Magnesium and Copper," Unpublished Manuscript (1982).

52. M. Pourbaix, Atlas of Electrochemical Equilibria 2nd Ed. NACE, Houston, Texas (1974).

IV. DEVELOPMENT OF THE SCANNING POTENTIAL MICROPROBE FOR STUDYING LOCALIZED CORROSION

A. Introduction

A primary mode of corrosion in aluminum alloys is pitting. When exposed to air or water, a protective aluminum oxide film is formed on the metal surface. The initiation of a pit requires the breakdown of this passive layer and attack of the underlying metal by the electrolyte. During this attack, several electrochemical reactions occur locally at the pit site. These electron-transfer reactions cause a perturbation in the potential field in the electrolyte above the sample and mark the initiation of a pit. With each pit (anode) there are one or more cathode sites which complete the charge transfer circuit. The Scanning Potential Microprobe (SPM) used in this study detects this event and maps the location of incipient pits and cathode sites over the sample surface. Therefore, pit sites can be detected before they are easily visible.

The mapping of incipient pits was accomplished by scanning the surface with a vibrating metal microelectrode held 100 μm above the sample. The vibration of the probe allows the use of frequency specific amplifier for recording a more noise-free signal from the sensitive microprobe tip. The probe motion and data collection are computer-controlled for flexibility and storage.

The advantage of using a metal microelectrode is that it has low resistance with a small diameter probe, not possible with a glass capillary filled with salt solution. The vibration of the microelectrode further reduces noise problems because the lock-in amplifier can be used instead of voltmeters, electrometers or oscilloscopes. In addition, a dedicated computer system to digitize the data and prepare the plots can be added. This gives further accuracy and ease of experimentation and data manipulation.

Scanning reference electrode techniques using traversing glass pipette electrodes and flat specimens were first developed and used by researchers in the early 1940's [1-3]. Such apparatus helped to determine the electrochemical nature of corrosion. A technique using rotating cylindrical samples and fixed metal electrodes or glass pipette

Luggin probes was developed in the 1950's and later modified by others [4-8]. Using this technique, regions of anodic activity on steel were mapped with a resolution level of 0.5 mm.

Isaacs et al. developed a scanning reference technique using a flat specimen and a traversing glass pipette electrode for studying stress corrosion cracking, weld line corrosion and grain boundary corrosion in stainless steels [9]. Later, a vibrating platinum microelectrode fashioned after Jaffe and Nucitelli [10] replaced the glass capillary electrode [11] giving a better signal-to-noise ratio.

When pitting is occurring on an aluminum surface, rgions of local potential perturbation occur in the electrolyte due to the current flow through the solution. The developing pit serves as the anode while the cathode may be a precipitate or inclusion particle. The SPM senses the potential gradient around a pit or a cathode. When examining aluminum samples which have been exposed to salt water or seawater using Auger electron spectroscopy, it is difficult to distinguish pits which were active at the time of removal from solution from pits which have passivated. Sites of cathodic activity also cannot be easily identified. This version of the SPM was built to address this problem.

The first requirement for a high resolution SPM is that the probe be very close to the surface. At a distance of several millimeters above the surface, the potential fields begin to flatten out, even in a solution of low conductivity. In the horizontal direction, the gradients drop off quickly after the border of the anode or cathode is reached. For this reason, the probe tip must be very small. Yeager and Kuta (12) have noted that the distance between the probe and the surface must be not less than the probe diameter to avoid perturbation of the current profile by the probe. Secondly, the best results will be achieved in solutions of low conductivity since the potential gradients will be strongest and will extend out far enough into the electrolyte to be sensed by the traversing probe.

Earlier versions of the SPM developed in the H. H. Uhlig Corrosion Lab at M.I.T. by Smith [13] also used a glass capillary probe electrode and a saturated calomel reference electrode to measure local surface potentials. The tip of the glass capillary was about 0.25 mm in diameter, limiting the resolution of the instrument. The resolution was

also limited by the noise level of the measuring electrometers. Strong anodic sites were detectable, but most cathodic sites were lost in the background noise.

In previous work by Smith et al. [14] where pure aluminum and aluminum alloy 5052 were exposed to salt water and natural seawater, some correlation was found between magnesium on the surface and pitting sites in seawater. The magnesium is believed to be adsorbed from solution since a magnesium-containing alloy, 5052, exposed to 3.5% NaCl showed no segregation of magnesium at the surface. It is not known whether the pits analyzed for Mg concentration were active or had passivated before removal from solution because correlation between SPM scans and Auger data could not be done with the early version of the SPM. The improvements described below, modeled after the work of Isaacs et al. [11] with the vibrating metal microelectrodes, allow this combination of electrical, visual and chemical surface analysis to be performed.

B. Apparatus and Experimental Procedures

The design and construction of the scanning potential microprobe was the major object of this study. To achieve higher resolutions, the microelectrode must be held very close to the sample surface during scanning. For this reason, the sample must have a very flat surface and be held very level with respect to the probe's horizontal motion. A flat sample was achieved by careful metallographic preparation. The sample mounting stage (Figure IV.1) was designed and machined to create a mounting surface parallel to the probe's axes of motion.

The probe is a thin platinum wire, 100 μm in diameter, coated with an insulating lacquer. It was partially encased in a glass capillary to further stiffen it. It is essential that the probe does not sway or bend as it travels through the solution so that the potential data and spatial location can be correlated. An auxillary platinum wire electrode was used to measure the overall solution potential at a distance several centimeters from the sample surface. The probe arm, a stainless steel tube holding the electrode cables and supporting a piezoelectric reed, is attached to the shaft of a micrometer with a non-rotating spindle. The micrometer is used to raise and lower the probe arm and

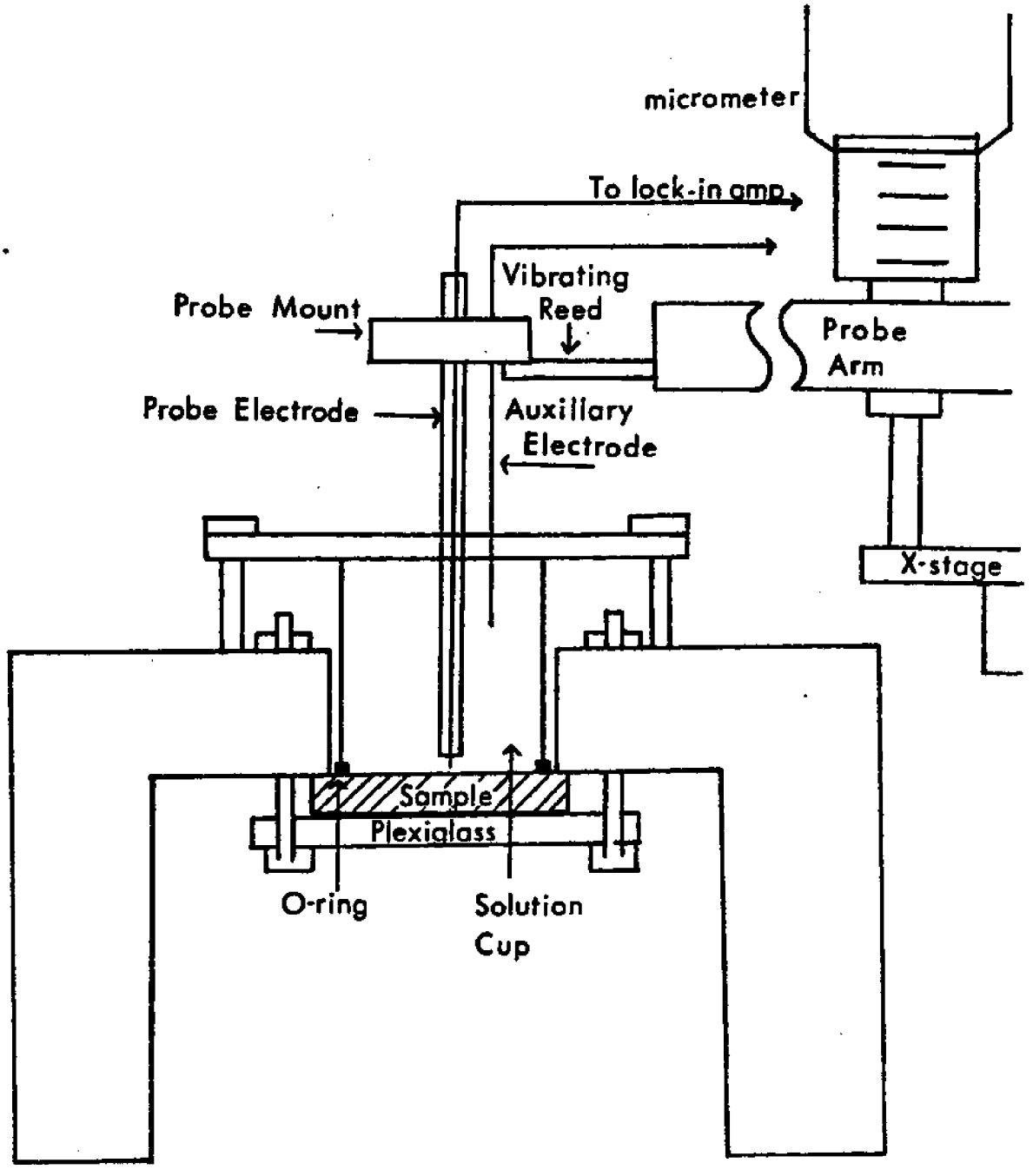

Fig. IV.1Detail of electrodes and sample stage.

electrodes and to position the probe close to the sample surface. The distance of the probe from the surface is measured by means of a 25X microscope with a measuring reticle.

The probe and auxillary microelectrodes are vibrated vertically by a piezoelectric vibrating reed. The piezoelectric bimorph ceramic reed responds to an applied voltage across it with a small amplitude vibration. The reed is driven by a six-volt sine-wave of fixed frequency. The same frequency signal is fed to the reference input of a precision lock-in amplifier which reads the signals from the vibrating probe. A vibration frequency of 267Hz was chosen for a strong, steady probe motion.

The lock-in amplifier is designed to read the voltage amplitude of an A.C. signal at a specific frequency. This measuring technique eliminates stray noise at other frequencies. When the probe is vibrated, a potential reading (relative to instrument ground) is made by the differential preamplifier of the lock-in amplifier at each extreme of the probe's vibration. The magnitude of the difference in the signal from the probe and from the auxillary electrode modulated the output from the lock-in amplifier. This signal is converted from an analog signal to a 12-bit digital signal by an analog-to-digital convertor designed to interface with the computer system (see Figure IV.2).

This digital signal is accessed by a program running on an Apple II+ computer. This program also moves the probe across the sample surface by advancing the stepping motors by a specified number of steps. Each time the probe is advanced one step, a data point is stored in an array by the program. Simultaneously, the pen of the X-Y plotter is advanced in the x-direction and its y-position is modulated by the voltage value corresponding to this position on the sample. The result is a quasi-three-dimentional plot where a peak indicates a region of anodic pitting activity and a valley indicates a cathodic area.

The solution used for the exposure of aluminum alloys with the SPM contained 2.453 mg NaCl, 0.52 mg $MgCl_2 \cdot 6H_2O$ and 0.41 mg Na_2SO_4 in one liter of distilled water. The specific conductivity, $K = 6.1 \times 10^{-3}$ $ohm^{-1}cm^{-1}$, was estimated using Ruppin's formula [15] for seawater

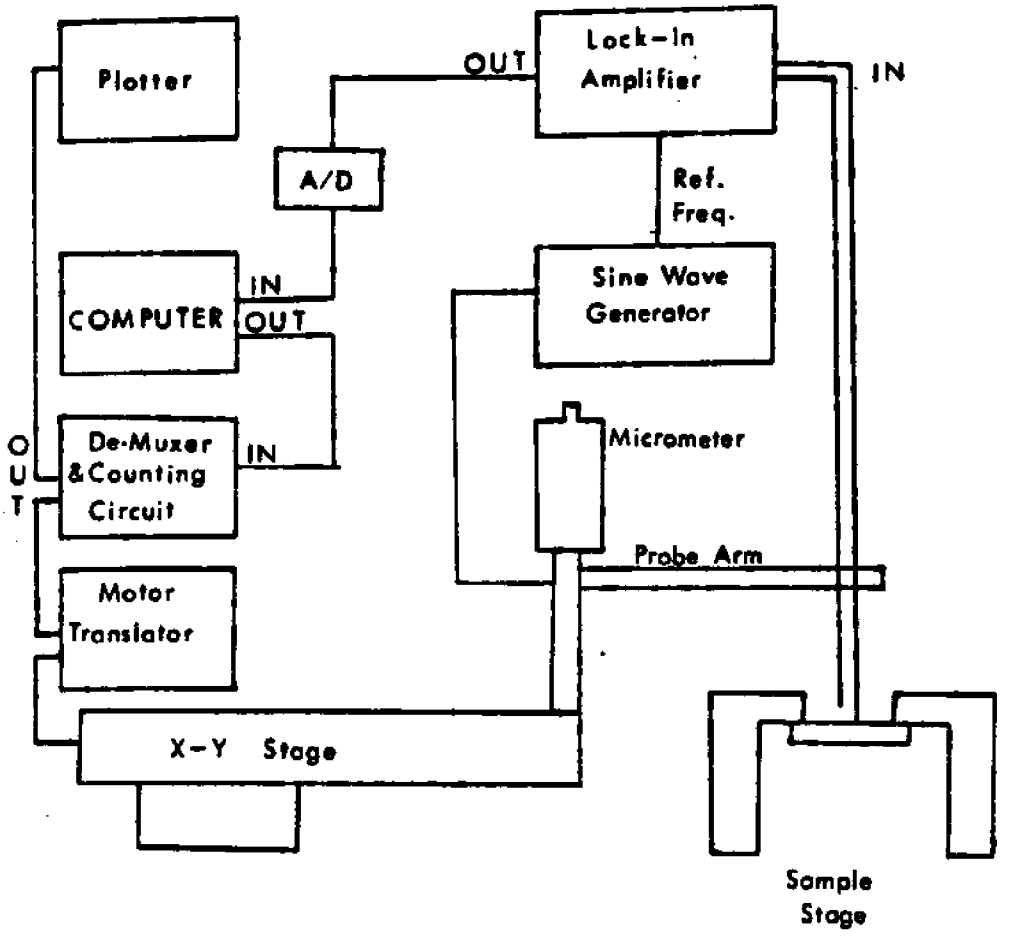

Fig. IV.2 Schematic of Scanning Potential Microprobe Apparatus.

conductivity based on salinity, S, the total weight in grams of all salts (NaCl, $MgCl_2$, etc.) per kg of seawater:

$$\text{At } 25°C;\ 10^6K = 1823S - 12.76S^2 + 0.1177S^3$$

This solution contains a subset of the components of ASTM substitute ocean water in diluted concentrations. This diluted solution was chosen so that the interaction of magnesium with corroding surface could be investigated while keeping the solution conductivity low.

The aluminum samples were cut into 1 cm square coupons for the pitting scans. They were polished on wet silicon carbide paper to 600 grit and then with 1 μm alumina slurry on a cloth wheel. After polishing, the aluminum oxide film was allowed to reform in air for 30-60 minutes before exposure to the salt solution. A reference starting point was marked on the sample with lacquer. The probe was positioned at this point at the start of the scan so that the data collected could be correlated to positions on the sample. After the scan was completed, the starting point was marked with a steel blade and the lacquer was removed to eliminate electron charging problems during subsequent Auger electron spectroscopy. The scanning electron microscope was used to identify pit sites on the sample which were active when the sample was scanned in solution with the SPM. Then the pits of interest were located again with the scanning Auger microscope (SAM) and surface analysis was performed. The surface was sputtered lightly to remove carbon contamination and the surface composition was determined.

C. Results

The real test of the resolution of the SPM is locating developing pits in an aluminum sample exposed to the salt water electrolyte. The spatial position of an SPM peak can be determined from knowledge of the scan step size and the x- and y-position of the feature with respect to the scan starting point. Then, the corresponding surface feature is located by measuring on the SEM photomicrograph from the reference point. This step of pit location must be done with the SEM because the image quality at high magnification is too poor to clearly identify pits.

The SPM scan of a sample of aluminum alloy 5052 which was exposed to the electrolyte is shown in Figure IV.3. Several regions of pitting activity are indicated. Most of the pitting activity shows only 1 or 2 μV difference from the background level. Electrical noise is still a problem in the scans. We cannot be certain that every peak corresponds to a pit site. The larger peaks, indicating a higher level of activity, are more likely to correlate to actual pits. Also, peaks which extend over two or more steps in the x- or y-direction are less likely to be caused by random noise.

The scan area was 0.94 mm by 0.78 mm. Several pitted regions are also visible in the photomicrograph of this sample (Figure IV.4). Correlation between many of the SPM peaks and surface features on the sample is indicated by the letters on Figs. IV.3 and IV.4. The feature marked "d" was selected for further study. It appears as a small peak in the SPM scan of this sample in line 64. This pit was located with the SAM using the SEM photomicrograph as a guide. The size of this pit is about 1-2 μm wide and 15 μm long. The surface region surrounding the pit was analyzed by Auger electron spectroscopy (AES). A line scan was taken across the pit. The region was sputtered for 20 seconds prior to the AES scan to remove surface contaminants.

The AES scan across the pit (Figure IV.5) showed an increase in carbon coincident with a decrease in aluminum, oxygen, and magnesium in the pit. Magnesium is present in higher concentrations 4 to 6 μm to the left of the pit. As discussed earlier, Smith et al. [14] has proposed that this surface excess of magnesium is due to an adsorption reaction. The decrease in Al, O, and Mg at the pit is probably not due merely to a change in surface topography since the carbon signal increases over the pit. A change in topography should affect the strength of all signals equally. However, this effect could be done to the sputtering done before the scan. If the pit interior were not sputtered as cleanly as the rest of the surface, then an increase in the carbon signal at the pit would result. A carbon layer in the pit would also obscure the Al, O and Mg signals.

To answer this question and to confirm the presence of magnesium around the pits, another pit on this sample was located and analyzed. This line scan (Figure IV.6) also showed decreases in Al, O and Mg at

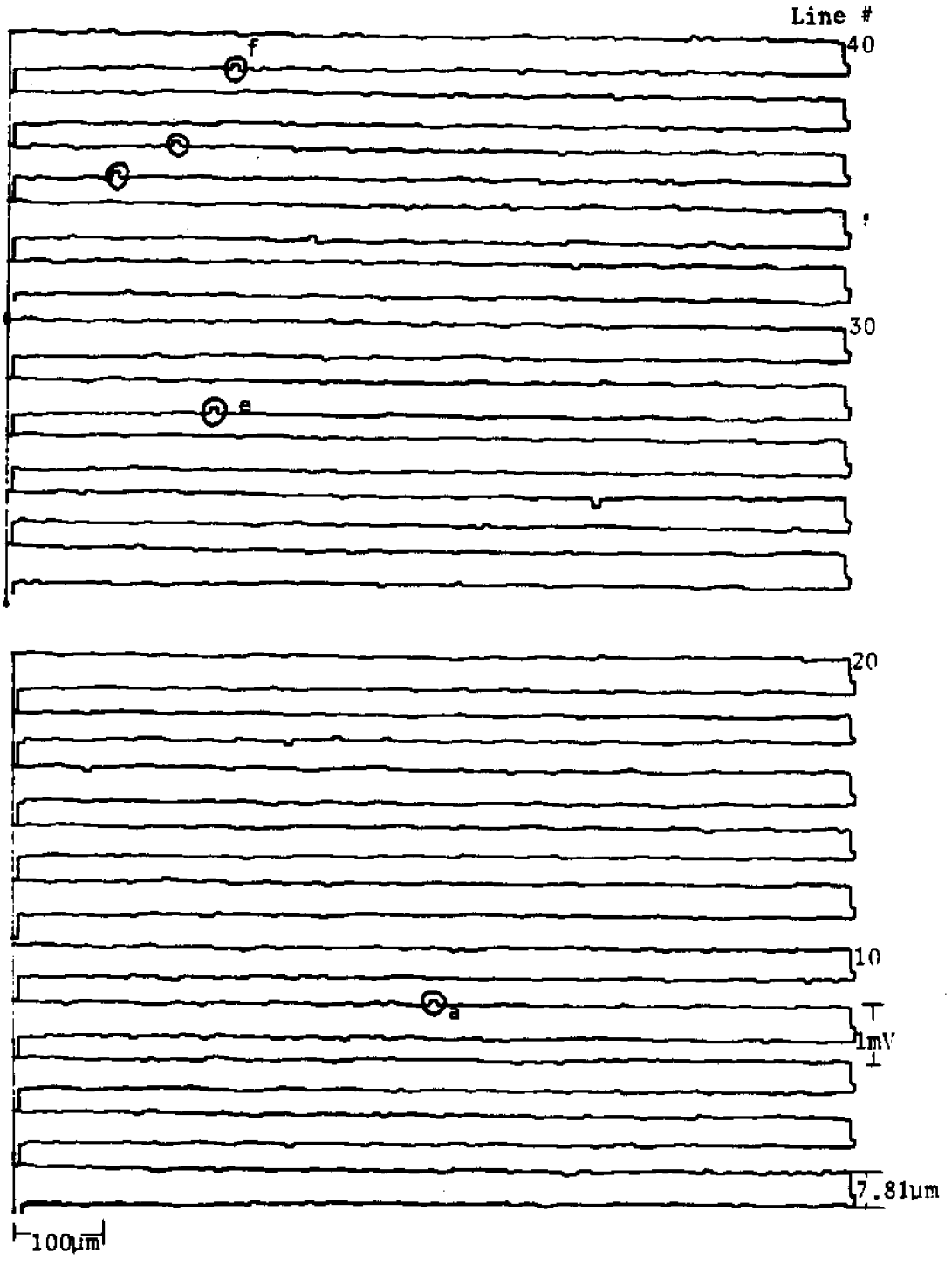

Figure IV.3 SPM scan of Al-5052 in dilute salt water electrolyte. Letters indicate pit sites on Figure IV.4.

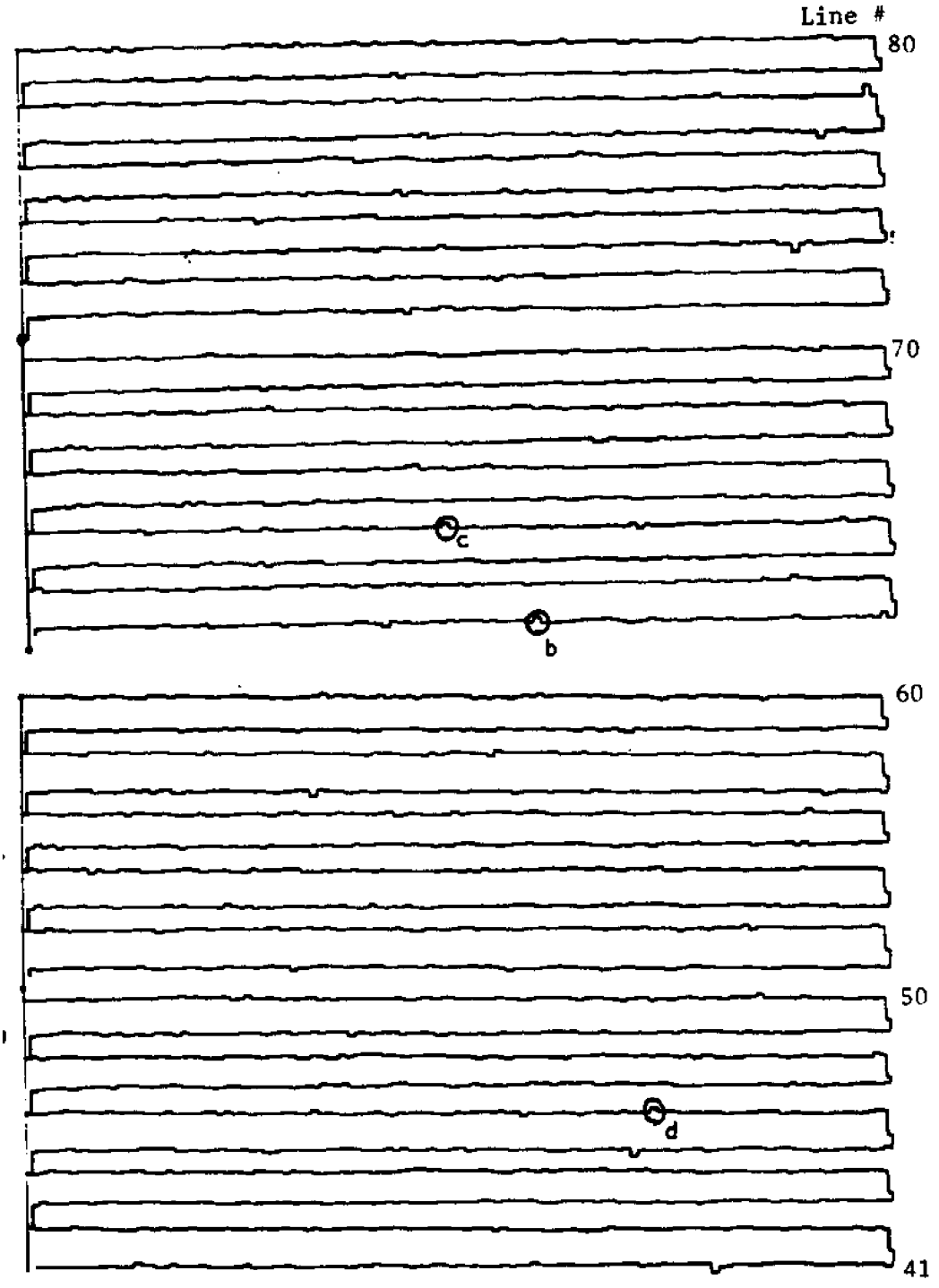

Fig.IV.3 continued.

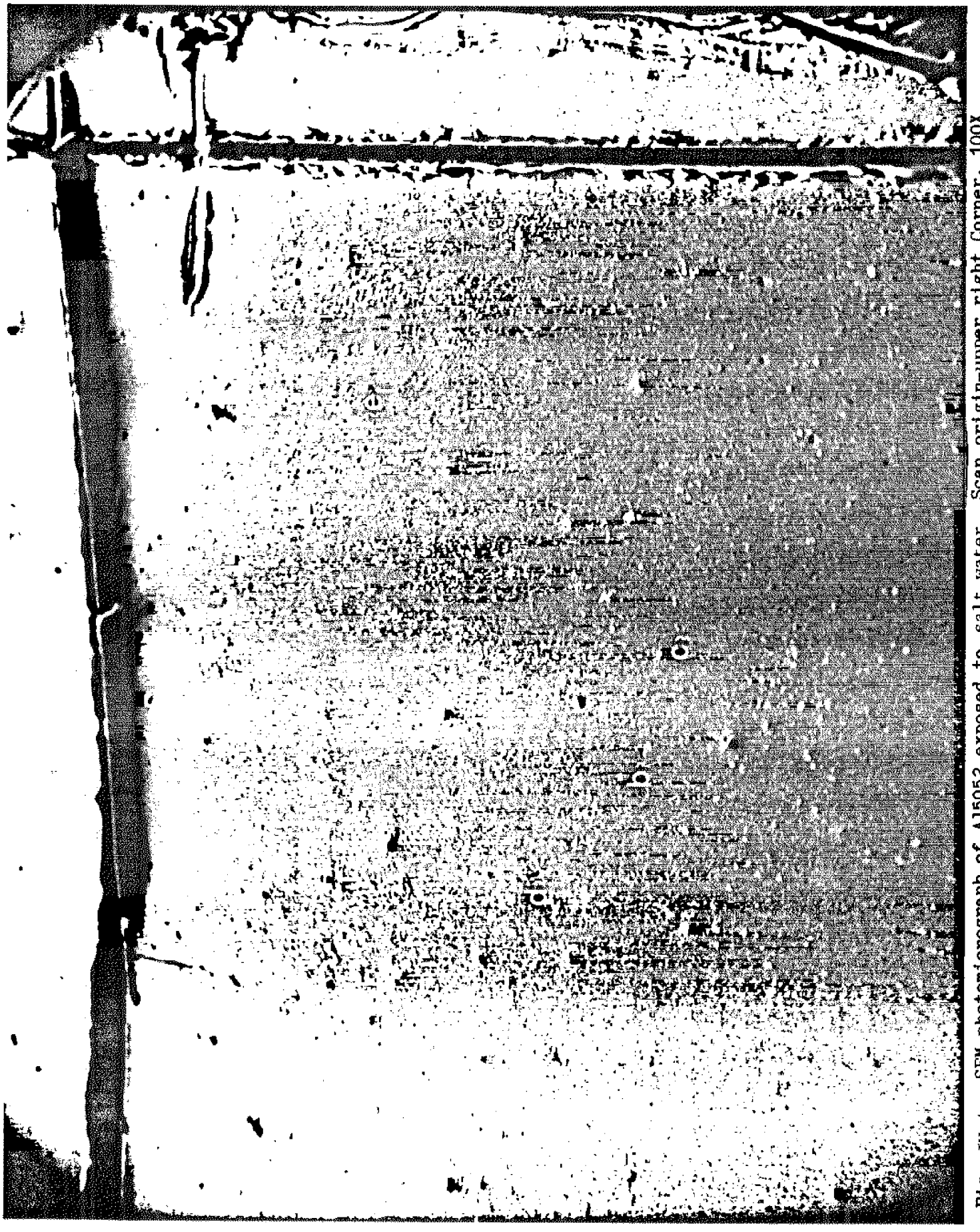

Fig. IV.4 SEM photomicrograph of A15052 exposed to salt water. Scan origin-upper right Corner. 100X

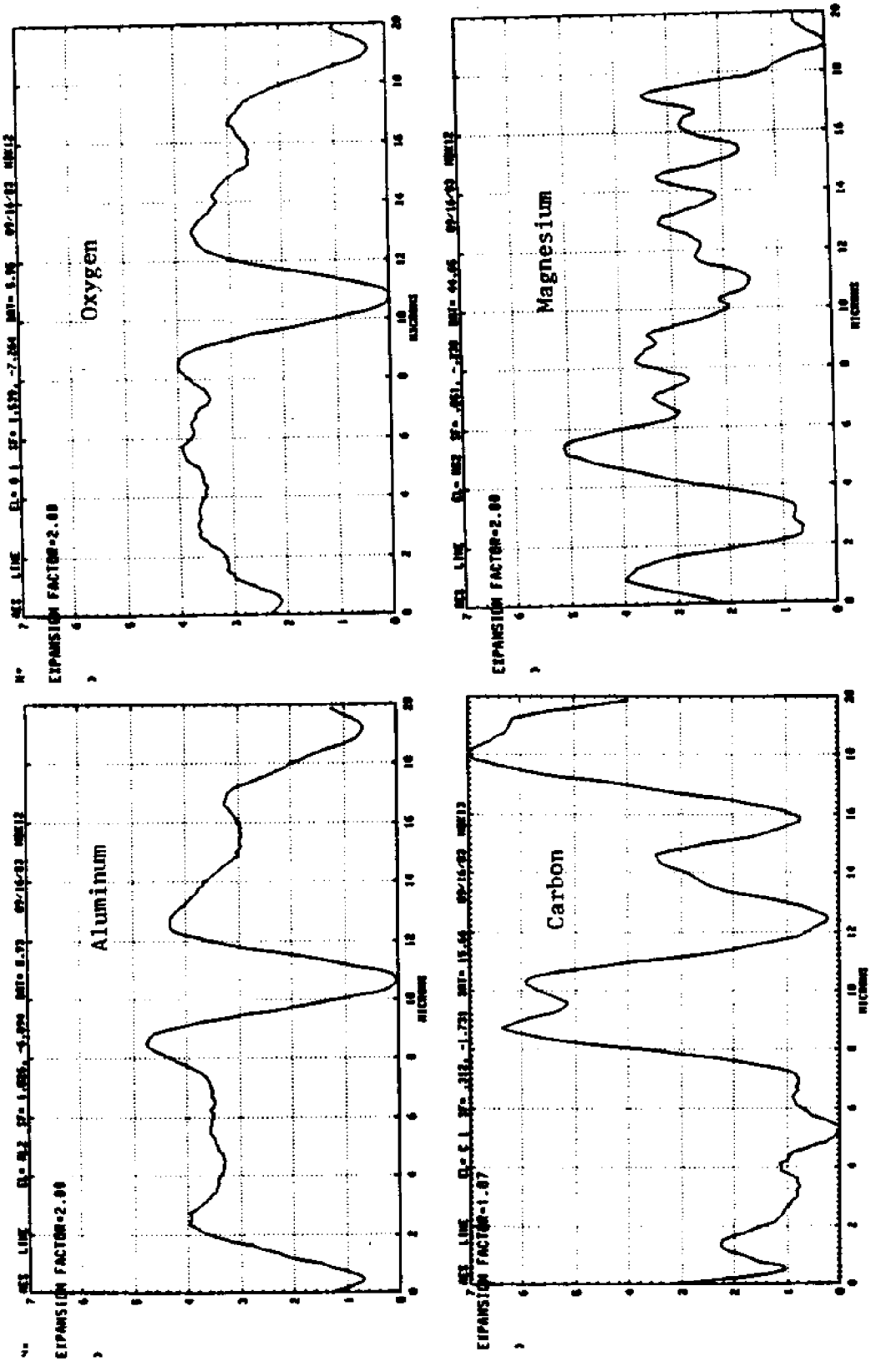

Fig. IV.5 Elemental line scans by Auger Electron Spectroscopy (AES) across pit in Fig.IV.4.

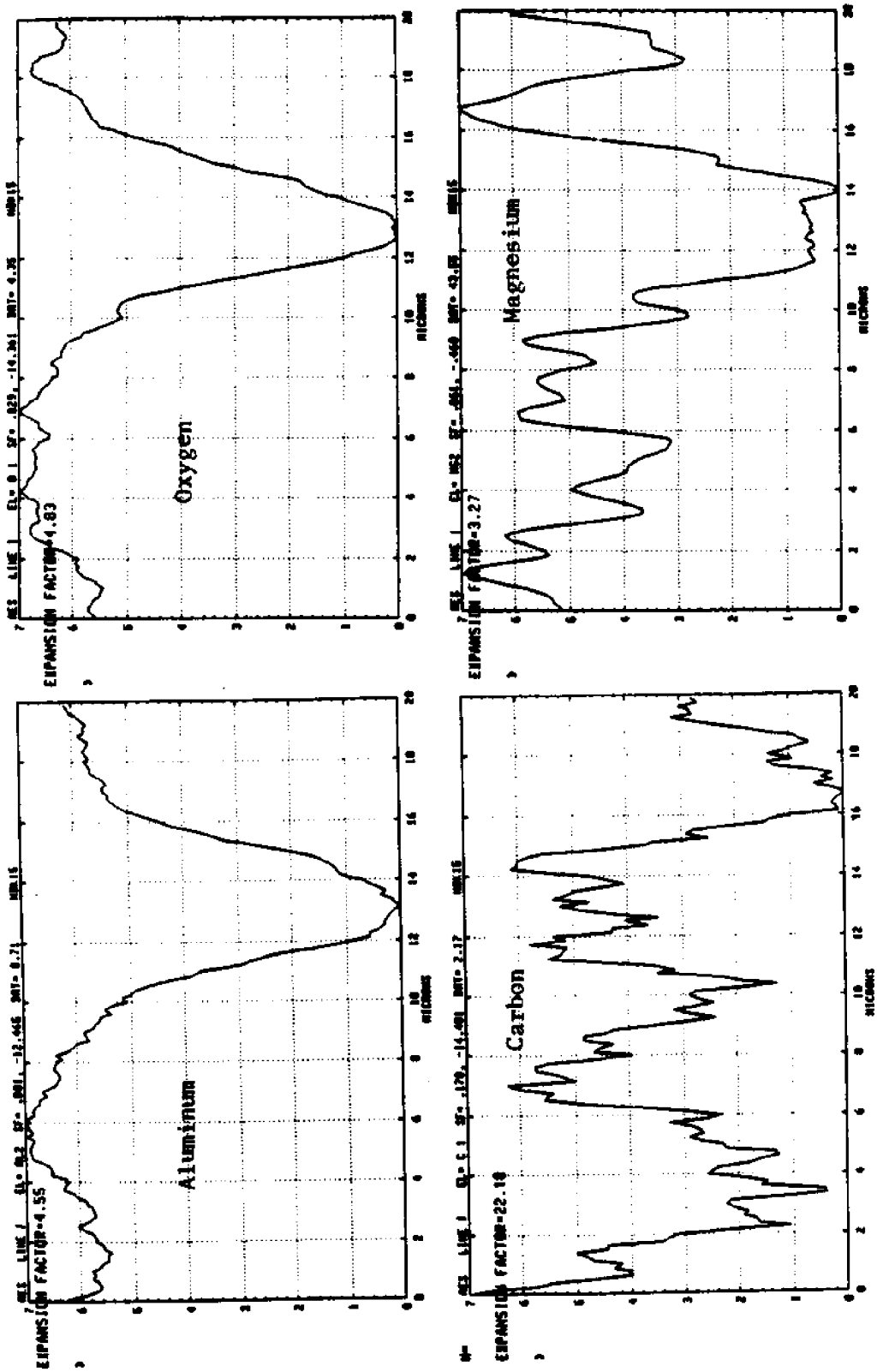

Fig. IV.6 Elemental line scans by AES across pit in Al-5052 exposed to dilute salt water.

the pit and relatively constant carbon levels across the pit. (Note the large expansion factor necessary to highlight the small variations in carbon signal across the surface.) This scan indicates that the relative excess of carbon in the pit is not a result of incomplete sputtering since no sputtering was done prior to these scans. Also, the decrease in the Al, O and Mg signals are not merely due to a topographical effect, but reflect actual decreases in these elements in the pit. Since no carbon compounds were intentionally added to the electrolyte, the carbon signal is probably due to contamination from exposure of the sample to air or from the vacuum system of the SAM.

These scans also show higher concentrations of magnesium at a distance of 4 to 6 μm from the pit center. After sputtering (Figure IV.7) even more magnesium is present 4 to 6 μm to the right of the pit. (Note lower expansion factors.) The carbon level has been decreased and shows an even more definite peak at the pit site, where Al, O and Mg signals decrease. Although the presence of magnesium near the pit has been confirmed on the surface of aluminum alloy 5052 exposed to magnesium containing salt solutions, the oxidation state of the surface magnesium should be determined to indicate whether this species is adsorbed onto the oxide film or is precipitated as $Mg(OH)_2$.

D. Summary and Conclusions

The SPM built in this study has significantly better resolution (tens of microns) than earlier versions of the scanning reference electrode technique [13]. This was confirmed by comparing SEM photomicrographs of the pitted surface with SPM scans showing regions of anodic and cathodic activity. To achieve this level of resoluton, three requirements must be met: 1) a small probe diamter, 2) a low noise measurement system and 3) a flat sample surface. The use of the vibrating probe and the lock-in amplifier address the first two requirements. The specially designed sample stage addresses the third requirement. A low conductivity solution was also necessary for clear indications of pitting on the SPM scan. This requirement might be overcome if a smaller probe were developed so that its distance from the surface could be decreased. However, the flatness of the sample surface would become even more vital if the probe were only 10 or 20 microns from the surface.

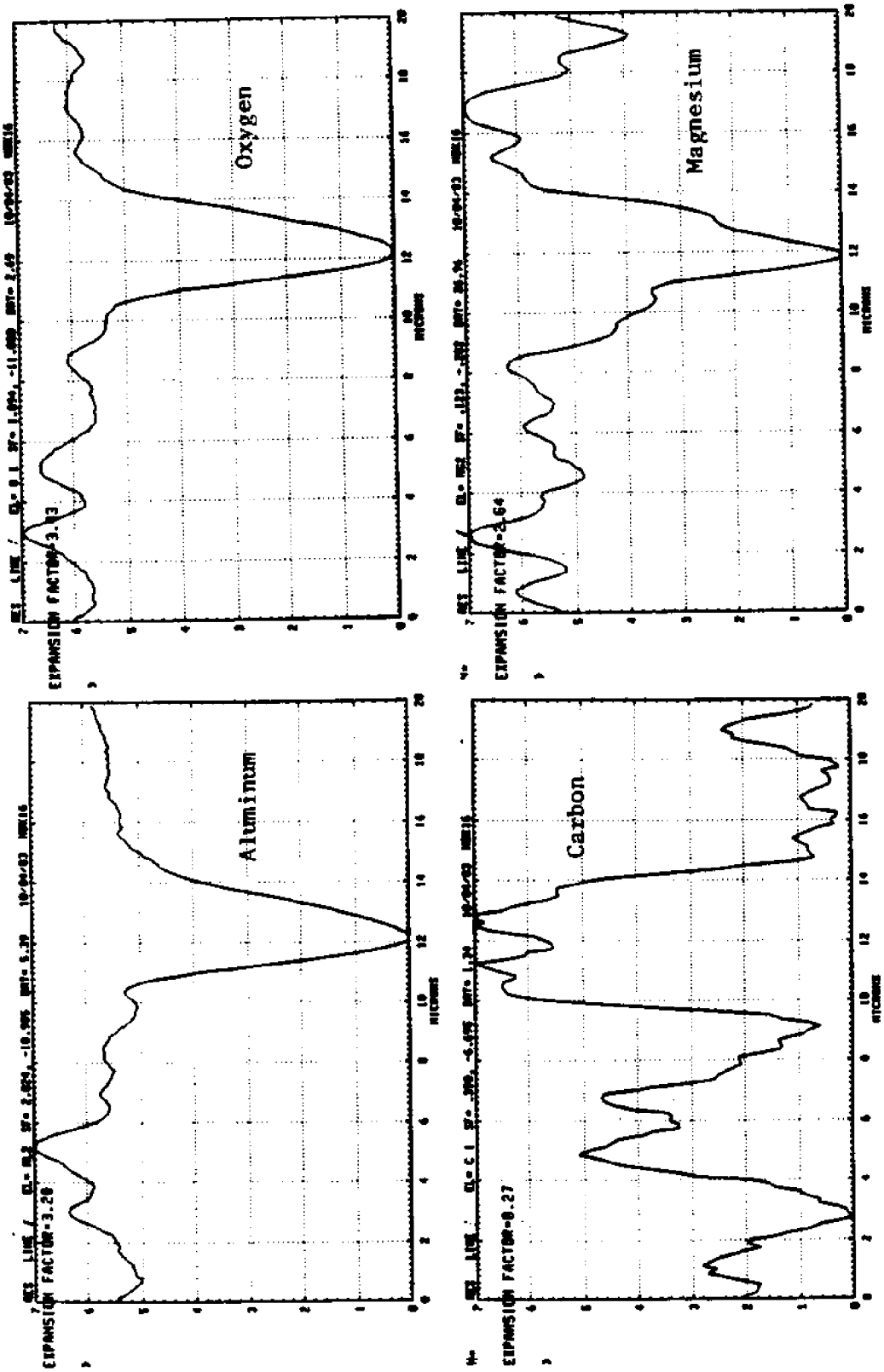

Fig. IV.7 Elemental line scans by AES across pit in Al-5052 after 20 sec. sputter.

Using the SPM, pits were located while the aluminum alloy 5052 sample was actively corroding in a salt water electrolyte. The SPM scan made it much easier to locate pits for chemical analysis using the scanning Auger microscope. Also, the pits studied with the SAM were definitely known to be active at the time of removal from the electrolyte. Therefore, pits which had passivated were eliminated from the surface analysis. When the surface around these pits was analyzed, excess surface concentrations of magnesium were found at a distance of 4 to 6 μm from the pit center. This result agrees with earlier work done with pure aluminum exposed to seawater [14]. These previous studies indicate that the magnesium on the surface is a result of an adsorption reaction, not deposition of magnesium hydroxide. Since no magnesium is seen when Al-5052 is exposed to 3.5% NaCl solution, the surface concentration is not due to the presence of magnesium as an alloying ingredient of the alloy.

This high-resolution implementation of the SPM may prove useful for studies of grain boundary attack, and chemical analysis of the cathodic sites participating in the corrosion process.

References

1. J. N. Agar, Unpublished Results; Summarized by U. R. Evans in "Report on Corrosion Research Interrupted by the Outbreak of War", J. Iron and Steel Inst. 141, 219 (1940).
2. H. R. Copson, "Distribution of Galvanic Corrosion", Trans. Electrochem. Soc. 84, 71 (1943).
3. R. H. Brown, Unpublished Results; Aluminum Research Laboratory; Summarized by E. H. Dix, Jr. in "Acceleration of the Rate of Corrosion by High Constant Stresses", Trans. AIME 137, 11 (1940).
4. J. B. McAndrew, W. H. Colner and H. T. Francis, "Roto-generative Detection of Corrosion Currents", National Advisory Committee for Aeronautics Technical Note 2523, November 1951.
5. J. K. Rice, "Corrosion Testing by Measurement of Local Cell Potentials", Corrosion 10, 25 (1954).
6. K. J. Bhansali and M. T. Hepworth, "The Corrodescope its Description and Application to the Study of Pitting Phenomena", J. Physics E; Scientific Instruments 7, 681 (1974).
7. R. R. M. Johnston, C. P. Lloyd and N. White, "Detection of Local Corrosion due to Microphases in Steel", Australasian Corros. Eng. 17(7) (1973).
8. L. J. Gainer and G. R. Wallwork, "An Apparatus for the Examination of Localized Corrosion Behavior", Corrosion 35, 61 (1979).
9. H. S. Isaacs and B. Vyas, "Scanning Reference Electrode Techniques in Localized Corrosion", In: Electrochemical Corrosion Testing, ASTM STP 727, (F. Mansfeld and U. Bertocci, eds.), American Society for Testing and Materials, p. 3 (1981).
10. L. F. Jaffe and R. Nuccitelli, "An Ultrasensitive Vibrating Probe for Measuring Steady Extracellular Currents", J. Cell Biology 63, 614 (1974).
11. H. S. Isaacs and Y. Ishikawa, "Application of the Vibrating Probe to the Study of Localized Corrosion", Paper given at: The Corrosion Research Symposium, NACE Corrosion/83, Anaheim, CA, 18-20 April 1983.

12. E. Yeager and J. Kuta, "Techniques for the Study of Electrode Processes", In: Physical Chemistry. An Advanced Treatise (H. J. Eyring, ed.), Vol. 9A, p. 359 (1970.

13. S. W. Smith, "Analysis of the Cathodic Behavior of Aluminum in Natural Seawater by Surface Chemistry", Sc.D. Thesis, M.I.T. 1981.

14. S. W. Smith, N. D. Kackley and R. M. Latanision, "Corrosion of Aluminum in Salt Water and Seawater as Influenced by Magnesium and Copper", Paper given at: Corrosion/83, Anaheim, CA, 1820 April 1983.

15. E. Ruppin, Z., Anorg. Chem. 49, 190 (1908); from Properties of Ordinary Water-Substance (N. E. Dorsey, ed.), Reinhold Pub., New York, p. 382 (1940).